
An Investigation into the Level of Fidelity Required to Model Heat Exchangers of a Heat Recovery Steam Generator

Hanon Lim

School of Engineering, Computer & Mathematical Sciences
December 2016

Supervised by:
Associate Professor David I. Wilson
Dr. Jonathan Currie

A thesis submitted to Auckland University of Technology in fulfilment of the
requirements for the degree of Master of Engineering.

Abstract

Process modelling has traditionally been used in the design and development of Combined Cycle Gas Turbine power stations. In recent years it has been applied across the complete process lifecycle, from initial concept testing, through design, development, and operation. In the operation of these plants the process model may be used for offline or online applications. Offline refers to the model being solved in isolation from the plant. Such studies typically look at optimising the operation of the plant, or investigating the affect of plant modifications. Online operation means the process model is run in parallel with the actual plant, receiving measured data from the plant information system. In this role the model can be used to monitor plant performance, allowing degradation of equipment to be tracked, and maintenance scheduled accordingly. In addition, model estimations can be used to reconcile sensor data, improving knowledge about the plant and aiding troubleshooting.

Combined Cycle Gas Turbine (CCGT) power stations consist of a gas turbine and steam cycle, linked by a heat recovery steam generator (HRSG). The HRSG extracts heat from the gas turbines exhaust gases by boiling water for the steam cycle. This facilitated by a series of heat exchangers within the HRSG.

Given the central role of heat exchangers within CCGT power stations, the performance and accuracy of heat exchanger models in the process model is of highest importance. A review of the current literature revealed two competing methods for modelling the variation in the overall heat transfer coefficient of a heat exchanger. The first utilises semi-empirical correlations developed specifically for a given heat transfer problem. The alternative method estimates the variation in the overall heat transfer coefficient with fluid conditions, by applying weights to a nominal value, usually chosen to be the design value for overall heat transfer coefficient. The weights are determined using the ratio of design condition fluid properties to those at the fluid conditions of interest, raised to some constant power. This constant is chosen based on the particular heat transfer problem. A final possibility is to assume the value of the overall heat transfer coefficient does not vary significantly from design conditions and maintain this value constant.

These three methods for estimating the overall heat transfer coefficient represent three levels of modelling fidelity which can be used in heat exchanger models. To determine the level of fidelity required to for modelling HRSG operation, each method was implemented into a heat exchanger model designated the Correlation, Weighted, and Basic heat exchangers. These were then incorporated into a model of the HRSG in the Otahuhu B CCGT power station located in Auckland, New Zealand. The model was then used to simulate the operation of the HRSG at four different load points, spanning the operating range of the plant. Results from the model were then compared to measured plant data.

Overall the Weighted heat exchanger model was found to be the most accurate in following the variation in heat exchanger behaviour in the actual plant, as the load was varied. The Correlation model accurately followed trends in the measure plant data, however, the results were often offset from the data due to an inaccurate estimate of the initial value for overall heat transfer coefficient. The Basic heat exchanger model was the least accurate, and was unable to follow trends in the measure plant data as the load varied. In addition the Correlation model, in general, took over ten times longer to solve than either of the other models.

Contents

1	Introduction	1
1.1	Combined Cycle Gas Turbine Overview	2
1.1.1	Otahuhu B	3
1.2	Heat Recovery Steam Generator	3
1.2.1	Heat Exchangers	4
1.3	Heat Exchanger Modelling	6
1.4	Research Aim	7
1.5	Thesis Outline	8
2	Literature Review	10
2.1	Process Flowsheeting	10
2.1.1	Sequential Modular	11
2.1.2	Equation Oriented	12
2.2	Process Modelling in CCGT Operation	13
2.3	Heat Exchanger Models	15
2.4	Conclusion	15
3	Development of the Theoretical Heat Exchanger Model	18
3.1	Heat Exchanger Model	18
3.1.1	LMTD Method	19
3.1.2	Sizing vs Rating	21
3.1.3	Effectiveness-NTU Method	21
3.1.4	Heat Exchanger Discretisation	23
3.2	The Overall Heat Transfer Coefficient	24
3.2.1	Correlation Based Model	24
3.2.2	Weighted Model	32
3.3	Conclusion	35
4	Heat Exchanger Model Implementation	37
4.1	Development Environment	37
4.2	Heat Exchanger Model	38
4.2.1	Software Architecture	38
4.2.2	Solution Method	40

4.3	Heat Exchanger Model Validation	44
4.4	Discussion	49
4.5	Conclusion	53
5	HRSG Simulation	54
5.1	Gas Turbine Model	54
5.1.1	Basic Operation	55
5.1.2	Model Development	55
5.1.3	Part-load Model	57
5.2	Otahuhu B HRSG Model	60
5.3	Simulation results	64
5.4	Discussion	70
5.5	Conclusion	71
6	Conclusions and Further Work	73
6.1	Conclusion	73
6.2	Further Work	75
	Bibliography	77
A	Correlations	82
A.1	ESCOA TURB-X HF Correlations	82
A.1.1	Heat Transfer Coefficient Correlation	86
A.1.2	Pressure Drop Correlation	88
A.2	Shah Flow Boiling Correlation (1982)	90
B	Simulation Results	91
C	DVD Contents	104

List of Figures

1.1	Process flow diagram of a single pressure level Combine cycle gas turbine power station.	3
1.2	Diagram showing a simplified heat exchanger layout of the Otahuhu B HRSG. LP, IP, and HP designate the low, intermediate, and high pressure circuits. The function of each heat exchanger is indicated by a four letter abbreviation. ECON is short for economiser, EVAP, evaporator, SHTR, superheater, PHTR, preheater, and RHTR, re-heater. When more than one stage of a particular heat exchanger is present for a given pressure level, a number is used to differentiate between them.	4
1.3	HRSG heat exchanger with staggered tube topology. The crosses indicate flow into the page and dots, flow out of the page. P_t and P_l are the transverse and longitudinal tube pitch (spacing) in m. N_t is the number of tubes per row, N_r is the number of rows, and N_{rpp} is the number of rows per pass of the fluid.	5
1.4	Schematic diagram of the segmented fin tube cross-section and top view. d_i and d_o are the inner and outer tube diameters. t_w is the tube wall thickness, d_f is the fin diameter, l_f is the fin length, t_f is the fin thickness, w_s is the segment width, and s_f is the fin spacing. All dimensions are in meters.	5
3.1	Typical temperature profile for parallel and counter flow heat exchangers.	19
3.2	Discretised heat exchanger.	24
3.3	Thermal network diagram of the tube wall cross-section in a tubular heat exchanger.	24
3.4	a). HRSG heat exchanger with staggered tube topology, b). Schematic diagram of the segmented finned tube cross-section and top view. . .	28
4.1	Class diagram of the base heat exchanger model.	39
4.2	Economiser temperature profile of each heat exchanger model, compared to simulation results from the GTPro software [61].	47

4.3	Evaporator temperature profile of each heat exchanger model, compared to simulation results from the GTPro software [61].	49
4.4	Evaporator temperature profile of each heat exchanger model, evaluated for 10 segments.	50
4.5	Variation in the tube side convective heat transfer coefficient as the water is heated from a subcooled liquid to a superheated vapour.	51
4.6	Time required to solve each heat exchanger model with an increasing number of segments.	52
4.7	Comparison of the routines for calculating the tube side heat transfer coefficient. Both routines use the Petukhov-Kirillov and Gnielinski correlations for calculating the heat transfer coefficient for single phase flows. For the black line, the Shah flow boiling routine uses the Petukhov-Kirillov and Gnielinski correlation to calculate the liquid fraction heat transfer coefficient. For the blue line, the Dittus-Boelter correlation was used.	53
5.1	Gas turbine process flow diagram.	55
5.2	Gas turbine model results for important operating parameters compared to measured plant data. In general the model shows good correlation with the plant data. The largest error occurs in the compressor efficiency at low load.	60
5.3	Simplified process flow diagram of the heat recovery steam generator in the Otahuhu B Combined Cycle Gas Turbine Power Station.	61
5.4	Pump unit operation symbol.	62
5.5	Mixer unit operation symbol.	62
5.6	Comparison of the outlet temperatures of the Preheater and LP superheater 2.	64
5.7	Comparison of the outlet temperatures of the IP and HP final stage superheaters.	65
5.8	Comparison of the outlet temperatures of the Reheater and last stage HP Economiser.	66
5.9	Comparison of the steam mass flows for the LP and IP evaporators.	67
5.10	Comparison of the steam mass flow for the HP evaporator and Reheater.	68
5.11	Comparison of the solution time required to solve the HRSG model, for each of the heat exchanger methods. The simulations were performed using MATLAB 2015b, on a laptop with a 64 bit, Intel Core i5-4200U CPU at 1.6 GHz.	69
A.1	a). HRSG heat exchanger with staggered tube topology, b). Schematic diagram of the segmented finned tube cross-section and top view.	82

List of Tables

1	Thesis nomenclature	ix
2	Thesis subscripts	x
2.1	Summary of heat exchanger modelling methods reviewed in literature.	16
3.1	Effectiveness relation for pure counter-flow heat exchangers and during a phase change ($C_r = 0$).	23
3.2	NTU relation for pure counter-flow heat exchangers and during a phase change ($C_r = 0$).	23
3.3	Typical fouling factor for natural gas combustion.	27
3.4	Typical fouling factor for treated boiler feedwater from the Standards of the Tubular Exchanger Manufacturers Association (TEMA 1988).	27
3.5	Heat transfer coefficient and pressure drop correlations used in the Correlation heat exchanger model.	33
4.1	Heat exchanger test data for the Economiser, Evaporator.	44
4.2	Economiser simulation results for each of the heat exchanger models compared to GTPro. Values in red have been calculated by the models.	48
4.3	Evaporator simulation results for each of the heat exchanger models compared to GTPro. Values in red have been calculated by the models.	50
5.1	Basic gas turbine model input parameters	57
5.2	Gas turbine model simulation results.	59
5.3	Design data used by the heat exchanger models.	63
5.4	Fixed pressures and temperatures for each simulation case study.	63
5.5	Variation in heat exchanger UA values with load, calculated by the Weighted model.	69
5.6	Variation in heat exchanger UA values with load, calculated by the Correlation model.	70
A.1	ESCOA correlation nomenclature.	83
A.2	ESCOA correlation nomenclature continued.	84
A.3	ESCOA correlation nomenclature continued.	85
A.4	Shah flow boiling correlation nomenclature	89

B.1	HRSG simulation results at 382 MW, for the Basic heat exchanger model.	92
B.2	HRSG simulation results at 326 MW, for the Basic heat exchanger model.	93
B.3	HRSG simulation results at 265 MW, for the Basic heat exchanger model.	94
B.4	HRSG simulation results at 222 MW, for the Basic heat exchanger model.	95
B.5	HRSG simulation results at 382 MW, for the Weighted heat exchanger model.	96
B.6	HRSG simulation results at 326 MW, for the Weighted heat exchanger model.	97
B.7	HRSG simulation results at 265 MW, for the Weighted heat exchanger model.	98
B.8	HRSG simulation results at 222 MW, for the Weighted heat exchanger model.	99
B.9	HRSG simulation results at 382 MW, for the Correlation heat exchanger model.	100
B.10	HRSG simulation results at 326 MW, for the Correlation heat exchanger model.	101
B.11	HRSG simulation results at 265 MW, for the Correlation heat exchanger model.	102
B.12	HRSG simulation results at 222 MW, for the Correlation heat exchanger model.	103
C.1	DVD contents.	104

Nomenclature

Table 1: Thesis nomenclature

Notation	Description	Unit
A	Area	m^2
c_p	Constant pressure specific heat	$\text{kJ}/\text{kg}\cdot\text{K}$
f_D	Darcy friction factor	
f_F	Fanning friction factor	
F_{corr}	LMTD correction factor	
FAR	Fuel air mass flow ratio	
FC	Mass flow correction factor	
h	Heat transfer coefficient	$\text{kW}/\text{m}^2\cdot\text{K}$
i	Enthalpy	kJ/kg
k	Thermal conductivity	$\text{kW}/\text{m}\cdot\text{K}$
\dot{m}	Mass flow	kg/s
n	Gas turbine compressor speed	rpm
NTU	Number of transfer units	
Nu	Nusselt number	
P	Pressure	bar
Pr	Prandtl number	
\dot{Q}	Heat (Thermal energy transfer)	kW
R	Thermal resistance	K/kW
Re	Reynolds number	
SEC	Compressor speed efficiency correction factor	
T	Temperature	$^{\circ}\text{C}$ or K as indicated.
TFC	Temperature correction factor	
u	Velocity	m/s
U	Overall heat transfer coefficient	$\text{kW}/\text{m}^2\cdot\text{K}$
VFC	Vane flow correction factor	
\dot{W}	Work	kW
X	Vapour fraction	
α	Thermal diffusivity	m^2/s
Δ	Change in a quantity	
ε	Heat transfer effectiveness	
ϵ	Surface roughness	m
η	Efficiency	
μ	Dynamic viscosity	$\text{Pa}\cdot\text{s}$
ν	Kinematic viscosity	m^2/s
ρ	Density	kg/m^3

Table 2: Thesis subscripts

Notation	Description
AMTD	Arithmetic mean temperature difference
avg	Average value
c	Cold fluid
comp	Compressor
d	Design point
des	Design point
f	Fouling
h	Hot fluid
i	Inside tube
in	Inlet
isen	Isentropic property
LMTD	Logarithmic mean temperature difference
max	Maximum value
o	Outside tube
out	Outlet
turb	Turbine
1	Inlet
2	Outlet

Attestation of Authorship

I hereby declare that this submission is my own work and that, to the best of my knowledge and belief, it contains no material previously published or written by another person (except where explicitly defined in the acknowledgements), nor material which to a substantial extent has been submitted for the award of any other degree or diploma of a university or other institution of higher learning.

Hanon Lim _____

Acknowledgements

I firstly wish to thank my academic supervisors, Associate Professor David I. Wilson and Dr. Jonathan Currie for offering me this project and providing invaluable support, both in knowledge and encouragement.

I also wish thank my family for supporting me throughout my academic career, and my partner, Hannah, without whom none of this would have been possible.

Chapter 1

Introduction

Numerical modelling of industrial processes is an important tool in both the design and operation of thermal power plants. In design, the models may be used to size equipment, or assess different plant configurations ability to meet design specifications. Simulations can be carried out over the operating range of the plant to ensure the plant behaves as expected in off-design conditions. Models also have many applications in the simulation of existing plants. Results from these simulations can be used in a number of analyses, for example, to determine the optimal operating parameters under different conditions, or in plant monitoring, where deviation of plant behaviour from model predictions may indicate equipment performance degradation or malfunction, informing maintenance scheduling.

This work is based on the Otahuhu B power station¹, which is a combined cycle gas turbine (CCGT) power station, operated by Contact Energy Ltd. in Auckland, New Zealand. Operation of the plant is monitored by a network of sensors feeding information about the plants current operating state to controllers, plant operators via the Human Machine Interface (HMI), and recorded in the plants PI Historian database for later review. The number and type of sensors is limited by cost and physical difficulty in measuring certain plant parameters. This is especially true for temperature measurements within the heat recovery steam generator (HRSG) where only a limited number of points are routinely measured. One solution for limited sensor data is to run a simulation in real-time to mirror plant operation. The model itself can be validated against the available plant measurement data and the results of the model used to estimate missing temperatures. In addition, these temperature estimates can be used to reconcile erroneous sensor readings. To simulate the operation of the HRSG requires models capable of accurately predicting

¹Since the start of this research the Otahuhu B power station has been decommissioned. Plant information required for this research including all operating data was gathered prior to decommissioning.

the performance of the constituent heat exchangers. Heat exchanger modelling is a mature topic in literature, however, even when just considering steady-state simulation a number of different modelling methodologies are still used in literature and in commercial software packages.

To determine the best approach, this work develops heat exchanger models implementing these methods, and incorporates them into a steady-state model of the Otahuhu B HRSG. The results from this model are validated using actual plant operating data, and the relative performance of each heat exchanger model compared.

The chapter continues by providing an broad overview of CCGT operation, then narrowing the focus to Otahuhu B. The heat exchangers present in the HRSG are then discussed, followed by an overview of the modelling framework used in the study. It then formalises the research aims and provides an outline for the rest of the thesis.

1.1 Combined Cycle Gas Turbine Overview

Currently the most efficient fossil fuel thermal power plants are Combined Cycle Gas Turbines (CCGT). A process flow diagram of a single pressure level CCGT power station is shown in Figure 1.1. These power stations operate on two cycles. The gas turbine operates on the Brayton cycle where air is compressed into the combustion chamber, mixed with natural gas and then combusted. The hot exhaust gases are then allowed to expand through the gas turbine generating work. This work is used to drive both the gas turbine compressor and a generator to generate electricity. The exhaust gases leaving the turbine are still very hot (over 500°C), and additional energy can be extracted. These exhaust gases are used as the heat source for the second stage which operates on the standard Rankine cycle. This heat is extracted by feeding the hot exhaust gases through the Heat Recovery Steam Generator (HRSG). The HRSG is essentially a large duct containing many heat exchangers. It is through these heat exchangers that heat from the exhaust gases is extracted and used to convert water at high pressure in the heat exchanger coils, to superheated steam. The steam is then allowed to expand through steam turbines, again generating work which is used to generate more electricity. The steam leaving the turbines is then condensed back into water and pumped back up to high pressure, completing the cycle. Modern CCGT power stations are capable of achieving efficiencies of greater than 60% compared to the approximately 40% for single cycle plants, [68, 41, 55].

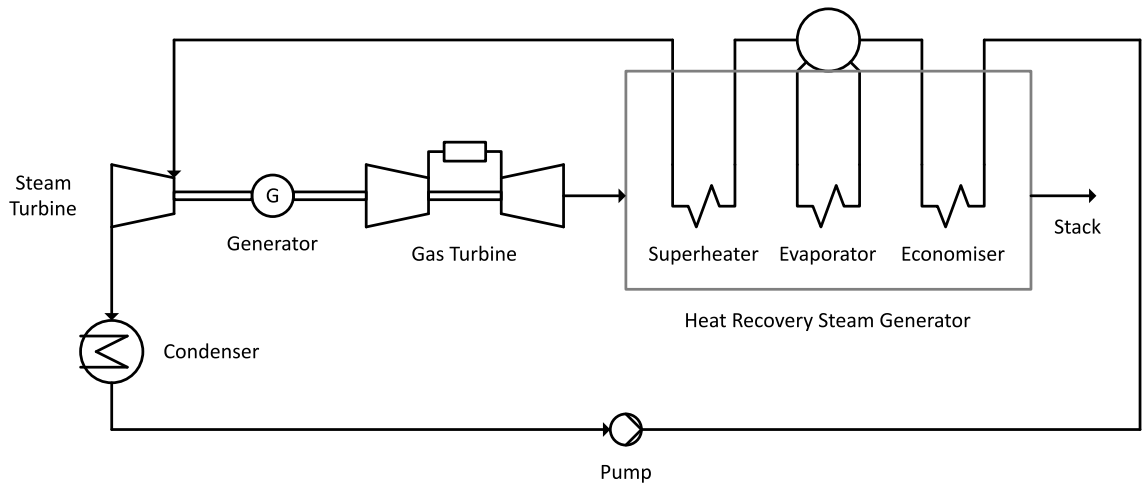


Figure 1.1: Process flow diagram of a single pressure level Combine cycle gas turbine power station.

1.1.1 Otahuhu B

Otahuhu B is a 400 MW CCGT power station in Auckland, New Zealand, operated by Contact Energy Ltd. It consists of a single Siemens SGT5-4000F V94.3A(2), 288 MW gas turbine and three pressure level with reheat HRSG. The steam produced drives three turbines designated low, intermediate and high pressure (LP, IP, and HP), with output of the HP turbine being mixed with the IP steam prior to entering the reheater. A deaerator, used to remove entrained gases from the circulating water, is located after the condensate preheater, but is only operated intermittently as deaeration is also achieved in the condenser. The steam exhausted from the LP turbine is still of high quality and is reduced to liquid water in the condenser. Cooling water for the condenser is sourced from the local estuary and is in turn cooled via an 8-cell evaporative, hybrid cooling tower.

1.2 Heat Recovery Steam Generator

The heat recovery steam generator consists of a large duct that contains the individual heat exchangers for each steam pressure level. For a given pressure level the heat exchangers are separated into three categories based on the phase of the water/steam they act upon. The economiser is designed to pre-heat the feed water to around $6 - 17^\circ\text{C}$ below saturation [37]. This is known as the approach point temperature difference, ΔT_{app} . The water is then fed into the evaporator where it is boiled to generate steam. The temperature difference between the exhaust gas leaving the evaporator and the saturation temperature is called the pinch point temperature difference, ΔT_{pinch} , and at design is typically in the range of $17 - 33^\circ\text{C}$, [37]. The steam then enters the superheater where it is brought up to the required outlet

temperature. The temperature differences, ΔT_{app} and ΔT_{pinch} , are important values in the design of the HRSG. From a thermal efficiency point of view the designer should seek to minimise their values. However, to achieve these low temperatures requires heat exchangers with a larger surface area, and proportionally larger size and cost.

Both the economiser and superheater stages may be divided among multiple heat exchangers. These heat exchangers, along with those of the other pressure levels if present, are then arranged both longitudinally and transversely to the gas flow in order to achieve the most thermally efficient layout. Figure 1.2 shows the layout of the Otahuhu B HRSG. It consists of a total of 14 heat exchangers. The Preheater heats the water before the IP and HP pressure levels are established by a multi-stage pump. The Preheater also serves as the economiser to the LP evaporator. A recirculation loop returns a portion of water from the outlet of the preheater to the inlet. This is done to ensure the temperature of the exhaust gas leaving the preheater is above the dew point, below which, acids in the gas will condense and cause corrosion of the Preheater tubes and HRSG surfaces. The HP turbine exhaust is returned to be mixed with the output steam of the second IP superheater and fed into the Reheater prior to entering the IP turbine.

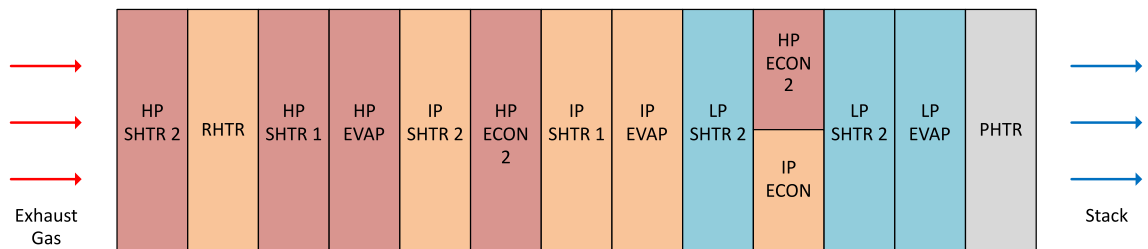


Figure 1.2: Diagram showing a simplified heat exchanger layout of the Otahuhu B HRSG. LP, IP, and HP designate the low, intermediate, and high pressure circuits. The function of each heat exchanger is indicated by a four letter abbreviation. ECON is short for economiser, EVAP, evaporator, SHTR, superheater, PHTR, preheater, and RHTR, reheater. When more than one stage of a particular heat exchanger is present for a given pressure level, a number is used to differentiate between them.

1.2.1 Heat Exchangers

The individual heat exchangers in the HRSG consist of a bundle of tubes oriented vertically within the HRSG. The tubes within the bundle are positioned in rows and arranged in a staggered formation as show in Figure 1.3. The staggered formation provides improved convective heat transfer over an in-line formation due to increased turbulence and mixing of the gas [39, 54]. However, the increased turbulence also results in a larger pressure drop across the tube bundle, adversely affecting gas

turbine performance. The exhaust gas flows over the outside surface of the tube bundle. Water enters the tubes from the opposite end moving up and down the tube rows in a cross-flow orientation, toward the exhaust gas inlet. While the water moves perpendicular to the exhaust gas in any given row, the overall flow orientation is counter to that of the exhaust gas. The flow orientation is therefore known as counter cross-flow [9].

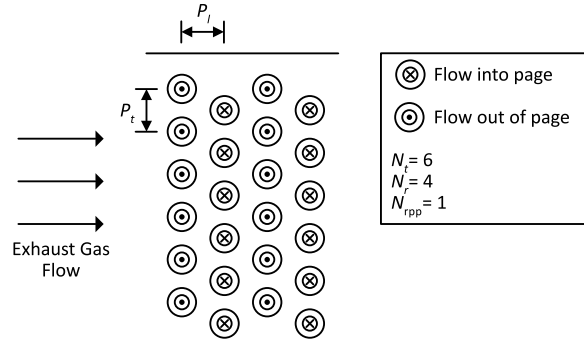


Figure 1.3: HRSG heat exchanger with staggered tube topology. The crosses indicate flow into the page and dots, flow out of the page. P_t and P_l are the transverse and longitudinal tube pitch (spacing) in m. N_t is the number of tubes per row, N_r is the number of rows, and N_{rpp} is the number of rows per pass of the fluid.

Extended surfaces called fins are added to the external surface of the tubes to increase the thermal energy transfer between the fluids. This is required due to the relatively lower convective heat transfer coefficient of gases compared to liquids [33]. The tubes in the Otahuhu B HRSG heat exchangers have segmented (also called serrated) fins as shown in Figure 1.4. These fins provide an increased surface area and greater turbulence and mixing within the exhaust gas stream, improving heat transfer, though again at the expense of increased pressure drop across the bundle.

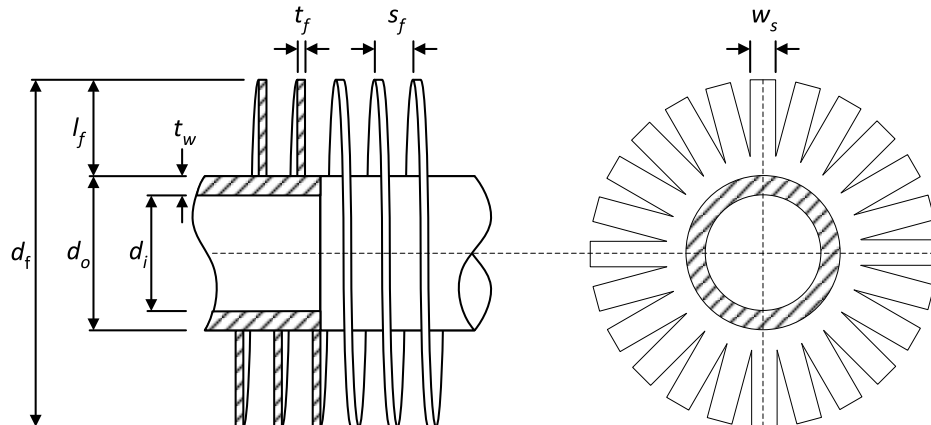


Figure 1.4: Schematic diagram of the segmented fin tube cross-section and top view. d_i and d_o are the inner and outer tube diameters. t_w is the tube wall thickness, d_f is the fin diameter, l_f is the fin length, t_f is the fin thickness, w_s is the segment width, and s_f is the fin spacing. All dimensions are in meters.

1.3 Heat Exchanger Modelling

Heat exchangers are typically modelled using either the logarithmic mean temperature (LMTD) method, or the effectiveness-NTU (ε -NTU) method. These methods are explained in detail in Chapter 3, however to aid the discussion the basic equations are repeated here. The equations relate the fluid properties and heat exchanger construction to the amount of heat transferred. While the methods look superficially different, they are effectively equivalent and give the same result.

LMTD Method:

$$\begin{aligned}\dot{Q} &= UA\Delta T_{LMTD} \\ \Delta T_{LMTD} &= \frac{\Delta T_1 - \Delta T_2}{\ln\left(\frac{\Delta T_1}{\Delta T_2}\right)}\end{aligned}\tag{1.1}$$

Where \dot{Q} is the heat transferred and ΔT_1 and ΔT_2 are the terminal temperature differences between the two fluids. The temperature difference ΔT_{LMTD} is the mean temperature difference between the two fluids as the pass through the heat exchanger. The value U is the overall heat transfer coefficient, and A is the area available for heat transfer [27].

ε -NTU method:

$$\begin{aligned}\varepsilon &= \frac{\dot{Q}_{\text{actual}}}{\dot{Q}_{\text{max}}} \\ NTU &= \frac{UA}{C_{\text{min}}}\end{aligned}\tag{1.2}$$
$$\varepsilon = f(NTU)$$

Where \dot{Q}_{max} is the maximum heat transfer possible, \dot{Q}_{actual} is the actual heat transfer achieved by the heat exchanger, C_{min} is the minimum heat capacity rate of the fluid and NTU is the number of transfer units. The heat exchanger effectiveness, ε , is a function of NTU and the fluid properties. Equations relating these values can be found in heat transfer text books for example [27, 44, 67].

The value of U is a function of the heat exchanger construction and the properties of the fluids. In the literature review in Chapter 2, two competing methods used to determine this value are identified. The first method is to calculate U using a

semi-empirical correlation developed for the specific heat transfer application.

$$U \approx \frac{1}{h_i} + \frac{1}{h_o} \quad (1.3)$$

$$(1.4)$$

Where h_i , h_o are the inner and outer fluid heat transfer coefficients. These values can be calculated using semi-empirical correlations of the general form

$$h = C \text{Re}^n \text{Pr}^m \quad (1.5)$$

Where Re and Pr are dimensionless numbers that are dependent on the fluid properties and duct geometry, and C , n , and m are experimentally determined constants. In this work, this is designated the Correlation heat exchanger model.

An alternative method is to calculate U by applying some weights to a nominal value of U , usually defined as the design value. The weights are determined by using ratios of fluid properties (often mass flow, \dot{m}) under the conditions of interest to nominal fluid properties, raised to some power. In this work, this is designated the Weighted heat exchanger model.

$$U = U_{\text{design}} \left(\frac{\dot{m}}{\dot{m}_{\text{design}}} \right)^x \quad (1.6)$$

where x is a constant determined for the specific heat transfer problem.

A final possibility is to assume the value of U does not vary from design conditions i.e. $U = U_{\text{design}}$. The value of U_{design} can then be simply determined from design fluid conditions, using Equations 1.1, or 1.2. In this work, this is designated the Basic heat exchanger model.

These three methods for estimating U represent three levels of modelling fidelity with the most complex being the Correlation model, followed by the Weighted and Basic models.

1.4 Research Aim

This work aims to determine the most appropriate level of model fidelity with regard to simulating heat exchanger performance in a heat recovery steam generator. Specifically it will focus on the source of the overall heat transfer coefficient, and how it's determination affects the performance of the heat exchanger model. The research has been divided into the following steps:

1. Develop a steady-state heat exchanger model utilising the three different methods to predict the overall heat transfer coefficient, described in Section 1.3.
2. Construct a steady-state model of the heat recovery steam generator in the Otahuhu B CCGT power station, incorporating the heat exchanger models.
3. Validate model outputs against measured plant data.
4. Compare the performance and accuracy of the different heat exchanger models.

1.5 Thesis Outline

This chapter has introduced the reader to the main focus of this thesis and reviewed background information. The rest of the thesis proceeds as follows:

Chapter 2 reviews existing literature on simulating CCGT power plant operation and the methodologies for modelling heat exchangers used in these simulations. This provides the motivation for developing such simulation models and exposes the gap in research on which methods are most suitable model heat exchangers in this application.

Chapter 3 develops the theoretical basis for the heat exchanger model based on well known principles. This leads to the need to determine the overall heat transfer coefficient for a given heat exchanger. Three different methods used in literature are detailed and applied to modelling the heat exchangers within the Otahuhu B HRSG.

Chapter 4 introduces the software environment used to develop the heat exchanger models and simulation of Otahuhu B. The development of the software model of the heat exchanger is then discussed including the architecture, solution strategy and performance. The simulation model of the Otahuhu B is developed and issues, solutions and approximations used are detailed.

Chapter 5 shows the results of a series of case studies. These involve simulating the operation of the Otahuhu B steam cycle at four points spanning the operating range of the plant for each of the three different heat exchanger models. Results from the heat exchanger models are then compared to existing plant data to validate their performance.

Chapter 6 concludes the study by reviewing the results of simulations and comparing the relative performance of each of the three heat exchanger models. Suggestions as to the most appropriate model for this application are made and oppor-

tunities for future research are discussed.

Chapter 2

Literature Review

2.1 Process Flowsheeting

Modeling is an important tool in the design, development, and operation of industrial processes. These processes are achieved through the interaction of the many pieces of equipment that make up the system. The analysis of these processes involves solving the heat and material balance of the system as a whole, as well as the sizing and costing of equipment. This analysis is known as process flowsheeting [56, 64].

Solving the flowsheet requires the solution of many, possibly thousands of equations. This system of equations may also need to be solved many times, for example, when exploring design alternatives, or if recycle streams or nonlinear equations are present. Solution by hand quickly becomes tedious and error prone, if not impossible for larger systems. To address this issue computer programs have been written to aid in the creation and solution of flowsheets. These programs began development in the 1950's. Early programs simply solved single unit operations. Through continuous development, by the 1970's general purpose flowsheeting programs had become an accepted tool in the industry [42, 64].

Modern flowsheeting programs consist of four main components:

- A library of unit operations that represent each piece of equipment.
- A physical properties library for materials used in the processes.
- Numerical solution methods for solving equations.
- A user interface for specifying the process model.

Flowsheeting programs can be generally split into two main categories. These are known as sequential modular (SM) and equation oriented (EO) [6, 50].

2.1.1 Sequential Modular

The vast majority of available flowsheeting programs use the sequential modular approach [37, 50]. Each unit operation is a module encapsulating the model equations, the solution method, and the user interface. Providing the appropriate inputs will enable the unit operation to solve the model and output the results. The process flowsheeting program will contain a library of unit operations to represent equipment commonly encountered in processes. More specialised software packages will also contain unit operations specific to a given problem domain. The unit operations may then be arbitrarily connected, output to input, as required to model the complete process.

When the unit operations are connected linearly from start to finish, then given the required parameters for the unit operations and any feed streams required by the process model, each unit operation may be solved sequentially with the output of the previous unit operation providing the input information for the next [50]. In many processes this is not the case as material or energy produced later in the process is returned as an input to a unit operation located earlier in the process. These are known as recycle streams. The value of these recycle streams are initially unknown. In a technique called stream tearing the value of these streams are guessed (torn). This allows the system to be solved sequentially with the newly calculated value for the recycle stream replacing the initial guess for the next iteration. These iterations continue until the recycle stream values converge with sufficient accuracy [37, 64, 50]. This is also called the outer iteration loop with reference to unit operations that also require solution by iteration which then constitute an inner iteration loop(s).

The sequential modular approach has a number of advantages. The solution methods are developed specifically to solve the model equations for a single unit operation. This results in an efficient and robust solution with the ability to provide detailed and specific error information should the unit operation fail to solve. Additionally, each unit operation may have a customised user interface facilitating the correct specification of parameters. There are also some disadvantages. This approach can be slow to find a solution. This is because most processes will have recycle streams as well as unit operations that require an iterative solution. The solution physical property models used by the software will also likely be iterative, generating multiple levels of iteration loops. While efficient solution algorithms may be used to solve the physical property models and unit operations, the lack of an-

alytic derivatives at the flowsheet level limits the available solution methods. The outer loop solver could use a finite difference approximation to find calculate the derivatives, increasing the number of model evaluations and time taken to solve, or successive substitution with tearing of recycle streams [50].

2.1.2 Equation Oriented

The equation oriented approach involves gathering all of the equations for the process model into a single system of equations (SOE) and attempting to solve the system simultaneously. The process flowsheet will be specified in much the same way as SM, with the user specifying the unit operations and their interconnection via the graphical interface. In this case each unit operation will only specify the model equations. These equations, along with those describing the interconnections between each unit operation will then be assembled into a large system of nonlinear equations (SNLE). The user must then specify enough information to leave a square, non-singular system. Upon initialising the unknown variables the system may then be solved simultaneously using a multi-dimensional root solver [6, 37, 64, 50].

Having the entire process model described in a single SOE enables a number of possibilities, not possible with the SM approach. The solution of the SOE is taken care of by the flowsheeting software allowing different algorithms to be applied depending on the structure and type of equations present. As the solution process is handled by the software, the addition of user defined unit-operations requires only the model equations be specified. This enables the unit-operations to be described in a declarative, rather than procedural programming language, making the addition of user defined unit-operations a more simple task than for SM. The model equations themselves are stated using a symbolic math notation. The use of symbolic math notation enables the software to perform complex mathematical operations on the SOE, such as determining analytical derivatives for the Jacobian [6, 46, 50, 56]. This is much faster than using numerical derivatives and will benefit optimisation as well as root solving algorithms [50]. The solution of the SOE is much more efficient than SM. This is especially so when recycle streams are present, as these are all contained within a single SOE, no addition iteration loops are added.

At face value this approach seems much simpler and more elegant than the sequential modular approach, in practice, implementing this method in software has proved difficult. This is due to the complexity software's architecture and the algorithms required to handle large systems linear, nonlinear, and/or differential equations [56]. This has meant relatively few commercial products have been developed. The main weakness in this approach compared to sequential modular,

has been the robustness of the solvers, specifically in relation to their initialisation [6, 50]. Root solvers are almost all based on Newton’s method which is only locally convergent, meaning the initial guesses for the unknowns must be close to the solution for the solver to converge [64]. In the case of the sequential modular approach single unit operations described by small systems of nonlinear equations will have custom algorithms developed on a case by case basis to provide good initial guesses. This, in general, is not possible with the equation oriented approach. To solve this problem two different approaches have been taken by commercial equation oriented flowsheeting programs. One method is to solve the system first using the sequential modular approach. The results of this simulation will then provide initial guesses for the equation oriented model. This is the method used by the ASPEN PLUS software package [3]. The other method uses a series of models of increasing complexity for each unit operation. The first model may require little or no initialisation, with the output from this model providing the initial guesses for the next. This continues until the model desired model is solved. This solution process is controlled by algorithms at the flowsheeting level. Once the initial steady-state simulation is solved the results may be used to initialise other algorithms for dynamic simulation, sensitivity analysis, optimisation, etc. without having to repeat the entire solution process. This is the approach taken by the gPROMS process modelling software [18, 50].

Process modelling can be further characterised as steady-state or dynamic. Steady-state models represent the process at one particular instant in time, while dynamic models capture the time dependent behaviour, effectively solving the steady-state model at many time steps, over some time interval. Dynamic models can be used to analyse start-up and shutdown behaviour of a plant. They are also used in the design of control systems and in process training simulators [48]. Steady-state modelling is less complex, and as it represents only a single point in time, is faster to solve than dynamic models.

This study is limited to the investigation of steady-state models. This is justified by the fact that the plant of interest is a CCGT power station which typically transitions quickly from one steady-state to the next, a fact that makes them useful as peaking power plants.

2.2 Process Modelling in CCGT Operation

Traditionally process modelling software has been used in the design and development of industrial processes. More recently, it has been applied across the complete process lifecycle, from initial concept testing, through design, development, and op-

eration. When used in the operation of industrial processes, the analysis can be performed offline, where the simulations are completed separate from the plant, or online, where there is some direct data connection between the plant and process modelling software. Pantelides et al. [49] provides a thorough review of current state of process modelling software in plant operation.

The combined cycle gas turbine (CCGT) power station, being at the forefront of efficient thermal power generation, has been the focus of a number of studies utilising process modelling software. Offline studies tend to focus on optimisation, where the goal is to optimise energy systems, taking into account economic factors. Barigozzi et al. [4, 5] modelled the steam cycle of a waste-to-energy plant in northern Italy, using THERMOFLEX software. Data generated by the model was then used in an optimisation application written in MATLAB to determine the optimal operating parameters for the cooling system. Pieve & Salvadori [52] developed a model of an air-cooled steam condenser installed in another waste-to-energy plant. The model was used to determine the optimal number for cooling units to operate depending on environmental conditions.

Online operation means the model is run in parallel with the actual plant, receiving measured data from the plant information system. In this way, the model is continuously updated and kept in sync with actual plant operation. This system also allows the model to act as a benchmark for plant performance, where discrepancies between model predictions and the actual plant may indicate equipment degradation. Once quantified, this degradation may be factored into analyses, allowing maintenance to be scheduled based on economic benefit, rather than the number of hours of operation. This system has been used in commercial plant performance monitoring software packages, and their implementation in CCGT power stations reported.

Kim & Joo [35] detailed the implementation and use of the EfficiencyMap commercial plant monitoring software at two Korean combined cycle gas turbine power stations, Seoincheon and Sinincheon. The software combines plant model outputs and real-time plant data to analyse system performance. The system also provides additional applications for assessing gas turbine compressor condition for maintenance scheduling, and the optimal load allocation for multi-train (multiple gas turbine/boiler units) configurations. The software monitors the condition of the plant by correcting current plant performance to reference load and ambient conditions. Using this method the corrected value should only vary due to changes in the physical condition of the equipment. A case study, monitoring gas turbine power output before and after an overhaul was used to demonstrate the performance monitoring system. The system revealed an immediate increase in gas turbine power output of

approximately 4.5 MW following the overhaul. This finding was verified by plant measurement data demonstrating the method is capable of detecting changes in the physical condition of plant equipment.

De Bobadilla et al. [13] reported the use of the 'EtaPRO' on-line performance monitoring system by General Physic Corporation at the Naco Nogales combined cycle plant in Mexico. The paper details the functionality provided by the software which is similar to that of the EFFICIENCYMAP software. Information from the monitoring system was used to assess the effects of changes to the heat rejection system configuration by stopping fans and circulation pumps at low loads and monitoring the resulting performance changes. Through this method improvements in heat rate of up to 0.2% were observed.

2.3 Heat Exchanger Models

As discussed in Chapter 1, heat exchangers play a central role in the operation of CCGT power stations. The studies reviewed thus far have utilised a range of methods for modelling the heat exchangers. This trend continues in the greater literature, allowing some generalisations to be made. Of the studies reviewed, which provide detailed information into how the models were developed, almost all use either the LMTD or effectiveness-NTU (ε -NTU) methods for the heat transfer model.

Where the models differ is how they determine the overall heat transfer coefficient, U . This value, combined with the heat transfer surface area, A , is a measure of how well the heat exchanger can transfer heat between two fluids. The overall heat transfer coefficient was introduced in Section 1.2.1 and is discussed in detail in Chapter 3. The overall heat transfer coefficient varies with fluid conditions and heat exchanger geometry. Given it's central role in determining the heat transfer in a heat exchanger, how the value is determined under changing fluid conditions, should have a large impact on the accuracy of the heat exchanger model. A summary of the heat exchanger models used in the reviewed literature is given in Table 2.1. The terms Correlation and Weighted models used to describe the methods for determining U are defined in Section 1.2.1 and again in Chapter 3.

2.4 Conclusion

This chapter has reviewed literature on process modelling and it's role in the operation of CCGT/Cogeneration power stations. Process modelling software has been

Table 2.1: Summary of heat exchanger modelling methods reviewed in literature.

Reference	Heat Exchanger Modelling Method
Aklilu & Gilani [1]	Use the LMTD method and Weighted method for determining U .
Barigozzi et al. [4, 5]	Method not stated. The study utilised the THERMOFLEX process modelling software.
Cafaro et al. [10]	ε -NTU, using the Weighted model for determining U .
De Bobadilla et al. [13]	Used the ETAPRO online performance monitoring software. They state that the model uses first principle models for the exchanger, so the Correlation model is likely used for determining U .
Diaz-Mateus & Castro-Gualdron [14]	The heat transfer model is not stated, but uses the Correlation method for determining U .
Dumont & Heyen [15]	Use the LMTD method and Correlation method for determining U .
Erbes & Gay [20]	Used the GATECYCLE software which uses the ε -NTU method and the Weighted method for determining U .
Ibrahim & Rahman [29]	Created models using the THERMOFLEX software. The heat exchanger modelling method is not given.
Ong'rio et al. [47]	Dynamic simulation using a distributed model. Correlation method was used for determining U .
Pieve & Salvadori [52]	LMTD methods using the Correlation method for determining U .
Kim & Joo [36]	Used the EFFICIENCYMAP software based on the GATECYCLE thermodynamic modelling software. This uses the ε -NTU method and the Weighted method for determining U .
Ibrahim & Rahman [29]	Created models using the THERMOFLEX software. The heat exchanger modelling method is not given.
Shin et al. [59]	Developed dynamic models and uses the Correlation method for determining U .

used offline to determine the optimal operating parameters of Cogeneration power stations. In online applications such software allowed accurate monitoring of plant performance, leading to efficiency gains, and the possibility of improved maintenance scheduling.

The review identified two competing methods for determining the overall heat transfer coefficient of heat exchangers used in the process models. With both methods used ubiquitously in the literature, it is natural to ask:

- Does the variation of U with fluid conditions have a significant affect on the heat exchanger operation?
- If it does, which of these methods is best for the application of CCGT power station modelling?

This work aims to answer these questions together by determining the appropriate level of model fidelity for simulating heat exchanger performance in the HRSG of a CCGT power station. In order to achieve this goal, three heat exchanger models are developed and incorporated into a model of the Otahuhu B HRSG. The results of the simulation are compared to measured plant data, allowing the performance and accuracy of each modelling methodology to be assessed.

Chapter 3

Development of the Theoretical Heat Exchanger Model

In this chapter the theoretical model of a heat exchanger is developed. The process starts with a heat and mass balance around the heat exchanger. Then the logarithmic mean temperature difference (LMTD) and effectiveness - number of transfer units (ϵ -NTU) methods are introduced as two common ways to calculate thermal energy transfer between the two fluids. Both methods assume constant isobaric specific heat capacities. The implications of this as well as solutions to possible issues are discussed. The analysis of methods for determining the overall heat transfer coefficient form the basis of this study. Three different approaches are discussed and specific solutions for modelling the exchangers present in the Otahuhu B HRSG are given.

3.1 Heat Exchanger Model

Heat exchangers can be broadly separated into categories based on the relative flow orientation of the two fluids. Figure 3.1 shows two possible flow orientations. The left is known as parallel-flow because the fluids enter at the same side and move in the same direction toward the outlet. The right is called counter-flow. Here the fluids enter at opposite ends and flow in opposite directions toward the outlet. In addition to these configurations there is also cross-flow. In this case the one fluid flows inside tubes while the other, usually in the gas phase, flows over the outside of the tubes, perpendicular to the flow direction of the internal fluid. The following discussion will focus on the counter-flow heat exchanger but will show how the model can be altered for parallel and cross-flow configurations.

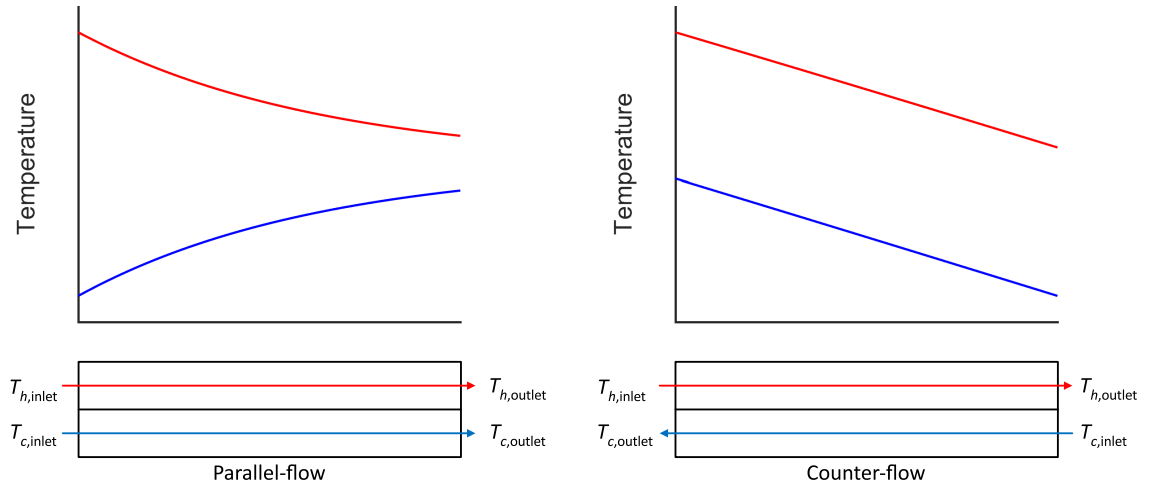


Figure 3.1: Typical temperature profile for parallel and counter flow heat exchangers.

Developing the model for the heat exchanger begins with a heat and mass balance at inlet and outlet.

$$\dot{Q} = \dot{m}_h c_{p,h} (T_{h,inlet} - T_{h,outlet}) \quad (3.1)$$

$$\dot{Q} = \dot{m}_c c_{p,c} (T_{c,outlet} - T_{c,inlet}) \quad (3.2)$$

Where \dot{m} is the mass flow in kg/s, c_p is the isobaric specific heat capacity in kJ/kg·K, T is the temperature in Kelvin (K), and \dot{Q} is the heat transfer in kW. The subscripts c , h , denote the cold and hot fluids respectively.

Equations 3.1 and 3.2 assume a constant fluid isobaric specific heat capacity. The accuracy of this assumption depends on the fluid, the change in temperature, and most importantly whether or not a phase change occurs. This will be explored in more detail in Section 3.1.4. Ignoring losses to the environment, \dot{Q} must be the same for both fluids, i.e. the thermal energy lost by the hot fluid must be transferred to the cold fluid. \dot{Q} is a function of the fluid temperatures and the physical construction of the heat exchanger. Two commonly used techniques for relating these quantities are the logarithmic mean temperature (LMTD) and effectiveness - number of transfer units (ϵ -NTU) methods.

3.1.1 LMTD Method

The rate of thermal energy transfer through a temperature difference, ΔT , is given by:

$$\dot{Q} = UA \Delta T \quad (3.3)$$

U is the overall heat transfer coefficient in kW/m²·K, A is the heat transfer surface area in m², and ΔT is the temperature difference in K. The product UA accounts for the thermal conductance of the two fluids and the separating wall. The determination of this value forms the basis of this study and will be discussed in detail Section 3.2. As the fluids move through the heat exchanger their temperatures will change, altering the value of ΔT . To determine a single value for representing the temperature driving force, the governing differential equations for the heat exchanger are integrated from the inlet to the outlet. This analysis is shown in [44, 67]. The result is the logarithmic mean temperature difference (LMTD).

$$\Delta T_{LMTD} = \frac{\Delta T_1 - \Delta T_2}{\ln\left(\frac{\Delta T_1}{\Delta T_2}\right)} \quad (3.4)$$

Where ΔT_1 and ΔT_2 are the terminal temperature differences between the two fluids:

Parallel flow:

$$\Delta T_1 = T_{h,inlet} - T_{c,inlet} \quad (3.5)$$

$$\Delta T_2 = T_{h,outlet} - T_{c,outlet} \quad (3.6)$$

Counter flow:

$$\Delta T_1 = T_{h,inlet} - T_{c,outlet} \quad (3.7)$$

$$\Delta T_2 = T_{h,outlet} - T_{c,inlet} \quad (3.8)$$

Counter-flow provides a larger ΔT_{LMTD} due to a higher overall temperature difference along the length of the heat exchanger, resulting in superior performance compared to a parallel-flow heat exchanger of the same size. Due to this the majority of heat exchangers are designed for a counter-flow configuration [33]. This is also true for cross-flow heat exchangers. While during a single pass the fluids flow perpendicular to one another, over multiple passes the fluids will often move in an overall counter-flow orientation. This hybrid arrangement is called counter cross-flow. Substituting this result for ΔT in Equation 3.3 gives,

$$\dot{Q} = UA\Delta T_{LMTD} F_{corr} \quad (3.9)$$

Where F_{corr} is a correction factor to account for heat exchanger geometries different from that of pure parallel-flow or counter-flow. This correction factor may be determined from curves developed for specific types of heat exchangers including cross-flow and shell and tube, and are provided in many heat transfer and heat exchanger textbooks, for example, [67] and [33]. For numerical solutions, equations have been fitted to correction factor curves for various heat exchanger types and are

available in literature. A general approximation is given in [62] where the coefficients are chosen for a specific type of heat exchanger. Equations 3.1, 3.2, and 3.9 form a system of non-linear equations (SNLE) and make up the core of the heat exchanger model.

3.1.2 Sizing vs Rating

Heat exchanger models are generally solved with the goal of either designing the heat exchanger to meet a set of specifications, which is known as the sizing problem, or for determining the performance of a particular heat exchanger design, the rating problem [33]. These two scenarios will dictate the information available, the unknowns to be solved for, and therefore, the solution strategy required to solve the SNLE. The sizing problem focuses on solving for UA given a set of design operating conditions. These will typically be the fluid properties at the inlet to the heat exchanger including temperature, pressure, and mass flow. To obtain a square system of equations an additional variable must be specified. Often the outlet temperature of one of the fluids will be fixed by design requirements of the greater system. With this information the SNLE may be solved directly for the value of UA required to achieve these design conditions.

In this study we are concerned with simulating the performance of existing heat exchangers. In this situation the inlet fluid properties may also be specified, however, the physical construction of the heat exchanger is fixed and UA will be determined from design data. The objective is then to solve for \dot{Q} from which the outlet fluid properties may be calculated. In this case the solution to the SNLE will be iterative. Non-linear equation solving algorithms implemented in software are available for the solution of such systems, but require the user to supply a good initial guess of the solution values. For the input specification discussed above ($T_{h,inlet}$, $P_{h,inlet}$, \dot{m}_h , $T_{c,inlet}$, $P_{c,inlet}$, \dot{m}_c , and UA) the effectiveness-NTU method provides a direct solution and is discussed next.

3.1.3 Effectiveness-NTU Method

The effectiveness-NTU method is an alternative to the LMTD method. It was developed by W. M. Kays and A. L. London and is detailed in their seminal text, Compact Heat Exchangers [34]. The method is based around three dimensionless numbers, the effectiveness, ε , the heat capacity rate ratio, C_r , and the number of transfer units, NTU. The relation between these values depends on the type of heat exchanger and may be obtained from design curves or equations for a limited number

of heat exchanger configurations. The effectiveness of the heat exchanger is the ratio of the actual thermal energy transferred to the maximum possible for the two fluids and is given by:

$$\varepsilon = \frac{\dot{Q}_{\text{actual}}}{\dot{Q}_{\text{max}}} \quad (3.10)$$

Where:

$$\dot{Q}_{\text{max}} = C_{\min} (T_{h,\text{inlet}} - T_{c,\text{inlet}}) \quad (3.11)$$

$$C_{\min} = \min(C_h, C_c) \quad (3.12)$$

$$C_h = \dot{m}_h c_{p,h} \quad (3.13)$$

$$C_c = \dot{m}_c c_{p,c} \quad (3.14)$$

C_h , and C_c are the heat capacity rates of the fluids and is a measure of the ability of each fluid to absorb or reject heat. \dot{Q}_{max} is given by the largest temperature difference between the two fluids ($T_{h,\text{inlet}} - T_{c,\text{inlet}}$) and limited by the minimum heat capacity rate. The NTU is:

$$NTU = \frac{UA}{C_{\min}} \quad (3.15)$$

As NTU is directly proportional to UA , the larger the value of NTU the larger the heat transfer area and therefore heat exchanger required. The final dimensionless value, C_r , is the ratio of the minimum to the maximum heat capacity rates:

$$C_r = \frac{C_{\min}}{C_{\max}} \quad (3.16)$$

$$C_{\max} = \max(C_h, C_c) \quad (3.17)$$

By definition $C_r \leq 1$. In the special case of a phase change, $C_r \rightarrow 0$, as $C_{\max} \rightarrow \infty$. Table 3.1 shows the effectiveness relation for a pure counter-flow heat exchanger. It also gives the effectiveness relation when one fluid is undergoing a phase change. This is applicable to all heat exchanger flow arrangements. Table 3.2 shows the same relations solved for NTU in terms of ε and C_r . Additional relations for common heat exchanger types (parallel, single pass cross-flow, shell and tube, etc.) including design curves are available in heat transfer and heat exchanger textbooks [67, 44, 33, 34]. Some relations for more complex heat exchanger flow arrangements may be sourced from literature. For example, Cabezas-Gómez et al. [9] develop ε -NTU relationships for multi-pass cross-flow heat exchangers with complex flow patterns.

Table 3.1: Effectiveness relation for pure counter-flow heat exchangers and during a phase change ($C_r = 0$).

Heat exchanger type	Effectiveness relation
Counter-flow	$\varepsilon = \begin{cases} \frac{1 - \exp[-NTU(1-C_r)]}{1 - C_r \exp[-NTU(1-C_r)]} & \text{for } C_r < 1 \\ \frac{NTU}{1 + NTU} & \text{for } C_r = 1 \end{cases}$
All heat exchangers with $C_r = 0$	$\varepsilon = 1 - \exp(-NTU)$

Table 3.2: NTU relation for pure counter-flow heat exchangers and during a phase change ($C_r = 0$).

Heat exchanger type	NTU relation
Counter-flow	$NTU = \begin{cases} \frac{\ln\left[\frac{1-\varepsilon C_r}{1-\varepsilon}\right]}{1-C_r} & \text{for } C_r < 1 \\ \frac{\varepsilon}{1-\varepsilon} & \text{for } C_r = 1 \end{cases}$
All heat exchangers with $C_r = 0$	$NTU = -\ln(1 - \varepsilon)$

3.1.4 Heat Exchanger Discretisation

Both the LMTD and effectiveness-NTU methods assume each fluid has a constant c_p . Over modest temperature changes this can be a good assumption, however, over larger temperature changes or if a phase change occurs the error introduced can be significant [44]. To increase the accuracy of the model one solution is to subdivide the heat exchanger into a number of segments as shown in Figure 3.2. Fluid properties may then be evaluated at the local average temperature for each segment. Depending on the number of segments chosen the heat exchanger can be solved to any desired accuracy. It should be noted that during a phase change there is no sensible heating/cooling. In order for the model to account for the latent heating/cooling that occurs during fluid phase changes the heat and mass balance must be solved in terms of enthalpy, i , instead of temperature. In this case the heat and mass balance results in:

$$\dot{Q} = \dot{m}_h (i_{h,\text{inlet}} - i_{h,\text{outlet}}) \quad (3.18)$$

$$\dot{Q} = \dot{m}_c (i_{c,\text{outlet}} - i_{c,\text{inlet}}) \quad (3.19)$$

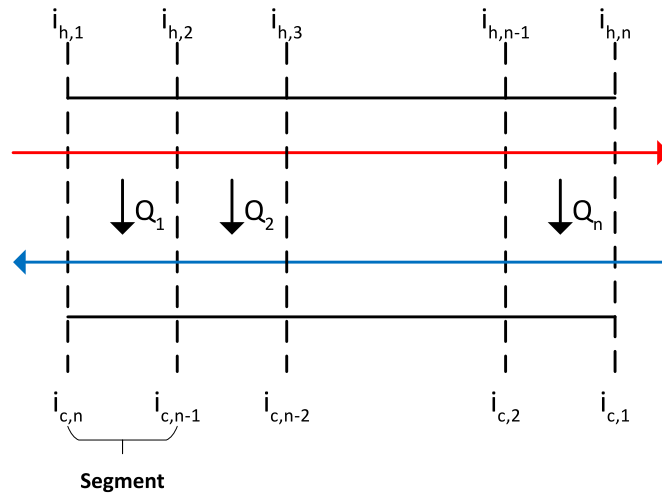


Figure 3.2: Discretised heat exchanger.

3.2 The Overall Heat Transfer Coefficient

To simulate the performance of an existing heat exchanger the value of UA must be determined. The simplest way is to solve equation 3.9 using design operating conditions. With the value of UA and the input conditions of both fluids known, the heat exchanger can be solved for the outlet states of the fluids. This assumes a constant value for UA , though as stated above, U is a function of fluid enthalpy and pressure. If the fluid input conditions change then the value of U will be different from the design point value. In this section two methods to account for the variation of U due to changes in fluid properties are detailed.

3.2.1 Correlation Based Model

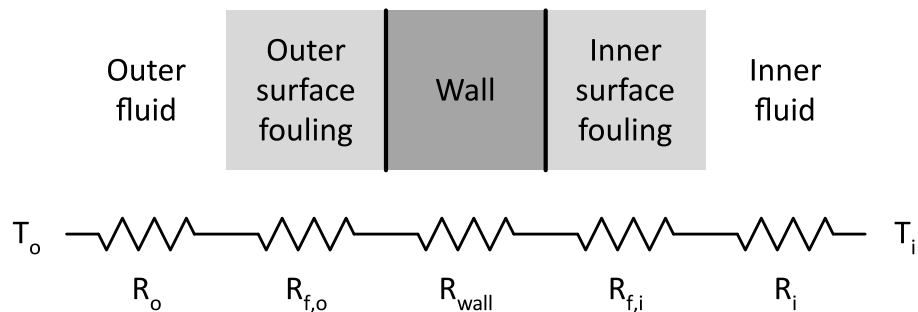


Figure 3.3: Thermal network diagram of the tube wall cross-section in a tubular heat exchanger.

Figure 3.3 shows a cross-section of the tube wall separating the two fluids in a heat exchanger as well as the corresponding thermal network diagram. The thermal network diagram represents the materials separating two different temperatures as thermal resistances in series forming a thermal resistance circuit. UA is the inverse

sum of the individual thermal resistances. For tubular heat exchangers the value is given by:

$$\frac{1}{UA} = R_t = R_o + R_{f,o} + R_{\text{wall}} + R_{f,i} + R_i \quad (3.20)$$

$$\frac{1}{UA} = R_t = \frac{1}{h_o A_o} + \frac{R_{\text{factor},o}}{A_o} + \frac{\ln(d_o/d_i)}{2\pi Lk} + \frac{R_{\text{factor},i}}{A_i} + \frac{1}{h_i A_i} \quad (3.21)$$

Where:

R_t - Total thermal resistance in K/kW.

R_i, R_o - Convection thermal resistance in K/kW.

$R_{f,i}, R_{f,o}$ - Thermal resistance due to fouling in K/kW.

$R_{\text{factor},i}, R_{\text{factor},o}$ - Fouling factor in $\text{m}^2 \cdot \text{K}/\text{kW}$.

h_i, h_o - Heat transfer coefficient in $\text{kW}/\text{m}^2 \cdot \text{K}$.

A - Surface area in m^2 .

d - Diameter in m.

L - Tube length in m.

k - Tube material thermal conductivity in $\text{kW}/\text{m} \cdot \text{K}$.

Subscripts:

o - Outer surface.

i - Inner surface.

Note that the overall heat transfer coefficient may be based on the either the outside or inside heat transfer surface areas:

$$\frac{1}{U_o} = \frac{1}{h_o} + R_{\text{factor},o} + \frac{A_o \ln(d_o/d_i)}{2\pi Lk} + \frac{A_o}{A_i} R_{\text{factor},i} + \frac{A_o}{A_i} \frac{1}{h_i} \quad (3.22)$$

$$\frac{1}{U_i} = \frac{A_i}{A_o} \frac{1}{h_o} + \frac{A_i}{A_o} R_{\text{factor},o} + \frac{A_i \ln(d_o/d_i)}{2\pi Lk} + R_{\text{factor},i} + \frac{1}{h_i} \quad (3.23)$$

However, the thermal resistances are equivalent:

$$\frac{1}{UA} = \frac{1}{U_o A_o} = \frac{1}{U_i A_i} \quad (3.24)$$

If the surface has structures such as fins to enhance heat transfer, then an additional factor called the overall surface efficiency, η , may be added to account for this effect

on the corresponding surface.

$$\frac{1}{UA} = R_t = \frac{1}{\eta_o h_o A_o} + \frac{R_{\text{factor},o}}{\eta_o A_o} + \frac{\ln(d_o/d_i)}{2\pi Lk} + \frac{R_{\text{factor},i}}{\eta_i A_i} + \frac{1}{\eta_i h_i A_i} \quad (3.25)$$

For a finned surface:

$$\eta = \left(1 - (1 - \eta_f) \frac{A_f}{A_t}\right) \quad (3.26)$$

Where η_f is the Fin efficiency, A_f is the surface area of the fins in m^2 , and A_t is the total combined surface area of the fins and exposed tube in m^2 . The fin efficiency is dependent of the type of fin present. Equations for calculating values for fin with simple geometries may be found in heat transfer and heat exchanger textbooks, [44, 33]. Equations for more complex geometries may be found in research literature. The addition of fins to enhance thermal energy transfer is common when the fluid is in the gas phase due to the low convective heat transfer coefficient associated with gases.

Thermal resistances reduce the rate of thermal energy transfer between two fluids at different temperatures. R_{wall} is the conduction thermal resistance of the tube wall. The equation for R_{wall} is obtained by integrating Fourier's law between the inner and outer radii of the tube wall [27]. The thermal conductivity, k , depends on the material of the tube and its temperature. The tubes of the Otahuhu B HRSG heat exchangers are made from carbon steel, where the range of thermal conductivity values is 29-55 kW/m-K [27], depending on temperature and carbon content. The thermal resistance due to fouling, R_f , is the build up of material on the heat transfer surfaces that acts to insulate the wall [33]. The extent of fouling is represented by the fouling factor, R_{factor} . Typical values are provided in the standards of the Tubular Exchanger Manufacturer Association (TEMA). These values can be used to design heat exchangers that will provide the required performance in fouled conditions that may be present between cleans. In modelling the performance of heat exchangers, typical fouling factors can be used to account for any fouling that has occurred. For the heat exchangers in the HRSG fouling on the outer surface is mostly due to the build up of combustion products (soot/ash) deposited on surfaces. On the inner surface fouling takes the form of scale and sludge deposited by the circulating water. Tables 3.3 and 3.4 give typical values for the fouling factors for flue gas from the combustion of natural gas and boiler feedwater respectively.

As shown in Equation 3.25, the convection thermal resistance of the fluids depend on the heat transfer coefficients, h_i and h_o . The heat transfer coefficients are in turn dependent on the heat exchanger type and the fluid's properties. In general, equations for the heat transfer coefficient cannot be developed directly from

Table 3.3: Typical fouling factor for natural gas combustion.

Source	Conditions	Fouling factor [$\text{m}^2\cdot\text{K}/\text{kW}$]
ESCOA Manual [22]	Fin spacing (s_f) ≥ 0.0018 m	0.1761 – 0.5283
Kakaç & Liu [33]	N\A	0.881
VDI Heat Atlas [62]	Water velocity 30 – 40 m/s	0.09 – 0.53

Table 3.4: Typical fouling factor for treated boiler feedwater from the Standards of the Tubular Exchanger Manufacturers Association (TEMA 1988).

Fouling factor [$\text{m}^2\cdot\text{K}/\text{kW}$]				
Temperature of heating medium	$\leq 115^\circ\text{C}$		$115 - 200^\circ\text{C}$	
Temperature of water	$\leq 50^\circ\text{C}$		$> 50^\circ\text{C}$	
Water velocity	< 0.9 m/s	> 0.9 m/s	< 0.9 m/s	> 0.9 m/s
Treated boiler feedwater	0.176	0.088	0.176	0.176

first principles for practical heat exchanger geometries. Correlations relating the heat transfer coefficient to fluid properties and heat exchanger configuration have been developed by fitting theoretical equations to experimental data. The next two sections describe the correlations used for determining the convection heat transfer coefficients for the inner and outer fluids of the HRSG heat exchangers.

3.2.1.1 External Correlations

External Heat Transfer Coefficient

The heat exchangers in the Otahuhu B HRSG consist of rows of vertical tubes with alternate rows offset to achieve a staggered layout as shown in Figure 3.4. In addition, the tubes have a helical strip of segmented fins welded to the external surface to enhance heat transfer. While many correlations for the heat transfer coefficient of tube bundles with plain (solid) fins are available in heat transfer textbooks, [27, 44, 67] and literature, very few have been developed for the segmented fin tube bundles. A correlation by Weierman in [63] was revised in 1979 and again in 1993 by the Extended Surface Corporation of America (ESCOA). The 1993 revision was made using data from their purpose built test facility. The data was gathered from tests on finned tube bundles in both inline and staggered arrangement, with a variety of fin types, including segmented; using tube diameters (1.5-2.4 in), and temperatures typical of large heat recovery boilers. The correlation is given in ESCOA Engineering Manual [22] and is widely used in literature to model heat transfer in finned tube bundles, for example, [16, 14]. The 1979 version of the ESCOA corre-

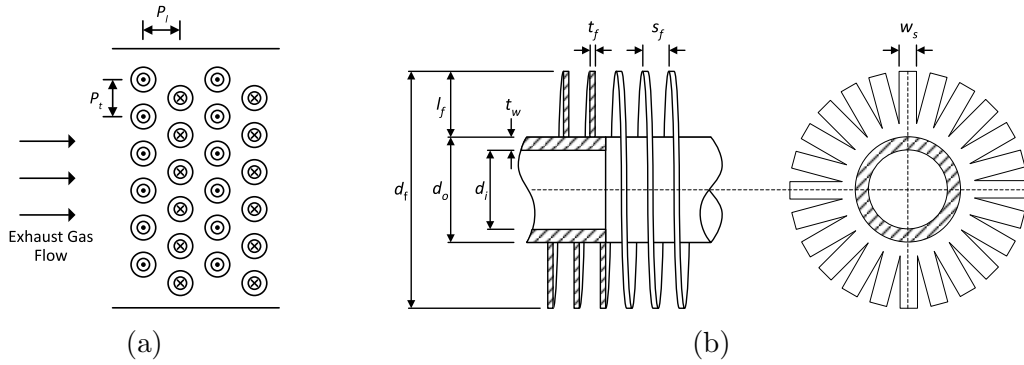


Figure 3.4: a). HRSG heat exchanger with staggered tube topology, b). Schematic diagram of the segmented finned tube cross-section and top view.

lation was recently compared to several other correlations in [39] using data from a test setup of a staggered arrangement of segmented fin tubes. The ESCOA correlation was found to match test data in the range of $\pm 10\%$ and provide the most consistent predictions across different tube bundle geometries.

External Pressure Drop Model

The ESCOA Engineering Manual also provides correlations for predicting the pressure drop across the tube bundle. Ma et al. [39] tested this and several other pressure drop correlations against pressure drop data gathered from their experimental setup. The ESCOA 1979 version of the pressure drop correlation was found to be the most consistent matching test data within $\pm 10\%$. The revised 1993 version of the correlations for both the heat transfer coefficient and pressure drop are given in Appendix A.

3.2.1.2 Internal Correlations

Within the tubes of the heat exchanger the water may exist as a single phase of either liquid or vapour, or during a phase transition, a combination of the two. The particular phase present will have a large impact on the heat transfer coefficient and pressure drop. The model must therefore detect which phase is present in a given segment and apply the appropriate correlations.

Internal Heat Transfer Coefficient

In the case of single phase liquid or vapour flow, one of the most well known and simple correlations for the heat transfer coefficient in fully developed turbulent flow

in smooth tubes, is the Dittus-Boelter equation [27]

$$\text{Nu} = 0.023 \text{Re}^{0.8} \text{Pr}^n \quad \begin{array}{l} 0.5 < \text{Pr} < 2000 \\ 2300 < \text{Re} < 10^4 \end{array} \quad (3.27)$$

$$n = \begin{cases} 0.4 & \text{for heating the fluid} \\ 0.3 & \text{for cooling the fluid} \end{cases}$$

Where Re is the Reynolds number, Pr is the Prandtl number, and Nu is the Nusselt number. Each of these numbers are dimensionless and are used to group properties of the system to describe a particular aspect of the flow. The Reynolds number is given by:

$$\text{Re} = \frac{u_{\text{avg}} d}{\nu} = \frac{\rho u_{\text{avg}} d}{\mu} = \frac{G d}{\mu} \quad (3.28)$$

Here, u_{avg} is the average velocity of the fluid in m/s, d is the hydraulic diameter (inner diameter of the tube) in m, and ρ is the fluid density in kg/m³. ν , the kinematic viscosity in m²/s and μ , the dynamic viscosity in Pa·s are related by

$$\nu = \frac{\mu}{\rho} \quad (3.29)$$

G , the mass flux in kg/m²·s is related to mass flow by the following relations

$$\dot{m} = \rho u_{\text{avg}} A_{\text{csa}} \quad (3.30)$$

$$G = \frac{\dot{m}}{A_{\text{csa}}} \quad (3.31)$$

Where A_{csa} is the cross-sectional area of the pipe in m². The Reynolds number is the ratio of inertial forces to viscous forces on the fluid [67]. It is used to indicate the flow regime present, with low Reynolds numbers indicating laminar flow, and high numbers indicating turbulent flow. The critical value of Reynolds number separating the two regimes is usually taken to be 2300 for flow in a pipe, though the transition from laminar to fully developed turbulent flow may occur from 2000 to 4000 [27].

The Prandtl number represents the relative thickness of the velocity to the thermal boundary layers developed in a fluid flowing near a surface [67]. This in turn is related to the ability of a fluid to transport momentum or energy [44]. The greater the ability of a fluid to transport (diffuse) momentum or energy, the greater the corresponding boundary layer thickness. The Prandtl number is defined as

$$\text{Pr} = \frac{\nu}{\alpha} = \frac{\mu c_p}{k} \quad (3.32)$$

Where α is the thermal diffusivity of the fluid, which has the same units as kinematic viscosity.

The Nusselt number represents the relative enhancement of heat transfer due to convection over what would occur in the case of pure conduction (no fluid motion, $\text{Nu} = 1$) [67]. It's value is given by

$$\text{Nu} = \frac{h d}{k} \quad (3.33)$$

where d is the hydraulic diameter in m, which is the tube inner diameter in this situation. k is fluid thermal conductivity in kW/m·K, and h is the sort after heat transfer coefficient in kW/m²·K.

The Dittus-Boelter correlation provides a simple method for calculating the heat transfer coefficient for internal convection, however, it can be in error by as much as $\pm 25\%$ [27]. A more accurate correlation was developed by Petukhov & Kirillov [51] and recommend in [27, 33]

$$\text{Nu} = \frac{(f_D/8) \text{Re} \text{Pr}}{1.07 + 12.7 (f_D/8)^{1/2} (\text{Pr}^{2/3} - 1)} \quad (3.34)$$

$$0.5 < \text{Pr} < 200 \quad \text{for } 6\% \text{ accuracy}$$

$$0.5 < \text{Pr} < 2000 \quad \text{for } 10\% \text{ accuracy}$$

$$10^4 < \text{Re} < 10^6$$

This was modified by Gnielinski in 1976 to better fit data at low Reynolds numbers [23]

$$\text{Nu} = \frac{(f_D/8)(\text{Re} - 1000) \text{Pr}}{1 + 12.7 (f_D/8)^{1/2} (\text{Pr}^{2/3} - 1)} \quad \begin{array}{l} 0.5 < \text{Pr} < 2000 \\ 2300 < \text{Re} < 10^4 \end{array} \quad (3.35)$$

Friction Factor

In these equations f_D is the Darcy friction factor. Note that it is four times larger than Fanning friction factor, f_F . The friction factor depends on the flow regime present. The friction factor for fully developed laminar flow, defined as $\text{Re} \leq 2300$ is given by the Hagen-Poiseuille equation [44, 27, 65, 11]

$$f_d = \frac{64}{\text{Re}} \quad (3.36)$$

For turbulent flow in a smooth duct the Petukhov gave the following formula [51]

$$f_D = (0.790 \ln(\text{Re}) - 1.64)^{-2} \quad (3.37)$$

The roughness of the pipes surface can have a significant effect on the friction factor [65]. It is denoted by ϵ and is measured as the height of the roughness in meters above the surface. To account for the effects of surface roughness, the standard design formula used is the Colebrook-White equation

$$\frac{1}{\sqrt{f_D}} = -2 \log \left(\frac{\epsilon/d}{3.7} + \frac{2.51}{\text{Re}\sqrt{f_D}} \right) \quad (3.38)$$

This equation was plotted in 1944 by Moody to generate the chart that now bears his name [65]. It describes the variation in the friction factor within a pipe, with Reynolds number and relative surface roughness (ϵ/d). The Colebrook-White equation is implicit in f_D , and therefore requires an iterative solution. A number of explicit approximations have been suggested. The Zigrang-Sylvester equation [69] was recommended by Nellis & Klein in [44].

$$\frac{1}{\sqrt{f_D}} = -2 \log \left(\frac{\epsilon}{3.7d} - \frac{5.02}{\text{Re}} \log \left[\frac{\epsilon}{3.7d} - \frac{5.02}{\text{Re}} \log \left(\frac{\epsilon}{3.7d} + \frac{13}{\text{Re}} \right) \right] \right) \quad (3.39)$$

$$4 \times 10^3 \leq \text{Re} \leq 10^8$$

$$4 \times 10^{-5} \leq \frac{\epsilon}{d} \leq 5 \times 10^{-2}$$

Explicit friction factor equations have been reviewed by a number of authors. In all cases the different equations were compared to the Colebrook-White equation. Zigrang & Sylvester [70] in 1985 and Jarić et al. [32] in 2011 both concluded that the Zigrang-Sylvester equation was the most accurate of the those surveyed. Winning & Coole [66] in 2013 reviewed a wide selection of equations measuring computational efficiency, and accuracy relative to the Colebrook-White equation. A relatively recent equation by Sonnad & Goudar (2006) [60] gained the overall highest rank when considering both computational efficiency and accuracy. While the Zigrang-Sylvester equation scored higher on accuracy with a mean percentage error of 0.019 compared to 0.174 for the Sonnad & Goudar (2006) equation, it scored lower on computation efficiency. A review by Asker et al. [2] in 2014 found the Sonnad & Goudar (2008) [24] equation to be the most accurate. While each of these studies highlighted a few exceptionally accurate equations, Brkić [8] found that aside from a few exceptions, most of the currently available equations provided, for all practical purposes, acceptable level of accuracy. It is also noted that while the Colebrook-White equation is the accepted standard, it is itself an approximation to the actual experimental data and may be more or less accurate than any of the equations it is

compared to.

Based on these results the Zigrang-Sylvester equation was chosen, primarily because it is well established, having remained relevant since development in 1982, and having filtered into reference materials, its performance is likely to have been more thoroughly investigated than the other more recent equations.

For the two-phase heat transfer coefficient, the model will only have to account for boiling heat transfer within the evaporator. Nellis & Klein [44] recommended the internal flow boiling correlation developed by Shah in 1982 [57]. This is because it was tested against a large collection of experimental data, with a mean deviation of less than 20%. It is also valid for annular flow, and both vertical and horizontal pipes, with vertical pipes being important in this application. Shah reviewed six of the most accepted flow boiling correlations in [58], including the Shah 1982 correlation. They were compared to a wide range of experimental data collected from 28 fluids including: water, refrigerants, hydrocarbons, and several gases. The Shah 1982 correlation was found to be the most accurate and consistent of the correlations tested. The correlation is given in Appendix A.

Internal Pressure Drop Model

To calculate the pressure drop within the tube the Darcy-Weisbach equation is used

$$\Delta P = f_D \frac{L}{d} \frac{\rho u_m^2}{2} \quad (3.40)$$

Where ΔP is the pressure drop in Pa, and f_D is determined from Equation 3.36 if the flow regime is laminar ($Re < 2300$), and Equation 3.39 if it is turbulent. As water within the evaporators of the Otahuhu B HRSG operate by natural circulation the internal pressure drop is zero, eliminating the need for a two-phase boiling friction factor relation.

A summary of the equations and correlations used by the Correlation based model is shown in Table 3.5.

3.2.2 Weighted Model

A simplified expression for the off-design overall heat transfer coefficient can be found by taking the ratio of the heat transfer correlations evaluated at off-design and design conditions. This eliminates variables that remain constant regardless of fluid conditions, leaving ratios of the off-design fluid properties to those at the

Table 3.5: Heat transfer coefficient and pressure drop correlations used in the Correlation heat exchanger model.

Flow regime	External flow	Internal flow
Heat transfer correlation		
Single phase	ESCOA Turb-X HF.	Gnielinski (1976), with Zigrang-Sylvester (1982) friction factor.
Two-phase	N/A	Shah (1982), boiling heat transfer coefficient.
Pressure drop correlation		
Single phase	ESCOA Turb-X HF.	Hagen-Poiseuille (Laminar flow), Zigrang-Sylvester (1982) (Turbulent flow)

design point raised to some power. This is the approach taken by Erbes & Gay in [19] where the developed models have been used to simulation a CCGT power station. A similar approach has also been used in the Weighted heat exchanger model in HYSYS [30]. The following equations used in the Scaled heat exchanger model are taken from [19].

3.2.2.1 Overall Heat Transfer Coefficient

In determining an equation for the off-design overall heat transfer coefficient, U_{des} , a number of simplifying assumptions can be used. The gas side heat transfer coefficient is much smaller than that of the water side and is thus the limiting value for heat transfer. As such, the overall heat transfer coefficient is dominated by the gas side fluid conditions and the water side effects can be ignored. The equation for the heat transfer coefficient in the turbulent flow regime can take the following general form [27, 21]

$$\text{Nu} = C \text{Re}^x \text{Pr}^y \quad (3.41)$$

Where C , x , and y are constants determined by the specific fluid and flow conditions. Taking the ratio of this equation evaluated at the off-design and design conditions

$$\frac{U}{U_{\text{des}}} = \frac{\text{Nu}}{\text{Nu}_{\text{des}}} = \left(\frac{\text{Re}}{\text{Re}_{\text{des}}} \right)^x \left(\frac{\text{Pr}}{\text{Pr}_{\text{des}}} \right)^y \quad (3.42)$$

Erbes & Gay [19] note that for a gas, viscosity, Prandtl number, and thermal conductivity are weak functions of temperature and will therefore remain reasonably

constant and can be eliminated. This results in

$$\frac{U}{U_{\text{des}}} = \left(\frac{\dot{m}}{\dot{m}_{\text{des}}} \right)^x \quad (3.43)$$

For the value of x , Erbes & Gay [19] used 0.805 for $40 \times 10^3 < \text{Re} < 400 \times 10^3$, as given in [27] for a cylinder in cross-flow.

3.2.2.2 External Pressure Drop Model

To evaluate the gas side pressure drop, a simplified pressure drop correlation by Holman [27] was used

$$\Delta P = \frac{2 f G_{\text{max}}^2 N}{\rho} \left(\frac{\mu_w}{\mu_b} \right)^{0.14} \quad (3.44)$$

Where G_{max} is the maximum mass velocity based on the available frontal flow area of the HRSG duct, obstructed by the heat exchanger tube bank, N is the number of longitudinal tube rows, and μ_w and μ_b are the dynamic viscosities of the fluid evaluated at the wall and bulk (average) fluid temperatures respectively. It is noted by Erbes & Gay [19] that for a gas, dynamic viscosity will not change very much with temperature, and as the ratio is raised to the power of a small exponent, the factor will remain reasonably constant and can be ignored. The friction factor f is given by Jakob [27]

$$f = K \text{Re}_{\text{max}}^{-0.16} \quad (3.45)$$

Re_{max} is the Reynolds number evaluated using G_{max} , and K , is a factor determined by the geometry of the tube bundle. This value remains constant as operation moves from design to off-design conditions, and is eliminated from the final equation. Substituting this into Equation 3.44 and simplifying gives

$$\frac{\Delta P}{\Delta P_{\text{des}}} = \left(\frac{\dot{m}}{\dot{m}_{\text{des}}} \right)^{1.84} \left(\frac{\mu_{\text{des}}}{\mu} \right)^{-0.16} \left(\frac{\rho_{\text{des}}}{\rho} \right) \quad (3.46)$$

To avoid evaluating fluid properties it is assumed that, for a gas, μ depends primarily on temperature, and by the perfect gas law given by Equation 3.47, ρ is proportional to pressure.

$$P = \rho R_{\text{gas}} T \quad (3.47)$$

$$R_{\text{gas}} = \frac{R}{M_{\text{gas}}} \quad (3.48)$$

where R is the universal gas constant (8.314 J/mol·K) and M_{gas} is the gases molar mass in kg/mol. Applying this to Equation 3.46 gives

$$\frac{\Delta P}{\Delta P_{\text{des}}} = \left(\frac{\dot{m}}{\dot{m}_{\text{des}}} \right)^{1.84} \left(\frac{T}{T_{\text{des}}} \right) \left(\frac{P}{P_{\text{des}}} \right)^{-1} \quad (3.49)$$

3.2.2.3 Internal Pressure Drop Model

To predict the water side pressure drop, the ratio of the Darcy-Weisbach equation (Equation 3.40) evaluated at off-design and design conditions, was taken. The simple Blasius friction factor equation was used

$$f_D = 0.046 \text{Re}^{-0.2} \quad (3.50)$$

Simplification results in

$$\frac{\Delta P}{\Delta P_{\text{des}}} = \left(\frac{\dot{m}}{\dot{m}_{\text{des}}} \right)^{1.8} \left(\frac{\mu}{\mu_{\text{des}}} \right)^{0.2} \left(\frac{\rho_{\text{des}}}{\rho} \right) \quad (3.51)$$

Again to avoid evaluating fluid properties it is assumed that μ depends primarily on temperature and ρ on pressure giving

$$\frac{\Delta P}{\Delta P_{\text{des}}} = \left(\frac{\dot{m}}{\dot{m}_{\text{des}}} \right)^{1.8} \left(\frac{T}{T_{\text{des}}} \right) \left(\frac{p}{p_{\text{des}}} \right)^{-1} \quad (3.52)$$

For liquids, viscosity will decrease with increasing temperature, however, as a liquid is essentially incompressible it is strange that density is related to pressure in this formulation. For a gas the converse is true, viscosity increases with temperature and density is a strong function of pressure.

3.3 Conclusion

This chapter has discussed the theoretical basis for the heat exchanger model and the different approaches taken to calculate the off-design overall heat transfer coefficient. Two approaches for modelling heat transfer within the heat exchanger were the LMTD and ε -NTU methods. Both methods assume a constant isobaric specific heat across the heat exchanger. For single phase flow with moderate temperature changes, this can be a good assumption, however, for large temperature changes, or during a phase change, this can result in significant errors. To solve this problem it was proposed that the heat exchanger be discretised into segments and the fluid properties evaluated at the local temperature for each segment.

Provided the inlet properties of the both fluids, and UA or \dot{Q} are known, the ε -NTU method allows the heat exchanger to be solved directly. However, for the discretised heat exchanger with fluids in counter-flow orientation, only the input fluid properties to the end segments are specified. The input fluid properties to the remaining segments must be initially guessed and these guesses iterated upon. In this scenario the ε -NTU method no longer gives a direct solution for the heat exchanger. In a study by Dumont & Heyen [17], it was found that the LMTD method can be converges faster than the ε -NTU method. This combined with the fact that the LMTD method is widely used in commercial thermodynamic modelling software such as HYSYS [30] and VMGsim [25], meant LMTD method was chosen to form the basis of the heat exchanger model.

Equations for modelling both the heat transfer coefficient and pressure drop of the gas (external) and water (internal) sides of the Correlation based heat exchanger were reviewed, and the most appropriate selected. The ESCOA correlations were chosen for the gas side. For the water side, the Gnielinski 1976 correlation was selected for the single phase heat transfer coefficient, with the friction factor determine by the Hagen-Poiseuille equation for laminar flow, and the Zigrang-Sylvester (1982) equation for turbulent flow.

The Weighted model utilised a simplified method for calculating the off-design overall heat transfer coefficient, detailed by Erbes & Gay [19]. It was noted that the pressure drop equation for the water side fluid in the liquid phase, incorrectly assumed dynamic viscosity and density were proportional to temperature and pressure respectively. In spite of this, Erbes & Gay were able to match plant performance to within 1% using these simplified equations [19]. Due to this the equations have been accepted unaltered for the Weighted heat exchanger model.

The next chapter focuses on the implementation of the heat exchanger models in software, and discusses the practical issues encountered in ensuring robust operation.

Chapter 4

Heat Exchanger Model Implementation

In the previous chapter the theoretical basis for the heat exchanger model was developed. This chapter shows how the theoretical model was implemented in software. The chapter starts by discussing the development environment and supporting software packages. The following section describes the heat exchanger model architecture starting with a high level perspective and moving on to the solution algorithm. The models are then validated against an available analogue. The results are then discussed, and any required modifications to the models are explained.

4.1 Development Environment

The model has been developed in MATLAB [40]. This software was chosen for a number of reasons. A high-level scripting language such as MATLAB enables rapid development and testing of software. This is further aided by an extensive library of built in functions and numerical solvers. The language is extensible through the addition of user defined classes and toolboxes. The language has support for modern software development techniques and tools including Object Oriented Programming (OOP), unit-testing and built-in source control via git. A toolbox is a collection of related functions and classes that add functionality to MATLAB. The model utilises two 3rd party toolboxes, JSteam [38] for it's fluid property packages and unit operation library, and OPTI [12], for it's non-linear equation solvers.

JSteam is a utility system and thermodynamic modelling package from Inverse Problem Ltd. The package consists of a library of functions accessible through a number of interfaces and available as a MATLAB toolbox. The functions include

fluid property routines for water based on the IAPWS Industrial 1997 Formulation [28]. It also includes property routines for a large number of components, for both pure fluids and mixtures. Routines for these fluid components are based on the NIST REFPROP package [45]. In addition to providing fluid property routines the package also has a library of unit operations commonly encountered in utility systems, including turbines and pumps.

OPTI is a free optimisation toolbox developed by the Industrial Information and Control Centre (I²C²). Of interest to this project, the toolbox contains solver algorithms for systems of non-linear equations. This provides alternatives to the standard solvers provided with MATLAB where performance can be compared and the best solver for a particular application selected.

4.2 Heat Exchanger Model

The model was to be developed using the sequential modular approach. This meant that the model was required to be self contained with respect to data storage and the solution algorithm. Such a model has three broad requirements. The ability to store, analyse, and manipulate user input data. Once a consistent input specification has been entered, the model must generate and solve the system of equations representing the heat exchanger. The results from the model solution must then be stored and made available for display, or use by other connected unit operations. Ultimately the goal was to produce heat exchanger models to simulate the performance of the HRSG economisers, evaporators and superheaters, utilising three different approaches for evaluating the overall heat transfer coefficient. The common base for these models was the set of equations given by the LMTD method, evaluated over an arbitrary number of segments. These requirements could best be met by using an object-oriented approach, where the different models would be realised through specialisations of the a minimal base heat exchanger class.

4.2.1 Software Architecture

The class diagram for the base heat exchanger model is shown in Figure 4.1. At the top of the hierarchy is the class `UnitOperation` which contains two additional classes, `UnitConversion` and `DataStore`. Class `UnitConversion` contains methods and data for converting between units and `DataStore` is a data structure for storing variables for the containing class. `DataStore` was created so a variables name, value and additional associated information could be stored together. Class

`UnitOperation` is the superclass of all other classes and contains methods for calculating fluid properties, unit conversions, storing data and error reporting.

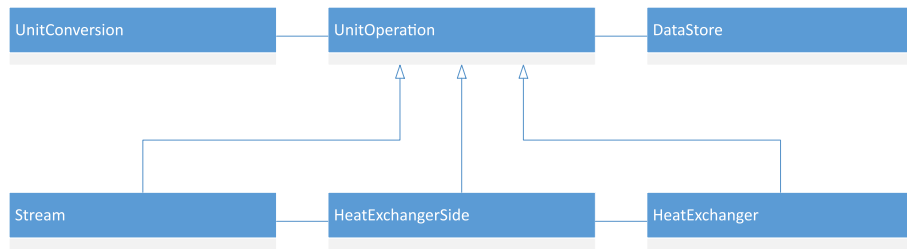


Figure 4.1: Class diagram of the base heat exchanger model.

Class `Stream` stores and manipulates data representing a process stream connected to the heat exchanger. The class contains a method for evaluating fluid properties, provided the fluid composition, pressure and at least one of temperature, enthalpy, entropy, or vapour fraction is given.

The `HeatExchangerSide` class represents a single side of the heat exchanger through which one of the fluids travel. The class contains two `Stream` objects representing the inlet and outlet ports of the side. The primary purpose of the class is to store and evaluate arrays of properties (also called property profiles) generated by discretising the heat exchanger over a number of segments between the inlet and outlet.

The `HeatExchanger` class implements the base heat exchanger model. It contains two `HeatExchangerSide` objects representing the two different sides of the heat exchanger and associated inlet and outlet ports. As many heat exchanger types have one fluid flowing over tubes while the second fluid flows through the tubes, they are often designated the shell and tube sides of the heat exchanger respectively. `HeatExchanger` directly stores and manages data relating to the overall heat exchanger, including variables such as UA and ΔT_{LMTD} , and their corresponding property profiles. `HeatExchanger` exposes an interface for accessing it's data and that of classes it contains. This is done so the `HeatExchanger` class can keep track of which data has been entered by the user and which data has been calculated. The solve method invokes the solution algorithm and is described in Section 4.2.2.

The economiser, evaporator and superheater models are represented as subclasses of `HeatExchanger`. Each class makes small changes to the solve method, where the solution algorithm can take advantage of knowledge of the type of heat exchanger when finding an initial guess of the solution. The design and correlation based heat exchanger models are also subclasses of `HeatExchanger`, with appropriate modifications made to implement their different solution methods.

4.2.2 Solution Method

Regardless of the particular heat exchanger model, the solution algorithm used follows a similar pattern. First the current user input specification is checked to ensure that sufficient information has been entered to allow the model to be solved. An initial guess for the solution is then calculated. A method for evaluating the heat exchanger system of equations for the current input specification, as well as the initial guess of the solution is then passed to the non-linear equation solver. Once the solver converges to the solution the results are stored and execution ends.

4.2.2.1 Solver Initialisation

The heat exchanger model is represented by the system of nonlinear equations given by:

$$0 = \dot{m}_{\text{shell}} (i_{\text{shell,in}} - i_{\text{shell,out}}) - \dot{Q} \quad (4.1)$$

$$0 = \dot{m}_{\text{tube}} (i_{\text{tube,out}} - i_{\text{tube,in}}) - \dot{Q} \quad (4.2)$$

$$0 = UA\Delta T_{LMTD} - \dot{Q} \quad (4.3)$$

Where for counter-flow:

$$\Delta T_{LMTD} = \frac{\Delta T_1 - \Delta T_2}{\ln\left(\frac{\Delta T_1}{\Delta T_2}\right)} \quad (4.4)$$

$$\Delta T_1 = T_{\text{shell,in}} - T_{\text{tube,out}} \quad (4.5)$$

$$\Delta T_2 = T_{\text{shell,out}} - T_{\text{tube,in}} \quad (4.6)$$

$$T_{\text{shell,in}} = f(i_{\text{shell,in}}, P_{\text{shell,in}}) \quad (4.7)$$

$$T_{\text{shell,out}} = f(i_{\text{shell,out}}, P_{\text{shell,out}}) \quad (4.8)$$

$$T_{\text{tube,in}} = f(i_{\text{tube,in}}, P_{\text{tube,in}}) \quad (4.9)$$

$$T_{\text{tube,out}} = f(i_{\text{tube,out}}, P_{\text{tube,out}}) \quad (4.10)$$

The numerical solvers used for solving the systems of non-linear equations are based on Newton's method. This method involves making an initial guess, x_0 , of the solution. By making a linear approximation of the function about this point and setting equal to zero, the intersection with the x-axis can be found. If the initial guess was sufficiently close to the actual solution, the value of x at the intersection should be closer to the actual solution. By repeating the process with $x_0 = x$, x can be converged arbitrarily close to the actual solution [7]. The most difficult part of this problem is consistently determining a good initial guess of the solution. If the initial guess is not sufficiently close to the solution then Newton's method can fail to converge. Finding an initial guess for the heat exchanger model is performed in two

steps. First the heat exchanger is solved as a single segment, then these values are interpolated to find initial guesses for each segment of the discretised heat exchanger. The method used to find an initial guess for a single segment depends on the input specification and whether a phase change occurs. For the case of no phase change, which is initially assumed, the arithmetic mean temperature difference (AMTD) is used place of ΔT_{LMTD} .

$$\Delta T_{\text{AMTD}} = \frac{\Delta T_1 + \Delta T_2}{2} \quad (4.11)$$

When c_p is assumed constant and evaluated at the specified fluid temperature, the system of equations for the heat exchanger becomes linear. This may then be directly solved for the solution. The closer ΔT_1 and ΔT_2 are to each other, the better the approximation. When $\Delta T_1 = \Delta T_2$, ΔT_{LMTD} is undefined and ΔT_{AMTD} is the correct value for the mean temperature difference between the fluids. As the system is linear, using the AMTD approximation is also computationally fast when compared to the other methods discuss next.

For the system to be linear, the AMTD approximation must use temperatures for the heat and mass balance of each side of the heat exchanger instead of enthalpy. This means a phase change occurring in a fluid will be ignored, resulting in a poor initial guess. Therefore, if a phase change is detected a different method must be used. The method used in the presence of a phase change depends on the input specification. If the input specification allows the value of heat transfer, \dot{Q} , to be bounded, the bisection method can be used to solve the system. The bisection method requires two values, x_1 and x_2 , that bound the root of a function of the form $f(x) = 0$, such that $\text{sign}(f(x_1)) \neq \text{sign}(f(x_2))$. The bounds can then be halved, and the interval that still bounds the root is selected for the next iteration [7]. An example is the situation in which the input temperatures, pressures and mass flows of the fluids, as well as the value of UA is specified. The maximum value of heat transfer, \dot{Q}_{max} , occurs when the value of ΔT_{LMTD} is a maximum. This happens when $T_{\text{shell,in}} = T_{\text{shell,out}}$ and $T_{\text{tube,in}} = T_{\text{tube,out}}$. The minimum occurs when $T_{\text{shell,out}} = T_{\text{tube,in}}$ and $T_{\text{tube,out}} = T_{\text{shell,in}}$, where $\Delta T_{\text{LMTD}} = 0$, so $\dot{Q}_{\text{min}} = 0$. The bisection method will then search for the value of \dot{Q} that satisfies

$$0 = UA\Delta T_{\text{LMTD}} - \dot{Q} \quad (4.12)$$

Where

$$i_{\text{shell,out}} = i_{\text{shell,in}} - \frac{\dot{Q}}{\dot{m}_{\text{shell}}} \quad (4.13)$$

$$i_{\text{tube,out}} = i_{\text{tube,in}} + \frac{\dot{Q}}{\dot{m}_{\text{tube}}} \quad (4.14)$$

$$T_{\text{shell,out}} = f(i_{\text{shell,out}}, P_{\text{shell,out}}) \quad (4.15)$$

$$T_{\text{tube,out}} = f(i_{\text{tube,out}}, P_{\text{tube,out}}) \quad (4.16)$$

and ΔT_{LMTD} is calculated as per Equation 3.4. The benefit of the bisection method is that provided that the root falls within the interval given by the bounds, and the function is continuous, it is guaranteed to converge to the solution. The downside is that the method converges slowly (linear convergence). As a compromise, once bisection has converged sufficiently close to the solution a Newton based method can be used to converge to the final solution. The MATLAB function `fzero` is used to implement the bisection method in the model. This function also uses the secant method to provide superlinear convergence, while not requiring the derivative of the function.

The bisection method is limited to the situation where the root of the equation can be bounded on some interval. This is not always possible, for example, if only the outlet temperature of the hot fluid is specified there is no obvious upper bound for the inlet temperature. An alternative technique used by the model is called homotopy. It works by modifying the system of equations to render it in a form where a consistent set of initial guesses can be easily determined. The system is then incrementally returned to its original form, updating the set of initial guesses at each step by solving the system using Newton's method. In this way the initial guesses are always close to the solution and Newton's method can converge quickly and robustly. For the case where the mass flow and *either* the input or output temperature and pressure of both fluids and UA are specified, the value of UA may be reduced to zero. Heat transfer will then be zero and the unknown temperatures will equal that of the specified values. The value of UA can be incrementally increased, and the previous values for the temperatures and heat transfer (zero in this case) used as the initial guess for solving the new system of equations. Eventually the value of UA will equal its specified value and the system is solved. Homotopy provides a robust solution, however it is very slow and is only used as a last resort. The algorithm used to implement the homotopy technique is the arc length continuation method given in [7].

Once an initial guess of the solution has been determined, the heat exchanger is divided up into the required number of segments. For the base heat exchanger model this is done by assuming uniform heat transfer distribution and pressure

drop per segment. As the mass flow through one side does not change, the enthalpy profile can be evenly divided over the number of segments. All other quantities can be calculated based on the enthalpy and pressure profiles for the side, i.e. the temperature profile is calculated from the enthalpy and pressure profiles, this allows ΔT_{LMTD} for each segment to be calculated which in turn allows the value of UA for each segment to be determined. The design and correlation based heat exchanger models must both calculate UA before the initial guess can be determined by the above procedures. The design based heat exchanger uses UA_{design} and ΔP_{design} as an initial estimate. The correlation based heat exchanger assumes there is no change in temperature across both sides, allowing the correlations to be solved for the initial values of UA and the pressure drop.

4.2.2.2 Solvers

The model has access to three solvers for the system of non-linear equations, `fsolve` [40], `HYBRJ` [12], and `MKLTRNLS` [12]. `fsolve` is a MATLAB built-in function. It is a Newton-Raphson based solver using the trust region dogleg algorithm for selecting the Newton step. `HYBRJ` is an open source solver from the MINPACK library and is based on the Powell Hybrid method [53]. If an analytic Jacobian is not provided the algorithm uses finite differences to find the initial Jacobian matrix and uses the rank-1 Jacobian update of Broyden's method for successive iterations. This reduces the number of function evaluations required by the algorithm, increasing the speed of solution. `MKLTRNLS` is from the Intel Math Kernel Library [31] and is a non-linear least squares solver. By fitting the SNLE to the zero vector, $\mathbf{0}$, `MKLTRNLS` can be used to solve SNLE as well. Both `HYBRJ` and `MKLTRNLS` are made available in MATLAB via the `OPTI` toolbox.

In practice best solver depends on the exact circumstances of the problem. `fsolve` performs well compared to the others if provided with an analytic Jacobian in sparse matrix form. Otherwise `HYBRJ` solves faster, but often less robustly. `MKLTRNLS` will generally require fewer iterations than `fsolve`, but is slower if an analytic Jacobian is available as `MKLTRNLS` does not take advantage of sparsity.

The system of equations for the base heat exchanger is simple enough to provide an analytic Jacobian. For the Weighted and Correlation heat exchanger models, finding analytic derivatives becomes more complex and the solvers use a finite-difference approximation.

4.3 Heat Exchanger Model Validation

The heat exchanger models were validated by comparing results to the commercial CCGT simulation software, GTPro [61]. This section demonstrates how each of the heat exchanger models is initialised and solved, for two test cases of an economiser and evaporator. The data for the two test cases are shown in Table 4.1.

Table 4.1: Heat exchanger test data for the Economiser, Evaporator.

		Economiser	Evaporator
d_o	m	0.03175	0.0381
t_w	m	0.001905	0.002108
P_t	m	0.08707	0.08704
P_l	m	0.1111	0.1111
n_f	m	216.4	226.7
l_f	m	0.01588	0.01588
t_f	m	0.0009906	0.0009906
w_s	m	0.00397	0.00397
N_t		38	38
N_r		10	8
N_{rpp}		1	8
$T_{shell,inlet}$	°C	200.6	248
$P_{shell,inlet}$	bar	1.01582	1.01659
\dot{m}_{shell}	kg/s	139.1	139.1
$T_{tube,inlet}$	°C	104.8	178.4
$P_{tube,inlet}$	bar	11.3	10.97
\dot{m}_{tube}	kg/s	21.19	3.466
UA	kW/K	194.33	201.55

The MATLAB code to set up each model for the economiser test case is given below. The first listing shows how an object of the Basic heat exchanger model is created, set up, and solved. Once an object is created properties can be entered using the objects `set` methods, which accept property-value pairs. For the Basic model the value of UA and the pressure drop for each side must be specified. The model also requires the inlet fluid properties, and fluid compositions. The fluid compositions are specified by a cell array in (component name, mole fraction) format. Having entered the required properties the model is solved using the objects `solve()` method. The results from the model are stored in the object and can be accessed by invoking the corresponding property `get` method.

```

%Fluid compositions

exhaustGas = {...
'carbondioxide', 0.040
'nitrogen', 0.761
'oxygen', 0.130
'water', 0.069};

water = {'water', 1};

% Basic Model

% Create basic heat exchanger object;
basicModel = HeatExchanger();

% Set heat exchanger properties
basicModel.set('UA', 194.33, 'solver', 'hybrj', 'nSegment', 1, ...
    'flowOrientation', 'counter', 'tubeDP', 0.3292, 'shellDP', ...
    0.002571);

% Set shell side properties
basicModel.setShellInput('t', 200.6, 'p', 1.01325, 'm', 139.1, ...
    'comp', exhaustGas);

% Set tube side properties
basicModel.setTubeInput('t', 104.8, 'p', 11.3, 'm', 21.19, 'comp', ...
    water);

% Solve model
basicModel.solve();

```

The code for the Weighted heat exchanger model is shown next. Instead of fixing the value of UA and the pressure drop for each side, the Weighted heat exchanger model requires a set of design (nominal) operating point properties from which it can calculate these values. These values are stored in a `designPoint` object which is a data member of the Weighted heat exchanger model class. The off-design fluid properties can then be entered, and the model solved in the same manner as the Basic model.

```

% Weighted Model

% Create correlation heat exchanger object;
weightedModel = weightedHeatExchanger();

% Set heat exchanger properties
weightedModel.set('solver', 'hybrj', 'nSegment', 1, ...
    'flowOrientation', 'counter');

% Set design point properties
weightedModel.getDesignPoint.setShellInput('t', 200.6, 'p', ...
    1.01325, 'm', 139.1);
weightedModel.getDesignPoint.setShellOutput('p', 1.01325);
weightedModel.getDesignPoint.setTubeInput('t', 104.8, 'p', 11.3, ...
    'm', 21.19);
weightedModel.getDesignPoint.setTubeOutput('t', 178.4, 'p', 10.97)

% Set off-design properties (Same as design in this case)
% Set shell side properties
weightedModel.setShellInput('t', 200.6, 'p', 1.01325, 'm', 139.1, ...
    'comp', exhaustGas);

% Set tube side properties
weightedModel.setTubeInput('t', 104.8, 'p', 11.3, 'm', 21.19, ...
    'comp', water);

% Solve model
weightedModel.solve();

```

The Correlation heat exchanger model uses the dimensions and material properties of the heat exchanger to calculate UA and the pressure drop for each side. Values for the average fouling factor as given by Tables 3.3 and 3.4, and surface roughness are set by default in the model. In addition, the model calculates the wall and fin material thermal conductivities, as a function of metal type and temperature, as specified in the ESCOA manual [22]. The nomenclature used in the code listing follows that of Figures 1.3, 1.4, and 3.4.

```

% Correlation Model

% Create correlation heat exchanger object;
correlationModel = CBEconomiser();

% Set heat exchanger properties
correlationModel.set('d1', (0.03175 - (2 * 0.001905)), 'd2', ...
    0.03175, 'tubeLength', 10.05, 'Nr', 1, 'Nt', 38, 'Nrpp', 1, ...
    'solver', 'hybrj', 'nSegment', 1, 'flowOrientation', 'counter');

% Set shell side properties
correlationModel.getShell.set('d2', 0.03175, 'tw', 0.001905, 'Pt', ...
    0.08707, 'Pl', 0.1111, 'lf', 0.01588, 'tf', 0.0009906, 'nf', ...
    216.4, 'ws', 0.00397, 'Le', 10.05, 'Nt', 38, 'Nr', 10);
correlationModel.setShellInput('t', 200.6, 'p', 1.01325, 'm', ...
    139.1, 'comp', exhaustGas);

% Set tube side properties
correlationModel.getTube.set('tubeOrientation', 'vertical')
correlationModel.setTubeInput('t', 104.8, 'p', 11.3, 'm', 21.19, ...
    'comp', water);

% Solve model
correlationModel.solve();

```

The temperature profile of each heat exchanger model for simulating the economiser of Table 4.1 is given in Figure 4.2. The temperature profile as determined by the GTPro software is also plotted for comparison, where it can be seen that the temperature profiles of the three models closely follow those calculate by GTPro. A more detailed comparison is given in Table 4.2. In the table red is used to highlight values calculated by the heat exchanger models, while black indicates values specified by the user.

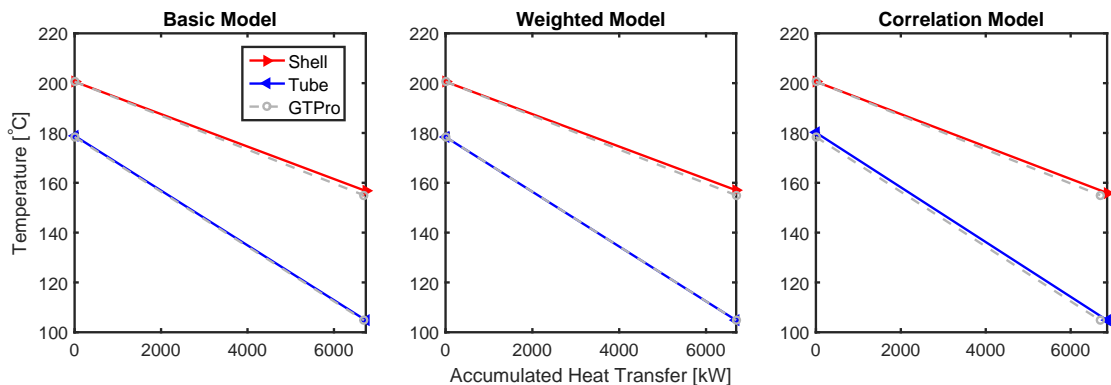


Figure 4.2: Economiser temperature profile of each heat exchanger model, compared to simulation results from the GTPro software [61].

Table 4.2: Economiser simulation results for each of the heat exchanger models compared to GTPro. Values in red have been calculated by the models.

Economiser		GTPro	Basic Model	Weighted Model	Correlation Model
$T_{\text{shell,inlet}}$	°C	200.6	200.6	200.6	200.6
$T_{\text{shell,outlet}}$	°C	155	156.7	157.0	155.9
$P_{\text{shell,inlet}}$	bar	1.01582	1.01582	1.01582	1.01582
$P_{\text{shell,outlet}}$	bar	1.01325	1.01325	1.01325	1.01334
ΔP_{shell}	bar	0.002571	0.002571	0.002571	0.002477
\dot{m}_{shell}	kg/s	139.1	139.1	139.1	139.1
$T_{\text{tube,inlet}}$	°C	104.8	104.8	104.8	104.8
$T_{\text{tube,outlet}}$	°C	178.4	178.9	178.4	180.2
$P_{\text{tube,inlet}}$	bar	11.3	11.3	11.3	11.3
$P_{\text{tube,outlet}}$	bar	10.97	10.9708	10.97	11.023
ΔP_{tube}	bar	0.3292	0.3292	0.33	0.2770
\dot{m}_{tube}	kg/s	21.19	21.19	21.19	21.19
\dot{Q}	kW	6694	6737	6694	6865
UA	kW/K	194.33	194.33	190.75	205.56

When simulating an evaporator the tube side outlet fluid is now a saturated vapour with a vapour fraction (X) of 1. The model will then be over-determined, leaving an additional degree of freedom. This allows the tube side mass flow (\dot{m}_{tube}) to be calculated, representing the rate of steam generation by the Evaporator. Setting up the Basic and Weighted heat exchanger models to operate as evaporators simply requires specifying the tube outlet vapour fraction to be 1, and not specifying the tube side mass flow, as shown below.

```

% Evaporator

% Basic Model

% Set tube side properties
basicModel.setTubeInput('t', 178.4, 'p', 10.97, 'comp', water);
basicModel.setTubeOutput('x', 1);

% Weighted Model

% Set tube side properties
weightedModel.setTubeInput('t', 178.4, 'p', 10.97, 'comp', water);
weightedModel.setTubeOutput('x', 1);

```

The Correlation heat exchanger model represents the evaporator with a separate class, `CBEvaporator`. This class implements an initialisation routine that estimates the shell outlet temperature using fixed pinch temperature difference (ΔT_{pinch}), which defaults to 20 °C. The modified object method calls are given in the listing below.

```

% Correlation Model

% Create Correlation evaporator object
correlationModel = CBEvaporator();

% Set tube side properties
correlationModel.setTubeInput('t', 178.4, 'p', 10.97, 'comp', water);
correlationModel.setTubeOutput('x', 1);

```

The temperature profiles calculated by the heat exchanger models for the evaporator test case is shown in Figure 4.3. Again the calculated outlet temperatures closely match those calculated by GTPro. The full results of the simulations are given in Table 4.3. It is interesting that the Weighted and Correlation models both calculated a lower value for UA than the value determine by GTPro, yet both models calculated a similar value for the tube side steam mass flow and heat transferred. This will be partially due to heat losses, and correction factors for reduced heat exchanger effectiveness, accounted for by GTPro but neglected in the models developed in this work.

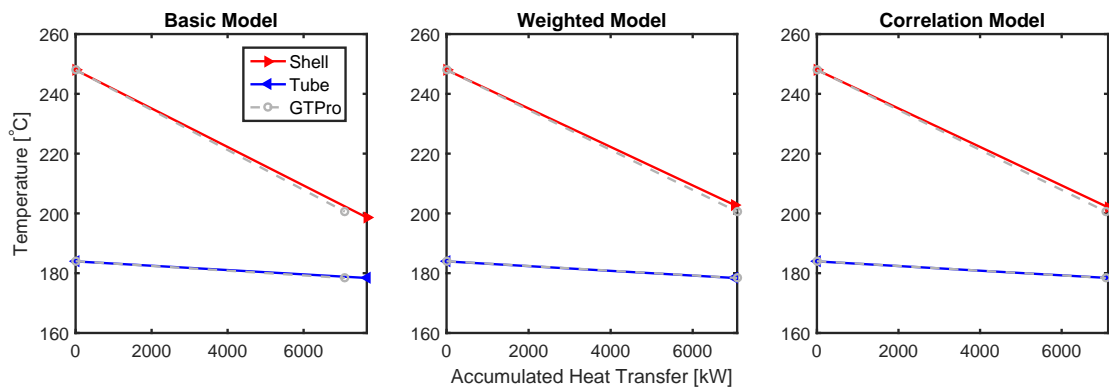


Figure 4.3: Evaporator temperature profile of each heat exchanger model, compared to simulation results from the GTPro software [61].

4.4 Discussion

In the previous section all of the simulations were run with the heat exchanger models evaluated over a single segment. This was done to match the way GTPro simulates

Table 4.3: Evaporator simulation results for each of the heat exchanger models compared to GTPro. Values in red have been calculated by the models.

Evaporator		GTPro	Basic Model	Weighted Model	Correlation Model
$T_{\text{shell,inlet}}$	°C	248	248	248	248
$T_{\text{shell,outlet}}$	°C	200.6	198.6	202.8	201.9
$P_{\text{shell,inlet}}$	bar	1.01659	1.01659	1.01659	1.01659
$P_{\text{shell,outlet}}$	bar	1.01325	1.01325	1.01325	1.01332
ΔP_{shell}	bar	0.003344	0.003344	0.003344	0.003272
\dot{m}_{shell}	kg/s	139.1	139.1	139.1	139.1
$T_{\text{tube,inlet}}$	°C	178.4	178.4	178.4	178.4
$T_{\text{tube,outlet}}$	°C	184	183.9	183.9	183.9
$P_{\text{tube,inlet}}$	bar	10.97	10.97	10.97	10.97
$P_{\text{tube,outlet}}$	bar	10.97	10.97	10.97	10.97
ΔP_{tube}	bar	0	0	0	0
\dot{m}_{tube}	kg/s	3.466	3.785	3.466	3.539
\dot{Q}	kW	7084	7664	7017	7165
UA	kW/K	201.55	201.55	170.73	177.30

individual heat exchangers, allowing more accurate comparisons to be made. All of the heat exchanger models are capable of subdividing the heat exchangers into an arbitrary number of segments to more accurately evaluate fluid properties at the local temperature for each segment. This is shown for the evaporator test case in Figure 4.4.

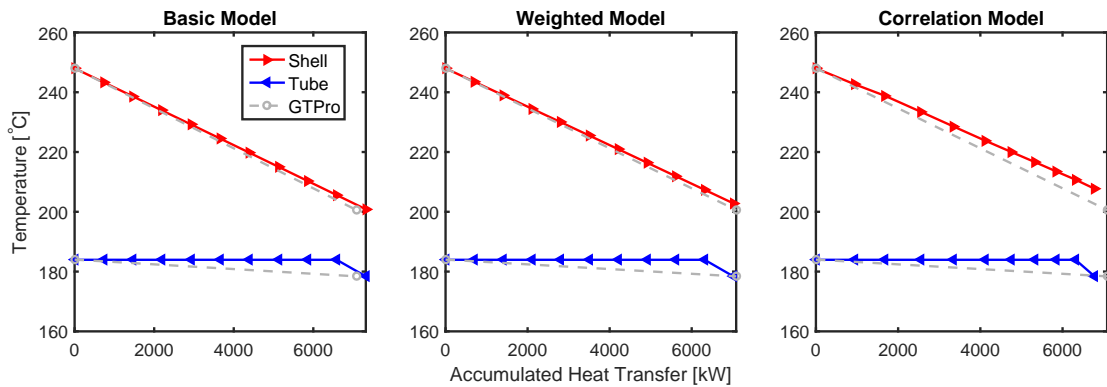


Figure 4.4: Evaporator temperature profile of each heat exchanger model, evaluated for 10 segments.

In an HRSG, each heat exchanger, under normal operation encounters water in either the liquid, two-phase, or vapour state. Therefore, the additional resolution provided by splitting the heat exchanger into multiple segments has lesser affect on the accuracy of the Basic and Weighted heat exchanger models. Where it does

have an impact is for the Correlation model when evaluating the tube side heat transfer coefficient in the evaporator. This is caused by the large variation in heat transfer coefficient as the water goes from subcooled liquid to saturated vapour. The variation in heat transfer coefficient is shown in Figure 4.5 The sharp changes

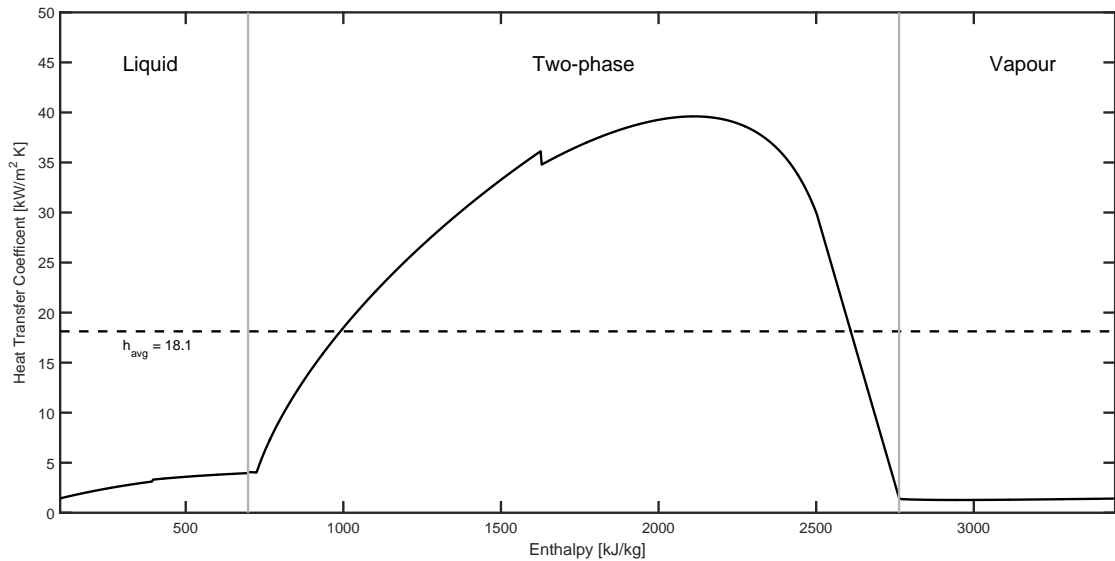


Figure 4.5: Variation in the tube side convective heat transfer coefficient as the water is heated from a subcooled liquid to a superheated vapour.

in the curve mark the transitions between laminar to turbulent flow, and between the Petukhov-Kirillov and Gnielinski correlations, as the Reynolds number changes. The Shah flow boiling correlation uses the single phase heat transfer correlation to determine portion of the heat transfer coefficient due to the liquid fraction of the flow. The amount of liquid water in the flow decreases as the vapour fraction increases, reducing the Reynolds number of the liquid fraction. This is why there is a shift from the Petukhov-Kirillov correlation to the Gnielinski correlation at the top of the curve, with the Reynolds number falling below 1×10^4 . If the Correlation heat exchanger were to be evaluated over a single segment, the heat transfer coefficient would be evaluated at the average of the inlet and outlet enthalpies. This would result in a heat transfer coefficient of 35–40 kW/m²·K, instead of the correct average value of 18.1 kW/m²·K.

This additional accuracy comes at the cost of longer solution times. Figure 4.6, shown the solution times for the heat exchanger models for an increasing number of segments. The Basic model's solution time remains reasonably constant, while the Weighted model increases from 0.0329 to 1.0783 s. The Correlation model clearly has the largest increase in solution time, increasing from 0.5252 at 1 segment to 35.006 s at 20 segments. For solving individual heat exchangers this does not pose a significant problem. However, once multiple heat exchangers are incorporated into a larger process model, requiring it's own iterative solution, the nested iterative loops result can result in extremely long solution times.

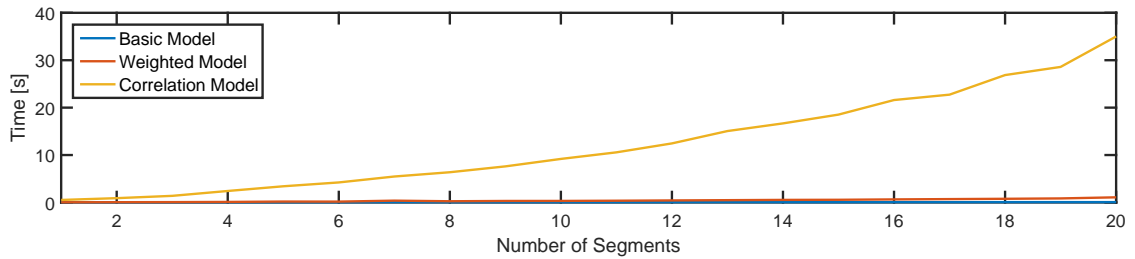


Figure 4.6: Time required to solve each heat exchanger model with an increasing number of segments.

As an example, consider the situation of the Correlation model being solved for 10 segments, as part of the Otahuhu B HRSG model, which is developed in the next chapter. The model is composed of 14 heat exchangers in a counter-flow arrangement. This results in an HRSG model with 17 unknown variables, 14 exhaust gas outlet temperatures, one for each heat exchanger, and three feed water mass flows, for the LP, IP, and HP pressure levels. According to Figure 4.6, solving the Correlation model for 10 segments results in a solution time of approximately 10 s. The solver must evaluate the model once per iteration plus an additional model evaluation per unknown variable to calculate the Jacobian using finite differences. If the HRSG model takes 10 iterations to solve, this results in

$$(10 \text{ s} \times 14 \times (1 + 17) \times 10) \frac{1 \text{ hr}}{3600 \text{ s}} = 7 \text{ hr} \quad (4.17)$$

To retain this accuracy but reduce the solution time, the Correlation model was altered to evaluate the tube side heat transfer coefficient and pressure drop over 10 segments, and use the average values to solve the heat exchanger for a single segment.

During the validation process it was found that the Shah flow boiling Correlation would produce erroneous values when Reynolds numbers decreased to low values ($Re < 1000$). This was linked to the Petukhov-Kirillov and Gnielinski heat transfer correlations used by the Shah flow boiling routine. To resolve this problem the correlations were replaced with the simpler Dittus-Boelter correlation. Figure 4.7 shows a comparison of the two routines. The reduced accuracy of the boiling heat transfer coefficient shouldn't be too much of a concern as the boiling heat transfer coefficient is much larger than the single phase heat transfer coefficient or the shell side heat transfer coefficient. Due to the nature of overall heat transfer coefficient, the smaller heat transfer coefficients tend to dominate it's value.

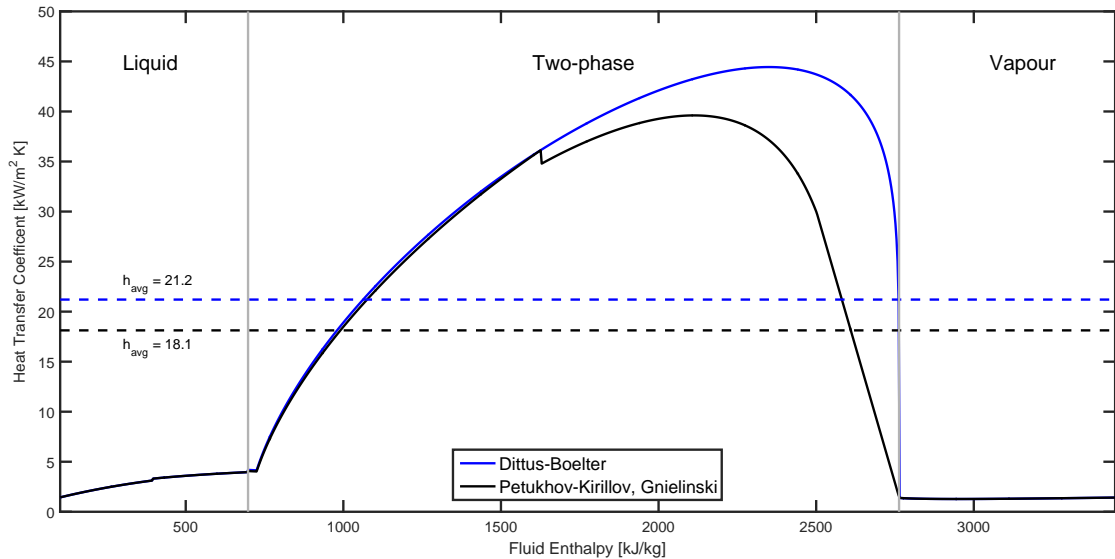


Figure 4.7: Comparison of the routines for calculating the tube side heat transfer coefficient. Both routines use the Petukhov-Kirillov and Gnielinski correlations for calculating the heat transfer coefficient for single phase flows. For the black line, the Shah flow boiling routine uses the Petukhov-Kirillov and Gnielinski correlation to calculate the liquid fraction heat transfer coefficient. For the blue line, the Dittus-Boelter correlation was used.

4.5 Conclusion

This chapter has introduced the development environment and supporting software used by the model. The implementation of the heat exchanger model was discussed and issues highlighted. As the problem required the development of multiple related heat exchanger models, an object-oriented approach to the software architecture was taken. This improved code reuse, maintenance and made changes easier to implement, speeding development. Consistently determining a good initial guess of the solution for the Newton based solvers proved to be this biggest challenge. There was no 'one best' approach, and ultimately multiple methods were implemented to handle different input specifications and fluid conditions. The models were then validated against two test cases of an economiser and evaporator, from the GT-Pro commercial CCGT simulation software. For the economiser test case, all of the models performed well, closely matching the temperature profiles of the GTPro simulation. The exception was the tube side pressure drop calculated by the Correlation model with a value of 0.2770 bar verse 0.3292 bar for GTPro. In the case of the evaporator, both the Weighted and Correlation models calculated a different UA value than that given by GTPro, 170.73, and 177.30, compared to 201.55 kW/K respectively. In spite of this difference, the temperature profiles and tube side mass flows calculated by the models closely matched the GTPro results.

Chapter 5

HRSG Simulation

In this chapter the heat exchangers are used to construct a model of the Otahuhu B HRSG. Due to a lack of measurement data for the gas turbine exhaust mass flow into the HRSG, an off-design model of the gas turbine is developed to predict this value for part-load conditions. These models are then used to simulate the operation of the HRSG at four points across the operating range of the power station. The results from these simulations are then compared to plant data to assess the performance of each heat exchanger model.

5.1 Gas Turbine Model

In a combined cycle gas turbine power station, the gas turbine exhaust provides the heat source that drives the steam cycle by transferring energy to the water via the HRSG. The primary focus of this study is the heat exchangers within the HRSG, however due to this connection, the operation of the HRSG is closely linked to that of the gas turbine. In order to simulate HRSG operation, the properties of the exhaust gas under specific operating conditions must be known. The manufacturer published specifications for the gas turbine at Otahuhu B are for ISO conditions (15 °C, 1.013 bar, 60 % relative humidity) at nominal load. Here nominal refers to the design operating point for the gas turbine which will be at the maximum power output. This is may also be referred to as base or full load. These nominal operating values will vary with changes in ambient conditions and gas turbine load. This section develops a gas turbine model to predict the part-load behaviour of the gas turbine as a function of ambient temperature and pressure and load requirement.

5.1.1 Basic Operation

The gas turbine has three main components, the compressor, combustion chamber and turbine. These components are shown in Figure 5.1. In this simple configuration the turbine, compressor and generator are connected via a single shaft, a set up common among large industrial gas turbines used in power plant applications [55]. Starting at the inlet to the compressor, the air at point 1 is at ambient conditions. It is pulled into the compressor where both the pressure and temperature are increased, exiting at point 2. This is then feed into the combustion chamber where it is mixed with natural gas and combusted. The temperature of the combustion products at point 3 are around $1200 - 1400\text{ }^{\circ}\text{C}$ [36] for modern gas turbines. This is commonly called the turbine inlet (or firing) temperature (TIT) and along with the compressor pressure ratio, (PR) is a key value in determining cycle performance. These combustion products expand through the turbine generating work. The resultant turbine work must drive the compressor with the excess used to generate electricity. The turbine exhaust temperature (TET) at point 4 is still greater than $500\text{ }^{\circ}\text{C}$ [68]. The exhaust gases are then feed into the HRSG where most of the remaining heat is extracted.

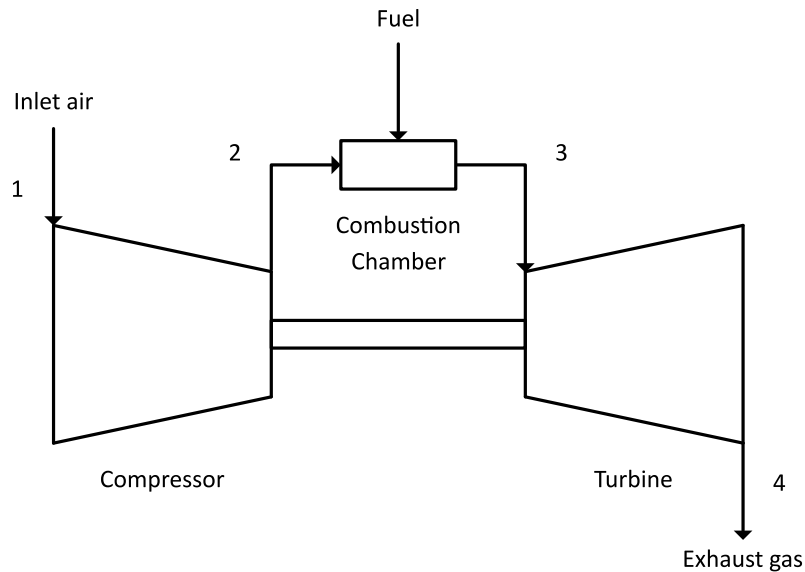


Figure 5.1: Gas turbine process flow diagram.

5.1.2 Model Development

The individual components can be modelled separately and combined to describe the overall operation of the gas turbine. Each component is analysed by performing a heat and balance around the control volume under steady state conditions. Both the compressor and the turbine are modelled by assuming the processes are isentropic and then applying an efficiency to account for the irreversibilities occurring in

the actual process [68].

Compressor:

$$\eta_{\text{comp}} = \frac{i_{2,\text{isen}} - i_1}{i_2 - i_1} \quad (5.1)$$

$$\dot{m}_1 = \dot{m}_2$$

Turbine:

$$\eta_{\text{turb}} = \frac{i_3 - i_4}{i_3 - i_{4,\text{isen}}} \quad (5.2)$$

$$\dot{m}_3 = \dot{m}_4$$

In the combustion chamber the fuel mass flow, lower heating value (LHV), and a combustion efficiency, η_b , are used to determine the energy contribution due to combustion of the fuel. The resulting equations may be solved for the combustion chamber outlet temperature T_3 , or the fuel or air mass flow, \dot{m}_{fuel} and \dot{m}_{air} respectively.

$$\frac{T_3}{T_2} = \frac{1 + \eta_b \text{FAR} (\text{LHV}/c_p) T_2}{1 + \text{FAR}} \quad (5.3)$$

$$\text{FAR} = \frac{(T_3/T_2) - 1}{\eta_b (\text{LHV}/c_p) T_2 - (T_3/T_2)} \quad (5.4)$$

$$\text{FAR} = \frac{\dot{m}_{\text{fuel}}}{\dot{m}_{\text{air}}} \quad (5.5)$$

Where FAR is the fuel air ratio. The overall efficiency of the gas turbine is the ratio of the net work produced by the turbine to the rate of fuel energy consumed [26] and is defined as

$$\eta_{\text{gt}} = \frac{W_{\text{turb}} - W_{\text{comp}}}{\dot{m}_{\text{fuel}} \text{LHV}} \quad (5.6)$$

With an appropriate set of input specifications describing a specific operating point, equations 5.1 to 5.6 completely describe the gas turbine. A typical input specification set is shown in table 5.1.

While this model allows the mass flows throughout the gas turbine to be determined from a set of input specifications, the model cannot accurately predict changes in gas turbine behaviour with changes in load and ambient conditions. This modelling of part-load or off-design behaviour is discussed in the next section.

Table 5.1: Basic gas turbine model input parameters

Input	Units	Output	Units
T_{amb}	$^{\circ}\text{C}$	\dot{m}_{fuel}	kg/s
P_{amb}	bar	\dot{m}_{air}	kg/s
T_{exhaust}	$^{\circ}\text{C}$	\dot{m}_{exhaust}	kg/s
PR			
η_{comp}			
η_{gt}			
Net power	kW		
Fuel LHV	kJ/kg		

5.1.3 Part-load Model

The previous discussion developed a model of a gas turbine which given the parameters shown in the first column of table 5.1 may be evaluated for the mass flow of air, fuel and importantly, exhaust gases. These input specifications may be sourced from the manufacturer or typical values may be assumed at nominal operating conditions. The gas turbine is designed to operate at these nominal operating conditions and therefore will achieve the highest efficiency at this point. Power plants, however, often have to operate away from these nominal conditions in order to meet power dispatch orders from the power system operator [?]. Moving away from the design conditions results in a reduction in gas turbine performance. To accurately predict the performance of the gas turbine under off-design conditions these effects must be accounted for.

In order to model the gas turbine behaviour as the operation shifts from the base load, knowledge of the control methodology and off-design behaviour of components is required [26, 37]. Gas turbines used in combined cycle applications have two methods of control, inlet guide vane (IGV) and fuel throttling. The IGV is a set of non-rotating vanes at the inlet to the compressor. Closing the IGV has the effect of reducing the air mass flow to the compressor and therefore the turbine, reducing the turbine work and power generated. As the air mass flow is reduced the firing temperature at the inlet to the turbine will increase. To maintain the TET at acceptable levels the fuel flow must be reduced as well.

Lowering the air mass flow through the compressor reduces compressor pressure ratio and efficiency, which in turn will reduce the overall cycle efficiency, η_{gt} . While the turbine efficiency will also be affected by the reduction in mass flow and pressure ratio the effects on the compressor dominate off-design performance and therefore changes in turbine performance at off-design are neglected [37]. There are multiple ways to capture the off-design characteristics of the compressor. Many off-design models utilise compressor maps [36, 55] or manufacturer supplied correction curves

[37]. The compressor maps are plots that relate the efficiency, pressure ratio, mass flow and temperature of the component through its operating range. Correction curves give the percentage change in design specifications as a function of off-design conditions such as ambient temperature. Both maps and correction curves are specific to a particular gas turbine model and are unavailable for the gas turbine at Otahuhu B. As an alternative [37] provides a set of equations to predict compressor off-design values for mass flow and efficiency as a function of design specifications and current operating conditions. This provides a simplified method to approximate off-design behaviour of the compressor and may be readily combined with the previously developed gas turbine model.

$$\dot{m}_{\text{air}} = \dot{m}_{\text{air,des}} \left(\frac{P_1}{P_{1,\text{des}}} \right) \left(\frac{T_{1,\text{des}}}{T_1} \right) (1 - (\Delta\text{IGV})(\text{VFC})) \left[1 + \text{TFC} \left(\frac{T_1 - T_{1,\text{des}}}{T_{1,\text{des}}} \right) \right] \quad (5.7)$$

$$\eta_{\text{comp}} = \eta_{\text{comp,des}} \left(1 - \text{FC} \left| \frac{\dot{m}_{\text{air}} - \dot{m}_{\text{air,des}}}{\dot{m}_{\text{air,des}}} \right| \right) \left[1 + \text{SEC} \left| \frac{n - n_{\text{max}}}{n_{\text{max}}} \right| \right] \quad (5.8)$$

$$\left(\frac{\dot{m}_{3,\text{des}} \sqrt{T_{3,\text{des}}}}{P_{3,\text{des}}} \right) = \left(\frac{\dot{m}_3 \sqrt{T_3}}{P_3} \right) \quad (5.9)$$

Where VFC, TFC, FC, and SEC are the vane flow, temperature flow, mass flow, and compressor speed efficiency correction factors respectively. ΔIGV is the change in IGV angle from design conditions, and n is the compressor speed. The design point speed may be substituted for n_{max} . Equation 5.7 gives the off-design air mass flow as a function of design point values (subscript des), and the current operating values for compressor inlet temperature and pressure, and change in IGV position. Equation 5.8 uses the new air mass flow value to compute the off-design compressor efficiency. For gas turbines used to generate electricity the operating speed is fixed at 3000 rpm (50 Hz) and the last term reduces to zero. Each of the correction factors may be altered to match the equations to a particular gas turbine. Equation 5.9 assumes that the turbine inlet remains choked during both design and off-design operation. This is required due to the lack of characteristic curves describing the operation of the turbine over its operating range. The greatest deviation from this condition will occur at reduced loads where the model may over predict the compressor pressure ratio. In practice only a portion of the turbines operating range is used during normal operation and flow will usually be choked or nearly so at the first stage inlet nozzle to the turbine [37, 55].

The part-load model solution proceeds as follows:

First, design data is used to establish design point values for the compressor, combustion and turbine efficiencies, as well as the fuel mass flow and TIT. These values are then supplied to the off-design model. In off-design operation it is most useful to solve the model for a fixed load rather than a fixed ΔIGV . In this situation the ΔIGV becomes an unknown and will be solved for. Initial guesses are made for the values of ΔIGV and PR. Equations 5.7 and 5.8 are then solved for the off-design values of air mass flow and compressor efficiency. The compressor may then be solved from Equation 5.1 for the outlet enthalpy i_2 . As the TET is more or less fixed at the maximum design value, the turbine is solved for the TIT required to maintain this value. This allows the fuel mass flow to be determined. The turbine inlet pressure is then calculated from Equation 5.9. The initial guess for PR and the required load are then compared to their calculated values. If they do not match a new guess for ΔIGV and PR is made and the next iteration begins.

Measured plant data for the compressor efficiency and pressure ratio as well as the gas turbine efficiency and fuel mass flow is available and has been used to validate the solution procedure. The results of the model are compared to measured plant data in figure 5.2. While the exhaust mass flow is not measured it has been assumed that if these key intermediate values from the model match measured plant data then the predicted exhaust mass flow should match the actual mass flow with a comparable accuracy. Results from the simulation of the Otahuhu B gas turbine, for each of the case studies are given in Table 5.2.

Table 5.2: Gas turbine model simulation results.

	Design	222 MW	265 MW	326 MW	382 MW
Net Power [kW]	267382	257196	210216	161775	127781
Compressor PR	17.5	17.41	15.06	12.51	10.6
η_{comp}	0.890	0.888	0.869	0.848	0.832
TIT [$^{\circ}\text{C}$]	1188	1184	1149	1104	1065
TET [$^{\circ}\text{C}$]	578.1	578.1	578.1	578.1	578.1
\dot{m}_{fuel} [kg/s]	17.1	16.65	14.28	11.73	9.855
\dot{m}_{air} [kg/s]	666.2	656.8	577.5	490.0	423.3
\dot{m}_{exhaust} [kg/s]	688.0	673.5	591.7	501.8	433.1
η_{gt}	0.348	0.344	0.328	0.307	0.288

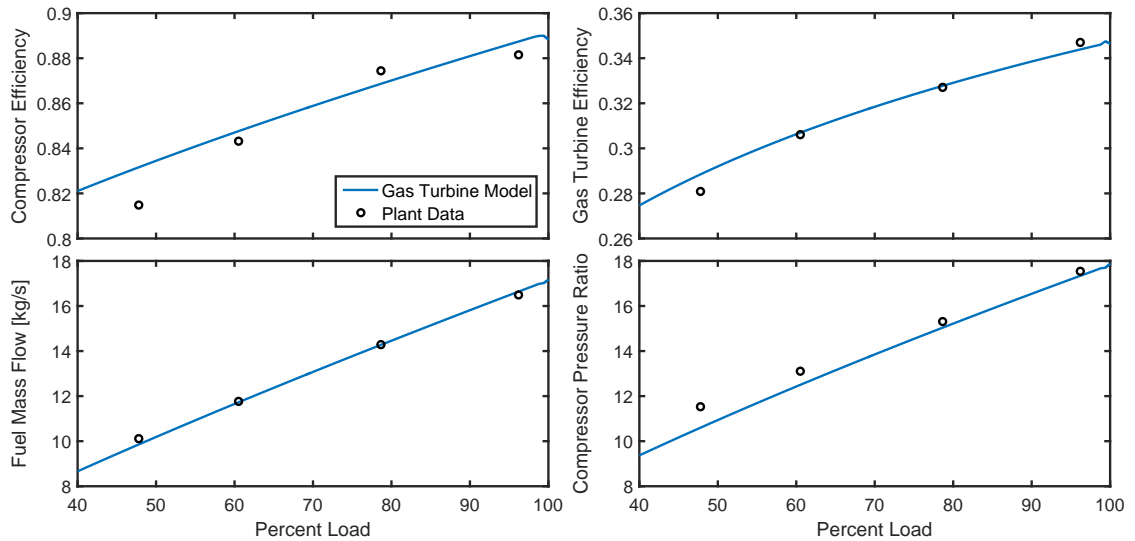


Figure 5.2: Gas turbine model results for important operating parameters compared to measured plant data. In general the model shows good correlation with the plant data. The largest error occurs in the compressor efficiency at low load.

5.2 Otahuhu B HRSG Model

A simplified process flow diagram (PFD) of the Otahuhu B HRSG simulation model is shown in Figure 5.3. The diagram excludes the deaerator and desuperheaters. The deaerator is only operated intermittently and is assumed to be switched off. The desuperheaters are located before and after the last stage superheater of the HP steam and reheater. They are also called attemperators, and are used to maintain the steam temperature at acceptable levels by spraying liquid water into the tubes, mixing with the steam. The desuperheaters have been excluded because the mass flows and inlet and outlet properties are not recorded in the available plant data. This may result in increased outlet temperatures for the final HP superheater and the reheater.

The heat exchangers are designated ECON, EVAP, and SHTR for economiser, evaporator, and superheater respectively. The gas turbine exhaust gas enters the HRSG from the left and exits via the stack on the right. Condensate at approximately 33 °C and 18 bar enters the Preheater. A certain amount of the outlet water of the Preheater is returned to the inlet to maintain the temperature of the exiting exhaust gas above the acid dew point. This value is recorded in the plant data and is considered fixed in the model. The water at the outlet to the Preheater is then split between the LP, IP and HP pressure levels. The LP pressure level is lower than that of the Preheater and the pressure is reduced to approximately 5.7 bar before entering the LP evaporator. The IP and HP pressure levels are approximately 33 and 121 bar. These are established by a fixed speed multi-stage pump, represented in the model as two discrete pump unit operations from the JSteam library.

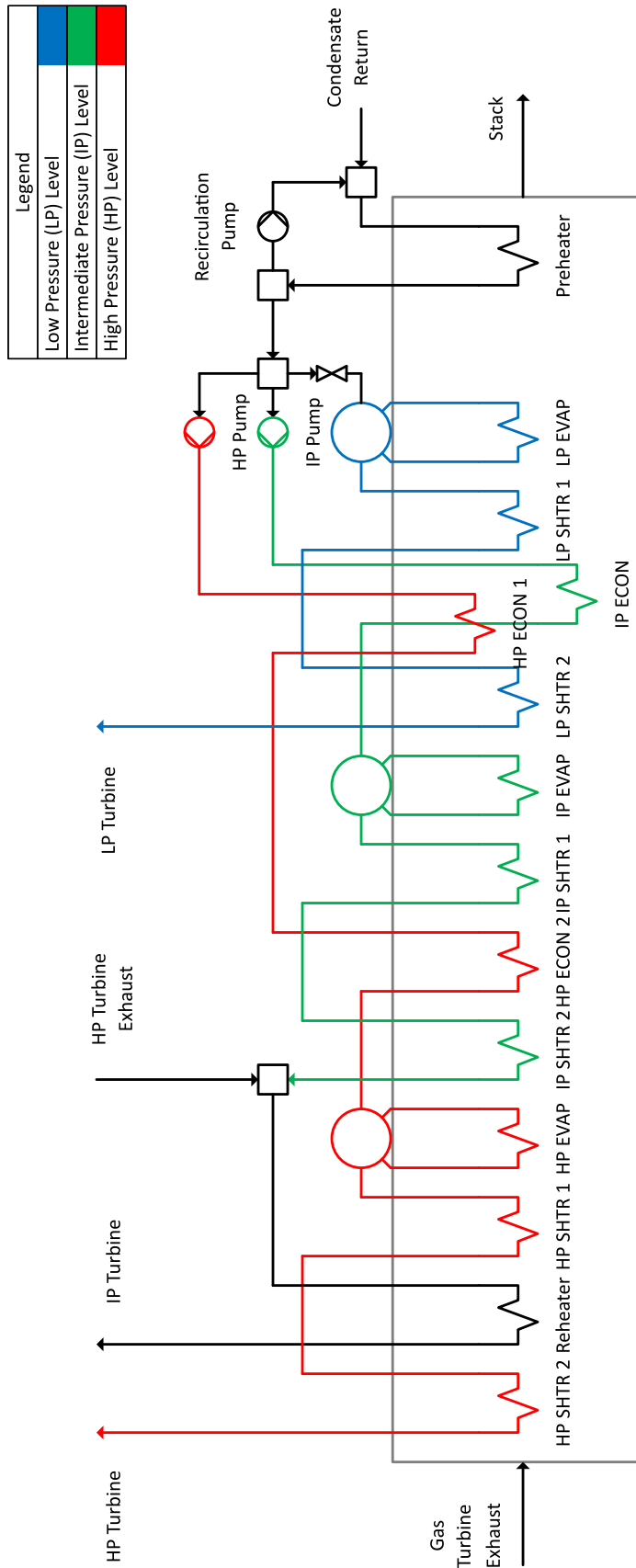


Figure 5.3: Simplified process flow diagram of the heat recovery steam generator in the Otahuhu B Combined Cycle Gas Turbine Power Station.

The pump unit operation uses an isentropic efficiency to account for irreversibilities within the pump, and a heat and mass balance to calculate the outlet enthalpy and work required. The unit operation symbol is shown in Figure 5.4, and the equations describing the pump are given by Equations 5.10.

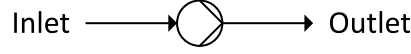


Figure 5.4: Pump unit operation symbol.

$$\eta_{\text{pump}} = \frac{i_{\text{outlet,isen}} - i_{\text{inlet}}}{i_{\text{outlet}} - i_{\text{inlet}}} \quad (5.10)$$

$$\dot{W}_{\text{pump}} = \dot{m}_{\text{inlet}}(i_{\text{outlet}} - i_{\text{inlet}})$$

The IP and HP streams then enter the first stage economisers. The IP and HP economisers are located next to each other in the same tube bundle, transverse to gas flow, with a roughly $\frac{1}{4}$ to $\frac{3}{4}$ share of the exhaust gas mass flow. The model, therefore, splits the exhaust gas path, with each economiser experiencing the same inlet temperature and pressure for the exhaust gas. At the gas side outlet, the two paths are recombined with a heat and mass balance, and the average of the two gas side outlet pressures is taken. The two gas paths are combined using a unit operation called a mixer. The symbol used to represent the mixer is given in Figure 5.5, and Equations 5.11 show how the outlet fluid properties are calculated.

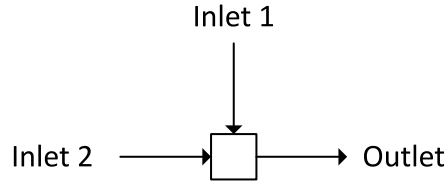


Figure 5.5: Mixer unit operation symbol.

$$i_{\text{outlet}} = \frac{\dot{m}_{\text{inlet},1}i_{\text{inlet},1} + \dot{m}_{\text{inlet},2}i_{\text{inlet},2}}{\dot{m}_{\text{inlet},1} + \dot{m}_{\text{inlet},2}} \quad (5.11)$$

$$\dot{m}_{\text{outlet}} = \dot{m}_{\text{inlet},1} + \dot{m}_{\text{inlet},2}$$

A number of other heat exchangers are located in the same tube bundle and only take up a fraction of the width of the HRSG duct. These heat exchangers are still situated approximately sequentially along the gas path but will experience only a fraction of the full gas side mass flow. These fractions have been determined from design data and are shown in Table 5.3. The fractions are constant across the plants operating range and are multiplied by the total exhaust gas mass flow to determine the mass flow entering each heat exchanger.

Table 5.3: Design data used by the heat exchanger models.

Heat Exchanger	Gas Side Mass Flow Fraction	Design UA [kW/K]	Gas Side Pressure drop [mbar]	Water Side Pressure Drop [bar]
HP Superheater 2	1	235.1	9.807	2.2
Reheater	1	551.4	30.40	1.3
HP Superheater 1	1	897.5	32.36	1.3
HP Evaporator	1	1979.2	50.01	0
IP Superheater 2	0.5758	53.5	5.884	0.6
HP Economiser 2	1	1639.1	38.25	1.7
IP Superheater 1	0.4571	68.3	7.845	0.2
IP Evaporator	1	900.0	23.54	0
LP Superheater 2	0.5714	44.6	5.884	0.5
HP Economiser 1	0.7990	1051.6	24.52	0.8
IP Economiser	0.2010	300.6	24.52	1.4
LP Superheater 1	0.3823	33.6	5.884	0.2
LP Evaporator	1	805.1	16.67	0
Preheater	1	2178.7	30.40	2.5

Table 5.4: Fixed pressures and temperatures for each simulation case study.

Load [MW]	382	326	265	222
Pressures [bar]				
Reheater	30.98	26.98	24.29	22.12
HP Economiser	120.5	106.4	95.87	88.15
IP Economiser	32.78	28.47	25.75	23.46
LP Evaporator	5.653	5.340	5.166	5.040
Condensate	18.33	19.23	19.71	19.84
Temperatures [°C]				
Reheater	355.5	357.8	356.3	358.1
Condensate	33.48	30.95	29.46	28.44
Mass flow [kg/s]				
Preheater	29.61	29.74	28.58	28.27
Recirculation				

Finally, referring back to the HRSG PFD, the steam exhausted from the HP turbine is returned to the HRSG where it is mixed with the outlet steam of the last IP superheater, prior to entering the Reheater. The fluid properties of the HP turbine exhaust are recorded in plant data and are specified for the model. All measured plant data specified in the HRSG model is given in Table 5.4. Values for the design point UA and pressure drops have been derived from design data for the HRSG and are given in Table 5.3.

5.3 Simulation results

To assess the performance of the heat exchanger models, the HRSG model was run through a series of four case studies spanning the operating range of Otahuhu B, specifically, 222, 265, 326, and 382 MW. While the plant is rated at 400 MW the highest output power achieved in the data is approximately 380 MW. The minimum load of 222 MW was indicated by the gas turbine IGV position approaching its minimum angle. The cases were chosen to have similar ambient conditions and to be close together in time to limit differences due to changes in plant condition, such as fouling. The model predictions are compared at a number of points to the available plant data with the results displayed graphically below. The top plot shows the model predicted values and corresponding plant data for each of the four operation points, while the bottom plot shows the absolute error in percent, for each of the heat exchanger models.

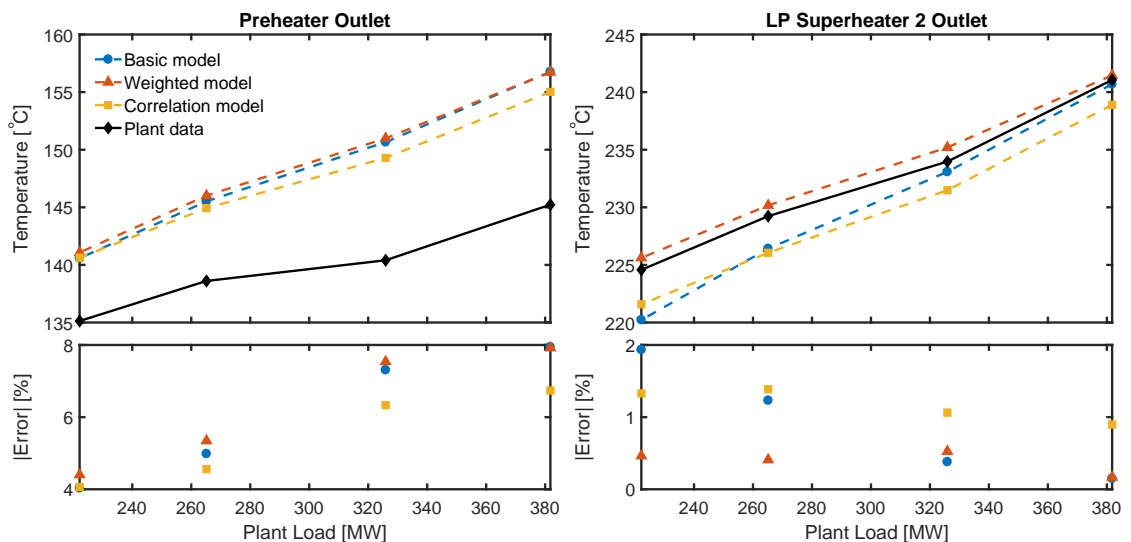


Figure 5.6: Comparison of the outlet temperatures of the Preheater and LP superheater 2.

Figure 5.6 shows the outlet temperature for the Preheater and LP superheater 2. The predicted temperatures for the Preheater outlet show an error ranging from

approximately 10 °C at full load to 5 °C at the minimum load studied. As all of the models show similar results the error might be due to an incorrect value in the HRSG model. This may be caused by a constant error in the measured recirculation mass flow data.

The next plot shows the outlet steam temperature for LP superheater 2. The off-design (Weighted and Correlation) models follow the plant data closely with an error under 1.5%. The temperature predicted by the Basic model starts off matching the off-design models and plant data at 382 MW, but decreases at a faster rate as the load is reduced. The fixed overall heat transfer coefficient of the Basic model maintains a higher heat transfer at reduced loads relative to the off-design models. This results in additional energy being extracted from the exhaust gas early along the HRSG, lowering the exhaust gas inlet temperatures for downstream heat exchangers. This in turn will reduce heat transfer and outlet water/steam temperatures. Due to this reduction in heat transfer, the initial decrease in exhaust gas temperature is damped by consecutive heat exchangers until, as seen in the Preheater outlet temperature, the effect is almost unnoticeable.

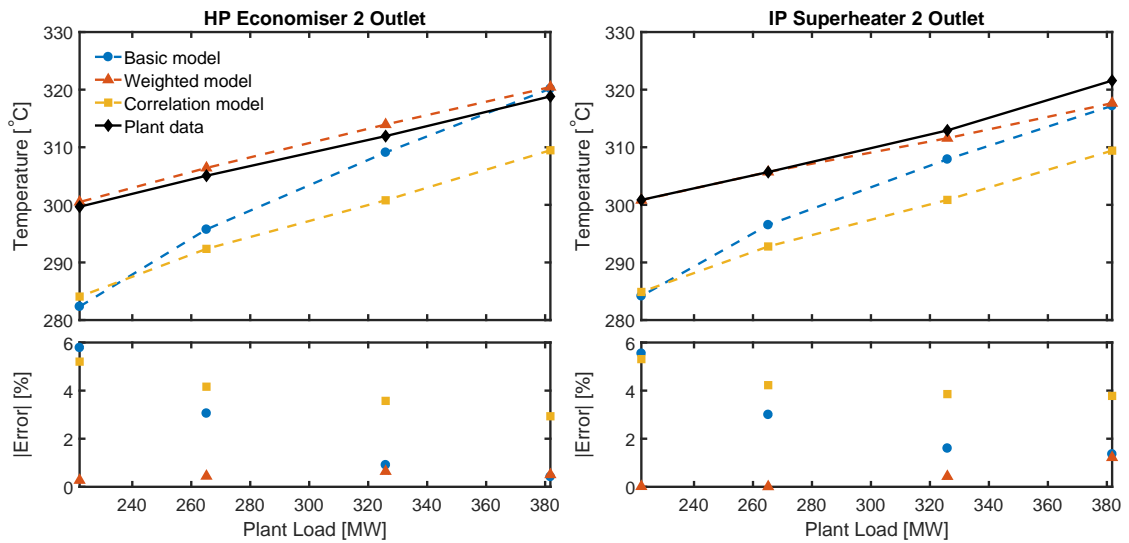


Figure 5.7: Comparison of the outlet temperatures of the IP and HP final stage superheaters.

The outlet temperature to the HP economiser 2 and IP superheater are shown in Figure 5.7. The heat exchangers sit next to each other in the HRSG and as a result the plots are nearly identical. The Weighted model closely follows the plant data across the load range of the plant, with errors of less than 2%. There is a large difference between the Correlation model and the plant data. The difference is fairly constant, ranging approximately from 10 °C below at maximum load to 15 °C below at minimum load. This offset has been caused by a reduced exhaust gas inlet temperature when compared to the Weighted model. The reduction in exhaust gas temperature occurs upstream at the HP evaporator, where the predicted value for

UA at maximum load is approximately 474 kW/K (24%) higher than the design point value, as shown in Table 5.6. This will affect all heat exchangers downstream of the HP evaporator. As with Basic model, the lower exhaust gas temperature results in reduced heat transfer, meaning the change in exhaust gas temperature across consecutive heat exchangers will be lower. This effect means the impact is most pronounced just after the HP evaporator, with the difference in exhaust gas temperature between the Correlation and Weighted models reducing to less than 2°C at the LP superheater 2 inlet.

Looking to the results for the Basic model, the affects of the lower exhaust gas inlet temperatures can be clearly seen by the large reduction in water/steam outlet temperature with load. As the heat exchangers are located further upstream, the reduction in exhaust gas temperature is greater when compared to LP superheater 2, with a commensurately large decrease in the water/steam outlet temperature.

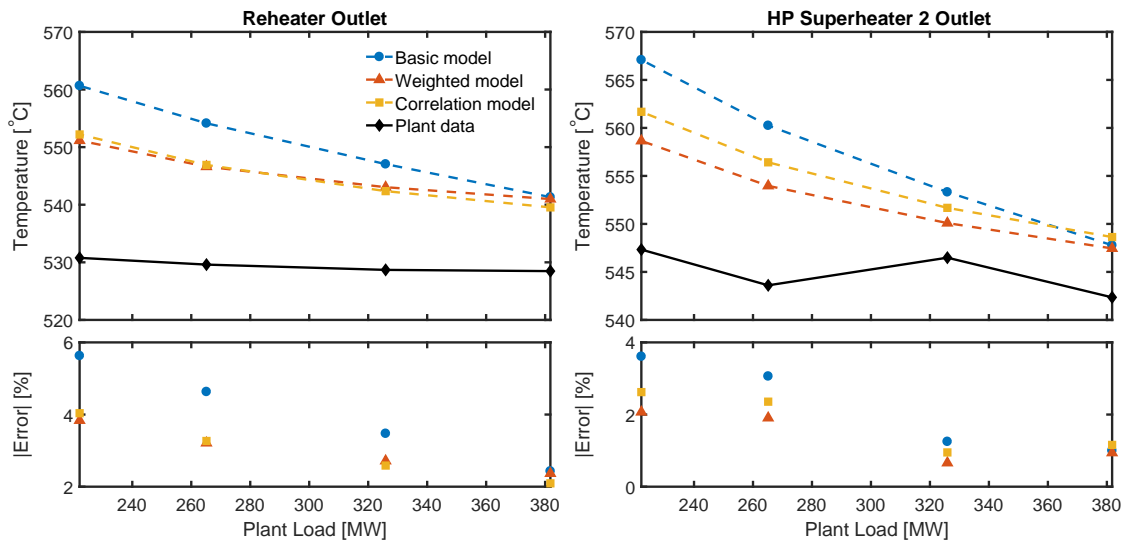


Figure 5.8: Comparison of the outlet temperatures of the Reheater and last stage HP Economiser.

The Reheater and HP superheater 2 outlet temperatures are shown in Figure 5.8. It is interesting that all of the models predict an increase in outlet temperature with decreasing load for these heat exchangers. As discussed in Section 5.1, inlet guide vane (IGV) control maintains a constant exhaust gas outlet temperature with decreasing load. This has a strong influence on HP superheaters 1 and 2, Reheater, and HP evaporator. With the inlet temperature of the exhaust gas held approximately constant, the decreasing steam mass flows reduce the heat capacity rate of the steam, resulting in an increased temperature change for a given amount of heat transfer. For the heat exchangers closest to the exhaust gas inlet, this is enough to offset the reductions in heat transfer due to decreased mass flows, UA and steam inlet temperature, resulting in an increased outlet steam temperature.

The Reheater outlet steam temperature predicted by the off-design models closely

agree, but are offset from the plant data by approximately 15 to 20 °C from the maximum to the minimum load. The Basic model matches the off-design models at the maximum load, but over predicts the outlet temperature as the load is reduced. This is due to the Basic model's fixed overall heat transfer coefficient, maintaining a high heat transfer over that of the off-design models and plant data. The large difference between the model predictions and plant data may be due to the HRSG model neglecting desuperheaters located at the inlet and outlet to both HP superheater 2 and the Reheater. These are used to maintain the steam temperatures within acceptable limits for the tubes and steam turbine inlets. This evidenced by the measured outlet temperature relatively constant throughout the load range. An additional factor would be a reduction in heat transfer due to fouling. According to [43], the highest level of fouling occurs at entrance to the HRSG, diminishing as temperature decreases and particles are filtered out of the exhaust gas. The results for HP superheater 2 show the same trends as those seen in the Reheater.

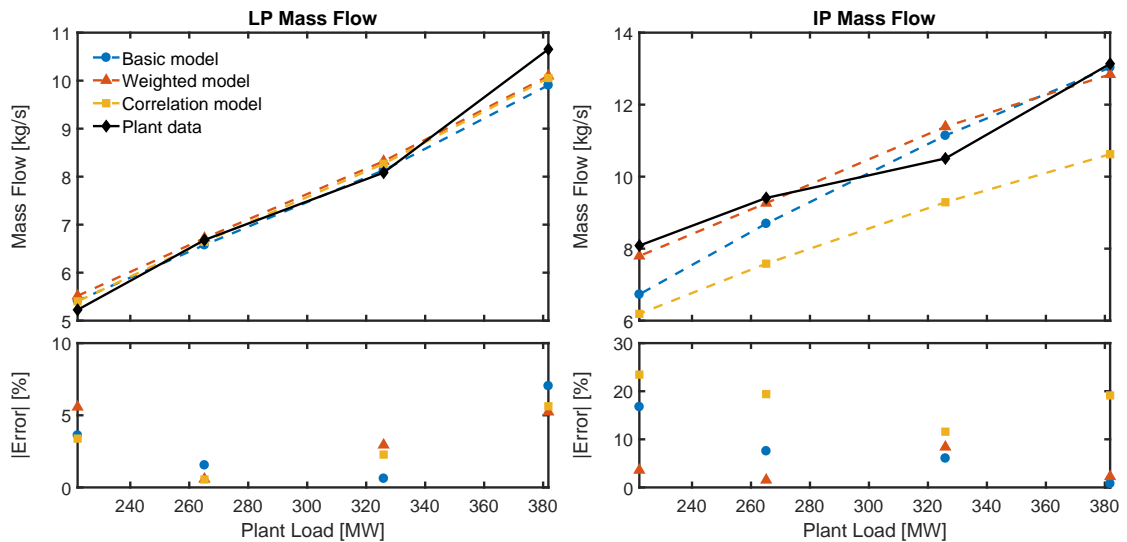


Figure 5.9: Comparison of the steam mass flows for the LP and IP evaporators.

The next two figures show the steam mass flows predicted by the evaporators. Figure 5.9 shows the steam generation for LP and IP evaporators. The LP mass flow predicted by all of the models closely matches the measured value. While the error may seem large, the magnitude of the LP mass flow is relatively small. For example, the error of 5.2% for the Weighted model at the maximum load equates to a difference of 0.56 kg/s. At the minimum load the error of 5.6% equates to a difference of just 0.29 kg/s.

The IP steam mass flow predicted by the Weighted model agrees with the measured values. As the IP evaporator is located further upstream than the LP evaporator, the reduced exhaust gas temperature affects the mass flows predicted by the Basic and Correlation models. The Predicted values follow a similar pattern to that seen in the outlet temperatures of Figure 5.7.

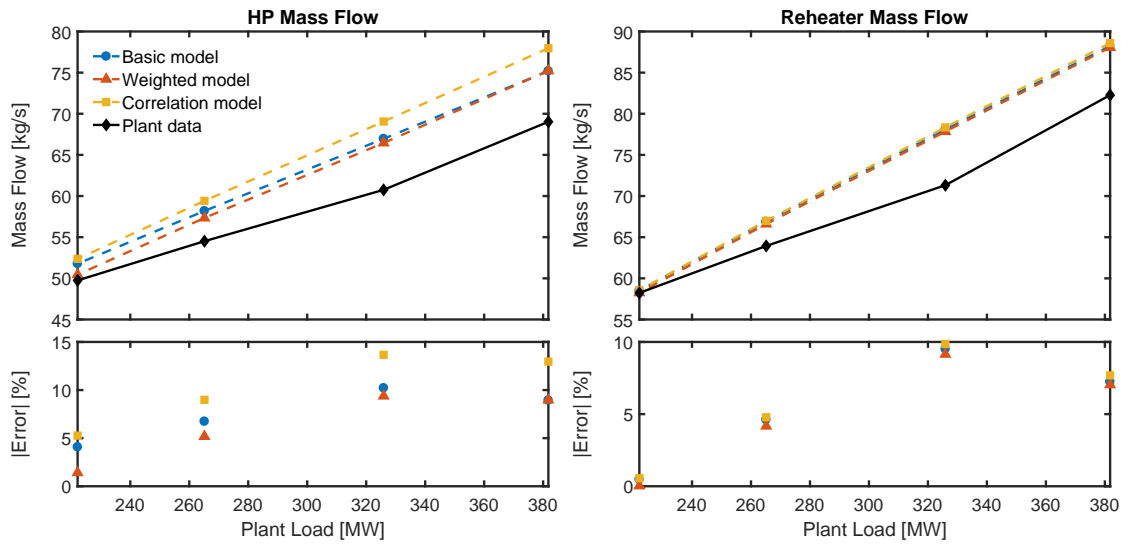


Figure 5.10: Comparison of the steam mass flow for the HP evaporator and Reheater.

The HP and Reheater mass flows are shown in Figure 5.10. The inlet exhaust gas temperature of the HP evaporator for each of the models remains relatively stable at approximately 450°C across the load range. Therefore the variation in predicted values will be due to differences in UA, with the Correlation model over predicting UA for the HP evpaorator, as discussed previously, and the Basic model using a fixed nominal value. Design data indicates that the HP steam mass flow should be nearly 75 kg/s at nominal load. The lower measured value may be due to fouling, reducing heat transfer and steam production or inaccuracies in the flow meter.

The predicted mass flow for the Reheater is simply the addition of the IP and HP mass flows. As the HP mass flow is much larger, it dominates and the plot resembles that of the HP mass flow. It is interesting to see that despite the variation in predicted mass flows for the different models, the total feed water, (LP, IP, and HP) mass flow, is approximately the same.

The solution times for the HRSG simulations are shown in Figure 5.11. The Correlation model takes much longer to solve (approximately $3600\text{-}5000\text{ s}$) than either the Basic or Weighted models. It also shows more variation, starting at approximately 5000 s at nominal load and reducing to 3600 s at the minimum load. This will be due to the fact that the model uses the solution to the previous case study to initialise the next, with a better initial guess resulting in faster, more robust convergence. The Basic and Weighted models take approximately 200 and 370 s respectively, and these values remain approximately the same for each case study.

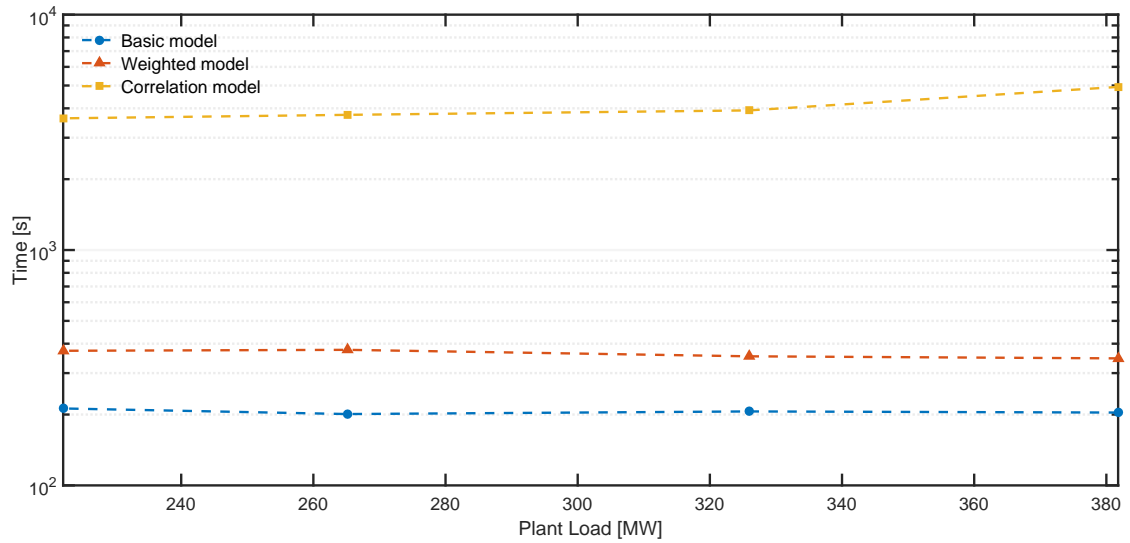


Figure 5.11: Comparison of the solution time required to solve the HRSG model, for each of the heat exchanger methods. The simulations were performed using MATLAB 2015b, on a laptop with a 64 bit, Intel Core i5-4200U CPU at 1.6 GHz.

Table 5.5: Variation in heat exchanger UA values with load, calculated by the Weighted model.

Heat Exchanger	UA [kW/K]				
	Design	Case Study			
		382 MW	326 MW	265 MW	222 MW
HP Superheater 2	235.1	232.5	209.2	183.2	162.7
Reheater	551.4	545.0	490.5	429.5	381.6
HP Superheater 1	897.5	891.7	802.4	702.6	624.3
HP Evaporator	1979.2	1967.1	1770.1	1550.0	1377.1
IP Superheater 2	53.5	52.9	47.6	41.7	37.0
HP Economiser 2	1639.1	1620.7	1458.4	1277.0	1134.6
IP Superheater 1	68.3	68.5	61.7	54.0	48.0
IP Evaporator	900.0	901.6	811.3	710.4	631.2
LP Superheater 2	44.6	44.1	39.7	34.8	30.9
HP Economiser 1	1051.6	1039.8	935.6	819.3	727.9
IP Economiser	300.6	297.3	267.5	234.2	208.1
LP Superheater 1	33.6	33.7	30.3	26.5	23.6
Weighted LP Evaporator	805.1	807.0	726.2	635.8	564.9
Preheater	2178.7	2154.3	1938.5	1697.4	1508.2

Table 5.6: Variation in heat exchanger UA values with load, calculated by the Correlation model.

Heat Exchanger	UA [kW/K]				
	Design	Case Study			
		382 MW	326 MW	265 MW	222 MW
HP Superheater 2	235.1	244.9	225.8	204.2	186.8
Reheater	551.4	532.6	489.2	439.7	400.1
HP Superheater 1	897.5	984.3	899.2	806.8	733.7
HP Evaporator	1979.2	2453.6	2268.9	2054.1	1890.7
IP Superheater 2	53.5	58.4	52.5	45.7	39.9
HP Economiser 2	1639.1	1899.1	1755.0	1587.2	1448.5
IP Superheater 1	68.3	56.2	50.5	43.9	38.4
IP Evaporator	900.0	885.5	845.4	772.7	670.0
LP Superheater 2	44.6	41.2	36.1	31.0	26.9
HP Economiser 1	1051.6	1161.8	1071.9	968.4	883.4
IP Economiser 1	300.6	285.9	263.6	237.8	217.7
LP Superheater 1	33.6	31.1	27.3	23.5	20.5
LP Evaporator	805.1	856.5	781.7	696.6	624.7
Preheater	2178.7	2211.5	2040.2	1842.1	1680.5

5.4 Discussion

In reviewing the simulation results of the previous section it should be noted that, while ideally the model predictions would accurately match the measured data, the primary focus of the study is to compare the performance of each of the three heat exchanger models in predicting the part-load behaviour of the heat exchangers within the HRSG. Model parameters can be later modified to better match the plant data at nominal load. Therefore, the models were assessed on their ability to predict the changes in heat exchanger behaviour with decreasing load rather than the absolute accuracy of those predictions.

For the majority of the points of analysed, the Basic model, with its fixed overall heat transfer coefficient, fails to follow the trends in the measured plant data in part-load conditions. This result was expected, however the simulation results demonstrated the complex interaction between heat exchangers within the HRSG. At decreased loads, the high UA values resulted in increased heat transfer in the heat exchangers located from the exhaust gas inlet up to and including the HP evaporator. The HP evaporator extracts the single largest amount of energy from the exhaust gas. The high UA value resulted in a reduction in the exhaust gas temperature at the outlet of the HP evaporator of approximately 23 °C below that

predicted by the Weighted model. This in turn reduced the heat transfer in the heat exchangers immediately following the HP evaporator. This lower heat transfer had the affect of reducing the difference in exhaust gas temperatures between the Basic and Weighted models as it moved toward the stack.

The Weighted model, in the majority of cases, accurately predicted measured data across the load range examined. There were a few notable exceptions, namely the Preheater, Reheater, and HP superheater 2 outlet temperatures, and the HP mass flow. Possible explanations for the discrepancies seen in the Reheater and HP superheater 2 were the HRSG model not taking into account the operation of desuperheaters at the inlet and outlet to these heat exchangers, which maintain the steam temperature within the operating limits of the equipment. Another possibility is the performance of the heat exchangers has been degraded by fouling. The greatest fouling occurs nearest the exhaust gas inlet, meaning these heat exchangers would be most affected.

The Correlation model, in general, predicted the correct trends in the plant data, but was usually offset by some value. Heat exchangers downstream of the HP evaporator were affected by reduced exhaust gas temperatures, caused by the over estimation of the HP evaporators UA value. By a similar mechanism as that explained for the Basic model, this lead to lower outlet temperature predictions for water/steam in the heat exchangers further downstream.

The Weighted and Correlation models both show very similar trends in their predictions across the load range. As the Correlation model calculates UA from first principles, this provides further validation of the Weighted models simplified method for determining variation of overall heat transfer coefficient with load.

5.5 Conclusion

Due to the absence of measured data for the gas turbine exhaust mass flow, a part-load model of the gas turbine was developed. The model parameters were manually tuned to ensure key properties such as compressor efficiency and fuel mass flow matched actual plant data, across the plants operating range. It is assumed that if these intermediate values match the available plant data, then the exhaust mass flow calculated based on these values should predict the actual exhaust mass flow with similar accuracy.

In this chapter the simulation procedure was detailed and the results of the simulations presented and analysed. It was found that the Basic model was unable

to correctly predict changes in heat exchanger performance with load. Both the Weighted and Correlation models followed trends in the measure data as the load was reduced. However, the Correlation model overestimated the UA value in the HP evaporator causing a large reduction in the exhaust gas temperature early along the HRSG. This in turn resulted in the predictions from heat exchangers situated downstream being offset from the measured data and Weighted model results.

Chapter 6

Conclusions and Further Work

6.1 Conclusion

The objective of this study was to determine the appropriate level of fidelity for heat exchanger models used in the simulation of existing Combine Cycle Gas Turbine (CCGT) power stations. The majority of heat exchanger models used in literature and commercial software packages utilised the LMTD or ε -NTU methods. With these as the accepted standard, the study focused on the variation of the overall heat transfer coefficient (U) in off-design conditions. Three methods used in literature for dealing with U were identified. These were to use a fixed design value, ignoring variation in U due to changes in operating conditions, scale the value of U with some related fluid properties, or calculate the value using empirical correlations developed for the specific heat transfer problem. Each of these methods were implemented in a separate heat exchanger model designated the Basic, Weighted, and Correlation models respectively.

The heat exchangers were then incorporated in the a model of the Otahuhu B CCGT power station's heat recovery steam generator (HRSG), and this model was used to simulate the operation of the HRSG at four load points, representing the operating range of Otahuhu B. The simulation results were then compared to plant data, and the performance of each heat exchanger model contrasted.

The Basic model matched plant data as well as the Weighted model when operating at nominal load. However, as load was decreased, the model predictions became increasing poor. This behaviour was expected due to the fixed value for U being specified for operation at nominal load.

The Weighted model was able to accurately follow trends in the plant data and,

for the majority of points investigated, accurately predict heat exchanger outlet temperatures and mass flows. There were a few exceptions, specifically: HP superheater 2, Reheater, and Preheater outlet water/steam temperatures, and the HP mass flow. It was suggested that this may have been caused by deficiencies in the HRSG model, though additional plant information would be required to confirm this.

Results from the Correlation model, in general, followed the trends in the plant data, and closely followed trends shown in Weighted model's results. In terms of absolute accuracy, the model's results tended to be offset from the plant data. This was attributed to an over-predicted U value for the HP evaporator, which is situated early along the exhaust gas path. The consequent reduction in exhaust gas temperature decreased heat transfer in downstream heat exchangers.

Ultimately each approach for modelling the heat exchangers has its own advantages and disadvantages depending on the application. The Basic model is the simplest to set up and fastest to solve. Provided operation does not shift too far away from where U is accurately known this model can perform well.

The Weighted model can predict the off-design performance of the heat exchanger. Variation in U is predicted relative to a known nominal point of operation, meaning the model is accurate near this point, with decreasing accuracy as it operation moves further away. Once an accurate nominal operating point is specified, adjusting the model to better match the off-design behaviour of the actual heat exchanger requires only the modification three exponents (x, y, z) . The model, however, requires a complete specification of some nominal operating point to make predictions from.

The Correlation model performs similarly to the Weighted model in terms of predicting changes in heat exchanger operation. In addition, being able to calculate U purely from the physical construction of the heat exchanger precludes the need for a complete set of nominal operating data. As seen in the simulation results, this does not guarantee the model will accurately predict the operation of the heat exchanger, even at the nominal operating point. Given the complexity of this approach, fine tuning the model to better match the operation of the plant requires greater effort than the other approaches. When attempting to simulate the plant in real-time, simulation time becomes an important factor. All simulation runs for the Correlation took over an hour to converge, and during this time the plant operation may have changed.

Overall, for the application of simulating heat exchangers in existing CCGT power stations, the Weighted model has been found to provide the most effective solution. The model was able to accurately match the plant at nominal operating

point, and follow the changes in operation in off-design conditions. In addition the model was simple to set up and converged in a reasonable time frame.

6.2 Further Work

There are a number of areas where improvements could be made to models developed in this study. Some have been omitted due to time constraints, while others are possible solutions to problems encountered during the simulation stages.

Performance of the Weighted model could be improved by the implementing analytical derivatives instead of the currently used finite differences.

The Correlation model, being the most complex has the most room for improvement and modification. As discussed in Chapter 3, the LMTD correction factor, F_{corr} , is used to adjust ΔT_{LMTD} to account for heat exchanger configurations other than pure counter-flow. Cabezas-Gómez, et al. in [9] found that as the number of rows increase, the performance of the counter cross-flow heat exchanger approaches that of the pure counter-flow. However, it was also found that for four rows, the lowest number of tube rows considered, the effectiveness of the counter cross-flow configuration, when compared to pure counter-flow, can be in error by as much as 6.7%, with an average of 1.5% over the range of fluid properties considered. The Otahuhu B HRSG has a number of heat exchangers with row numbers of less than four, so an even greater error can be expected in these cases. The VDI Heat Atlas [62] provides an equation to calculate F_{corr} as a function of fluid properties and the number of tube rows, which could be implemented in the Correlation model.

To account for variation in fluid properties with distance from the tube surface a correction factor can be used to multiply the heat transfer coefficient and friction factor correlations. For liquids, changes in viscosity with temperature are indicative of the variation in other fluid properties [33]:

$$\left(\frac{\mu_b}{\mu_w}\right)^n \quad (6.1)$$

For gases, fluid properties vary directly with absolute temperature [33]:

$$\left(\frac{T_w}{T_b}\right)^m \quad (6.2)$$

Where the subscripts b and w indicate the bulk (average) and wall (tube surface)

properties. The wall temperature may be found by solving [27]:

$$\dot{Q} = hA(T_w - T_b) \quad (6.3)$$

Where h is the convective heat transfer coefficient of the fluid. Clearly the process is iterative and these equations must be incorporated into the iterative loop of the model.

The HRSG model is slow to solve because each heat exchanger models must iteratively converge, one at a time, before one iteration of the outer loop, formed by the HRSG model solver, is complete. This process is completed many times until the outer loop converges to the solution. While this has not been a too much of an issue for the Basic, or even the Weighted model, the Correlation model takes an extremely long time to solve, greater than an hour for all case studies. This is long enough that it excludes this method for use in real-time monitoring applications for CCGT power stations. A way to decrease the solution time would be to avoid discrete heat exchanger unit operations and combine the equations describing the heat exchangers directly into the HRSG model. In this way, a single large system of non-linear equations can be solved simultaneously. The major draw backs are increased system complexity, difficulties in debugging, model initialisation, and possibly reduced flexibility, depending on the complexity of the supporting software framework [64, 50]. However, with the appropriate framework, as discussed in Chapter 2, such a system could provide a much faster solution, making heat exchanger models based on correlations a more viable option for this application.

Bibliography

- [1] AKLILU, B., AND GILANI, S. Mathematical modeling and simulation of a cogeneration plant. *Applied Thermal Engineering* 30, 16 (2010), 2545–2554.
- [2] ASKER, M., TURGUT, O. E., AND COBAN, M. T. A review of non iterative friction factor correlations for the calculation of pressure drop in pipes. *Bitlis Eren Univ J Sci & Technol* 4, 1 (2014), 1–8.
- [3] ASPEN TECHNOLOGY, I. Aspen Plus, v8.8. <http://www.aspentech.com/products/engineering/aspen-plus/>, 2016.
- [4] BARIGOZZI, G., PERDICHIZZI, A., AND RAVELLI, S. Wet and dry cooling systems optimization applied to a modern waste-to-energy cogeneration heat and power plant. *Applied Energy* 88, 4 (apr 2011), 1366–1376.
- [5] BARIGOZZI, G., PERDICHIZZI, A., AND RAVELLI, S. Performance prediction and optimization of a waste-to-energy cogeneration plant with combined wet and dry cooling system. *Applied Energy* 115 (feb 2014), 65–74.
- [6] BARTON, P. I. *The Equation Oriented Strategy for Process Flowsheeting*, 2000.
- [7] BEERS, KENNETH, J. *Numerical Methods for Chemical Engineering*. Cambridge University Press, New York, NY, 2007.
- [8] BRKIĆ, D. Review of explicit approximations to the Colebrook relation for flow friction. *Journal of Petroleum Science and Engineering* 77, 1 (2011), 34–48.
- [9] CABEZAS-GÓMEZ, L., APARECIDO NAVARRO, H., AND MARIA SAIZ-JABARDO, J. Thermal Performance of Multipass Parallel and Counter-Cross-Flow Heat Exchangers. *Journal of Heat Transfer* 129, 3 (jun 2007), 282.
- [10] CAFARO, S., TRAVERSO, A., AND MASSARDO, A. F. Heat recovery steam generator performance and degradation in a 400Å MW combined cycle. *Proceedings of the Institution of Mechanical Engineers, Part A: Journal of Power and Energy* 223, 4 (jun 2009), 369–378.
- [11] CENGEL, Y. A., AND CIMBALA, J. M. *Fluid Mechanics Fundamentals and Applications*. McGraw-Hill Education, New York, NY, 2006.
- [12] CURRIE, J. OPTI Toolbox v2.16. <http://www.i2c2.aut.ac.nz/Wiki/OPTI/index.php>, 2013.

- [13] DE BOBADILLA, F., RAMOS, F., NASAL, J., SUTHERLAND, S., AND NOE, G. Savings Achieved From Installation of an On-Line Performance Monitoring System at the Naco Nogales Combined Cycle Plant. In *Volume 4: Cycle Innovations; Electric Power; Industrial and Cogeneration; Manufacturing Materials and Metallurgy* (jan 2006), ASME, p. 519.
- [14] DÍAZ-MATEUS, F.-A., AND CASTRO-GUALDRÓN, J.-A. Mathematical model for refinery furnaces simulation. *CT&F-Ciencia, Tecnología y Futuro* 4, 1 (2010), 89–99.
- [15] DUMONT, M. Mathematical modelling and design of an advanced once-through heat recovery steam generator. *Computers & Chemical Engineering* 28, 5 (may 2004), 651–660.
- [16] DUMONT, M.-N., AND HEYEN, G. Mathematical modelling and design of an advanced once-through heat recovery steam generator. *Computer Aided Chemical Engineering* 14 (2003), 89–94.
- [17] DUMONT, M.-N., AND HEYEN, G. Row by row simulation of heat recovery steam generators: comparing different types of initialization as well as the LMTD and ϵ -NTU simulation methods. In *17th European Symposium on Computer Aided Process Engineering* (2007), V. Plesu and P. S. Agachi, Eds.
- [18] ENTERPRISE, P. S. gPROMS, v5.0. <https://www.psenterprise.com/products/gproms>, 2016.
- [19] ERBES, M. R., AND GAY, R. R. GATE/CYCLE Predictions of the Off Design Performance of Combined Cycle Power Plants. *Simulation of Thermal Energy Systems, ASME Winter Annual Meeting* 124 (1989), 43–51.
- [20] ERBES, M. R., GAY, R. R., AND COHN, A. Gate: a simulation code for analysis of gas-turbine power plants. In *ASME 1989 International Gas Turbine and Aeroengine Congress and Exposition* (1989), American Society of Mechanical Engineers, pp. V001T01A018–V001T01A018.
- [21] ERBES, M. R., EUSTIS, R. H. A Computer Methodology for Predicting the Design and Off Design Performance of Utility Steam Turbine Generators. In *Proceedings of the American Power Conference* (Chicago, IL, 1986).
- [22] FINOTUBE TECHNOLOGIES, INC. ESCOA Engineering Manual v2.1, 2002.
- [23] GNIELINSKI, V. New equations for heat and mass transfer in turbulent pipe and channel flow. *Int. Chem. Eng* 16, 2 (1976), 359–368.
- [24] GOUDER, C. T., AND SONNAD, J. R. Comparison of the iterative approximations of the Colebrook-White equation. *Hydrocarbon Processing* 87, 8 (2008), 79–83.
- [25] GROUP, V. M. VMGSim, v7.0. <https://www.virtualmaterials.com/VMGSim>, 2015.
- [26] GULEN, S. C. A Simple Parametric Model for the Analysis of Cooled Gas Turbines. In *Volume 1: Aircraft Engine; Ceramics; Coal, Biomass and Alternative Fuels; Education; Electric Power; Manufacturing Materials and Metallurgy* (2010), ASME, pp. 749–759.

- [27] HOLMAN, J. P. *Heat Transfer*, 10 ed. McGraw-Hill Education, London, 2009.
- [28] IAPWS. IAPWS. Revised Release on the IAPWS Industrial Formulation 1997 for the Thermodynamic Properties of Water and Steam. <http://www.iapws.org/>, 2007.
- [29] IBRAHIM, T. K., AND RAHMAN, M. M. Study on effective parameter of the triple-pressure reheat combined cycle performance. *Thermal Science* 17, 2 (2013), 497–508.
- [30] INC., A. T. HYSYS, v8.8. <http://www.aspentech.com/products/asp-hysys/>, 2016.
- [31] INTEL. Math Kernel Library. <https://software.intel.com/en-us/intel-mkl>, 2016.
- [32] JARIC, M., KOLENDIĆ, P., JARIĆ, M., BUDIMIR, N., AND GENIĆ, V. A Review of Explicit Approximations of Colebrook’s Equation. *FME Transactions* 39 (2011), 67–71.
- [33] KAKAÇ, S., PRAMUANJAROENKIJ, A., AND LIU, H. *Heat Exchangers Selection, Rating and Thermal Design*, 2nd ed. Taylor & Francis Inc, Bosa Roca, United States, 2002.
- [34] KAYS, W. M. W. M., AND LONDON, A. L. A. L. *Compact Heat Exchangers*, 3rd ed. Krieger Publishing Company, Melbourne, 1998.
- [35] KIM, S.-M., AND JOO, Y.-J. Implementation of on-line performance monitoring system at Seoincheon and Sinincheon combined cycle power plant. *Energy* 30, 13 (oct 2005), 2383–2401.
- [36] KIM, T. Comparative analysis on the part load performance of combined cycle plants considering design performance and power control strategy. *Energy* 29, 1 (2004), 71–85.
- [37] KNOPF, F. C. *Modeling, analysis and optimization of process and energy systems*. John Wiley & Sons, 2011.
- [38] LTD., I. P. JSteam, v3.16. <http://www.inverseproblem.co.nz/Software/JSteamExcel.html>, 2013.
- [39] MA, Y., YUAN, Y., LIU, Y., HU, X., AND HUANG, Y. Experimental investigation of heat transfer and pressure drop in serrated finned tube banks with staggered layouts. *Applied Thermal Engineering* 37 (may 2012), 314–323.
- [40] MATHWORKS. Matlab v2015b. <https://au.mathworks.com/>, 2015.
- [41] MORAN, M. J., AND SHAPIRO, H. N. *Fundamentals of Engineering Thermodynamics*, 5 ed. John Wiley & Sons, Chichester, UK, 2016.
- [42] MOTARD, R. L., SHACHAM, M., AND ROSEN, E. M. Steady state chemical process simulation. *AIChE Journal* 21, 3 (may 1975), 417–436.
- [43] MU, L., ZHAO, L., AND YIN, H. Modelling and measurements of the characteristics of ash deposition and distribution in a HRSG of wastewater incineration plant. *Applied Thermal Engineering* 44 (2012), 57–68.

- [44] NELLIS, G., AND KLEIN, S. *Heat Transfer*, 1st ed. Cambridge University Press, Cambridge, 2009.
- [45] NIST. RefProp. <https://www.nist.gov/srd/refprop>, 2014.
- [46] OH, M., AND PANTELIDES, C. A modelling and simulation language for combined lumped and distributed parameter systems. *Computers & Chemical Engineering* 20, 6-7 (jun 1996), 611–633.
- [47] ONG'IRO, A., UGURSAL, V., AL TAWHEEL, A., AND WALKER, J. Modeling of heat recovery steam generator performance. *Applied Thermal Engineering* 17, 5 (may 1997), 427–446.
- [48] PANTELIDES, C., AND BARTON, P. Equation-oriented dynamic simulation current status and future perspectives. *Computers & Chemical Engineering* 17 (jan 1993), S263–S285.
- [49] PANTELIDES, C., AND RENFRO, J. The online use of first-principles models in process operations: Review, current status and future needs. *Computers & Chemical Engineering* 51 (2013), 136–148.
- [50] PANTELIDES, C. C., NAUTA, M., AND MATZOPOULOS, M. EQUATION-ORIENTED PROCESS MODELLING TECHNOLOGY: RECENT ADVANCES & CURRENT PERSPECTIVES.
- [51] PETUKHOV, B. S. Heat Transfer and Friction in Turbulent Pipe Flow with Variable Physical Properties. *Advances in Heat Transfer* 6 (1970), 503.
- [52] PIEVE, M., AND SALVADORI, G. Performance of an air-cooled steam condenser for a waste-to-energy plant over its whole operating range. *Energy Conversion and Management* 52, 4 (apr 2011), 1908–1913.
- [53] POWELL, M. J. D. An efficient method for finding the minimum of a function of several variables without calculating derivatives. *The Computer Journal* 7, 2 (feb 1964), 155–162.
- [54] REID, D. R., AND TABOREK, J. Selection Criteria for Plain and Segmented Finned Tubes for Heat Recovery Systems. *Journal of Engineering for Gas Turbines and Power* 116, 2 (1994), 406.
- [55] SARAVANAMUTTOO, H. I. H., COHEN, H., AND ROGERS, G. F. C. *Gas Turbine Theory*, 5th ed. Pearson Education Ltd, Essex, 2001.
- [56] SHACHAM, M., MACCHIETO, S., STUTZMAN, L., AND BABCOCK, P. Equation oriented approach to process flowsheeting. *Computers & Chemical Engineering* 6, 2 (jan 1982), 79–95.
- [57] SHAH, M. Chart correlation for saturated boiling heat transfer: Equations and further study. *ASHRAE Transactions* 88 (1982), 185–195.
- [58] SHAH, M. M. Evaluation of General Correlations for Heat Transfer During Boiling of Saturated Liquids in Tubes and Annuli. In *Heat Transfer: Volume 2* (2005), ASME, pp. 1–11.
- [59] SHIN, J. Analysis of the dynamic characteristics of a combined-cycle power plant. *Energy* 27, 12 (dec 2002), 1085–1098.

- [60] SONNAD, J. R., AND GOUDAR, C. T. Turbulent Flow Friction Factor Calculation Using a Mathematically Exact Alternative to the Colebrook-White Equation. *Journal of Hydraulic Engineering* 132, 8 (aug 2006), 863–867.
- [61] THERMOFLOW. GTPro v23.0. https://www.thermoflow.com/combinedcycle_GTP.html, 2013.
- [62] VDI GESELLSCHAFT, Ed. *VDI Heat Atlas*, 2nd ed. Springer-Verlag Berlin Heidelberg, 2010.
- [63] WEIERMAN, C. Correlations ease the selection of fin tubes. *The Oil and Gas Journal* 74, 6 (1976), 94–100.
- [64] WESTERBERG, A. W., HUTCHISON, H. P., MOTARD, R. L., AND WINTER, P. *Process Flowsheeting*. Cambridge University Press, 1979.
- [65] WHITE, F. M. *Fluid Mechanics*, 7 ed. McGraw-Hill, London, 2010.
- [66] WINNING, H. K., AND COOLE, T. Explicit Friction Factor Accuracy and Computational Efficiency for Turbulent Flow in Pipes. *Flow, Turbulence and Combustion* 90, 1 (jan 2013), 1–27.
- [67] YUNUS A. CENGEL. *Heat and Mass Transfer A Practical Approach*, 3rd ed. McGraw-Hill Education, Singapore, 2006.
- [68] YUNUS A. CENGEL, M. A. B. *Thermodynamics: An Engineering Approach*, 6 ed. McGraw-Hill Education, 2007.
- [69] ZIGRANG, D. J., AND SYLVESTER, N. D. Explicit approximations to the solution of Colebrook’s friction factor equation. *AIChE Journal* 28, 3 (may 1982), 514–515.
- [70] ZIGRANG, D. J., AND SYLVESTER, N. D. A Review of Explicit Friction Factor Equations. *Journal of Energy Resources Technology* 107, 2 (1985), 280.

Appendix A

Correlations

This appendix chapter provides the equations used for the ESCOA TURB-X HF heat transfer coefficient and pressure drop correlations, and the Shah 1982 flow boiling heat transfer coefficient correlation.

A.1 ESCOA TURB-X HF Correlations

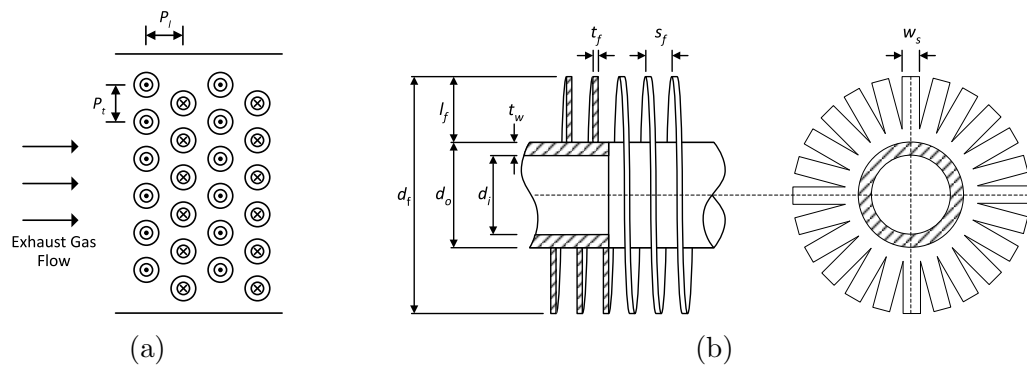


Figure A.1: a). HRSG heat exchanger with staggered tube topology, b). Schematic diagram of the segmented finned tube cross-section and top view.

Table A.1: ESCOA correlation nomenclature.

Notation	Description	Units
A_b	bare tube outside surface area per unit length of tube	ft ² /ft
A_c	finned tube projected cross sectional area per unit length of tube	ft ² /ft
A_d	total cross sectional area of the duct enclosing the bundle	ft ²
A_{fo}	fin or stud surface area only per unit length of tube	ft ² /ft
A_n	net free flow area in a tube row	ft ²
A_o	total outside surface area per unit length of tube	ft ² /ft
A_{po}	exposed bare tube outside surface per unit length of tube	ft ² /ft
A_t	total outside surface of a bundle	ft ²
A_w	average area of the tube wall per unit length of tube	ft ² /ft
a	pressure drop acceleration loss term	
B	pressure drop flow area contraction factor	
b_s	width of base of segmented fins, ($l_f - l_s$)	in.
C_1	Reynolds number correction to j-factor	
C_2	Reynolds number correction to f-factor	
C_3	fin geometry correction to j-factor	
C_4	fin geometry correction to f-factor	
C_5	tube layout correction to j-factor	
C_6	tube layout correction to f-factor	
c_p	specific heat capacity of outside fluid at T_b	Btu/lb·F
ρ_b	average outside fluid density at T_b	lb/ft ³
d_f	outside diameter of fins or studs	in
d_i	inside diameter of tube	in
d_o	outside diameter of bare tube	in
ρ_1	outside fluid inlet density at T_1	lb/ft ³
ρ_2	outside fluid outlet density at T_2	lb/ft ³
E	fin or stud thermal efficiency	
f	Fanning friction factor	
G_n	outside fluid mass velocity based on the net free area in a tube row	lb/hr·ft ²

Table A.2: ESCOA correlation nomenclature continued.

Notation	Description	Units
h_c	average actual outside convective heat transfer coefficient	Btu/hr·ft ² F
h_e	effective outside heat transfer coefficient	Btu/hr·ft ² F
h_i	average inside heat transfer coefficient	Btu/hr·ft ² F
h_m	maximum actual outside heat transfer coefficient	Btu/hr·ft ² F
h_n	natural convection outside heat transfer coefficient	Btu/hr·ft ² F
h_o	average actual outside heat transfer coefficient	Btu/hr·ft ² F
h_r	average outside radiation heat transfer coefficient	Btu/hr·ft ² F
j	Colburn heat transfer factor	
k_b	average outside fluid thermal conductivity at T_b	Btu/hr·ft·F
k_f	average fin material thermal conductivity at T_s	Btu/hr·ft·F
k_w	average tube material thermal conductivity at T_w	Btu/hr·ft·F
L	mean radiating beam length	ft
L_e	effective finned or studded length of the tube exposed to gas flow	ft
L_f	overall finned or studded length of the tube	ft
L_t	overall length of the tube	ft
l_f	fin or stud height	in.
l_s	segment length of segmented fins	in.
N_r	number of tube rows in the direction of flow	
N_t	number of tubes per row	
n_f	number of fins or rows of studs per unit length of tube	1/in.
n_s	number of studs per row or segments per wrap	
P	total pressure drop across bundle	in. of water
P_l	longitudinal (parallel to the fluid flow) tube spacing	in.
P_t	transverse (perpendicular to the fluid flow) tube spacing	in.
Re	Reynolds number	
R_{fi}	inside fouling resistance based on inside surface	hr·ft ² ·F/Btu
R_{fo}	outside fouling resistance based on total outside surface	hr·ft ² ·F/Btu
R_{io}	total inside thermal resistance based on total outside surface area	hr·ft ² ·F/Btu
R_o	total outside thermal resistance including fin efficiency based on total outside surface area	hr·ft ² ·F/Btu
R_{to}	total overall thermal resistance based on total outside surface area	hr·ft ² ·F/Btu
R_{wo}	tube wall thermal resistance based on total outside surface area	hr·ft ² ·F/Btu
s_f	clear space between fins or rows of studs	in.

Table A.3: ESCOA correlation nomenclature continued.

Notation	Description	Units
T_b	average outside fluid temperature	F
T_f	average fin or stud tip temperature	F
T_i	average inside fluid temperature	F
T_s	average fin or stud surface temperature	F
T_w	average tube wall temperature	F
T_1	outside fluid inlet temperature	F
T_2	outside fluid outlet temperature	F
t_f	average fin thickness, stud diameter or stud thickness	in.
t_w	average tube wall thickness	in.
t_1	inside fluid inlet temperature	F
t_2	inside fluid outlet temperature	F
U_o	overall heat transfer coefficient based on total outside surface area	Btu/hr·ft ² ·F
μ_b	average outside fluid dynamic viscosity at T_b	lb/hr·ft
W_o	outside fluid mass flow rate	lb/hr
w_s	fin segment width or elliptical stud width	in.
X_c	cross sectional area of flow obstructions other than finned tubes such as return bends, headers and baffles	ft ²

A.1.1 Heat Transfer Coefficient Correlation

Area calculations:

$$A_d = \frac{P_t N_t L_e}{12}$$

$$A_d = \frac{P_t N_t L_e}{12}$$

$$d_i = d_o - 2 t_w$$

$$A_i = \frac{\pi d_i}{12}$$

$$A_b = \pi d_o / 12$$

$$A_w = \frac{\pi (d_o - t_w)}{12}$$

$$d_f = d_o + 2 l_f$$

$$s_f = \left(\frac{1}{n_f} \right) - t_f$$

$$A_{po} = \frac{\pi d_o (1 - n_f t_f)}{12}$$

$$A_o = \frac{\pi d_o (1 - n_f t_f)}{12} + 0.4 \pi n_f \frac{d_o + 0.2}{12} + \pi n_f (d_o + 0.2) ((2 l_f - 0.4) (w_s + t_f) + w_s t_f) / (12 w_s)$$

$$A_{fo} = A_o - A_{po}$$

$$A_c = \frac{d_o + 2 l_f t_f n_f}{12}$$

$$A_n = A_d - A_c L_e N_t - X_c$$

$$A_t = N_t N_r L_e A_o$$

$$G_n = \frac{W_o}{A_n}$$

$$\text{Re} = \frac{G_n d_o}{12 \mu_b}$$

Staggered tube arrangement:

$$C_1 = 0.091 \text{Re}^{-0.25}$$

$$C_3 = 0.35 + 0.65 \exp\left(\frac{-0.17 l_f}{s_f}\right)$$

$$C_5 = 0.7 + (0.70 - 0.8 \exp(-0.15 N_r^2)) \exp\left(\frac{-P_l}{P_t}\right)$$

$$j = C_1 C_3 C_5 \left(\frac{d_f}{d_o}\right)^{0.5} \left(\frac{T_b + 460}{T_s + 460}\right)^{0.25}$$

Inline tube arrangement:

$$C_1 = 0.053 (\text{Re}^{-0.21}) \left(1.45 - 2.9 \left(\frac{P_l}{d_o}\right)^{-2.3}\right)$$

$$C_3 = 0.25 + 0.60 \exp\left(\frac{-0.26 l_f}{s_f}\right)$$

$$C_5 = 1.1 - (0.75 - 1.5 \exp(-0.7 N_r)) \exp\left(\frac{-2 P_l}{P_t}\right)$$

$$j = C_1 C_3 C_5 \left(\frac{d_f}{d_o}\right)^{0.5} \left(\frac{T_b + 460}{T_s + 460}\right)^{0.50}$$

$$h_c = j G_n c_p \left(\frac{k_b}{c_p \mu_b}\right)^{0.67}$$

$$h_o = \frac{1}{R_{fo}} + \frac{1}{h_c + h_r}$$

$$b = l_f + \frac{t_f}{2}$$

$$m = \left(\frac{h_o (t_f + w_s)}{6 k_f t_f w_s}\right)^{0.5}$$

$$E = \frac{\exp(m b) - \exp(-m b)}{\exp(m b) + \exp(-m b)} / (m b)$$

$$h_e = h_o \frac{E A_{fo} + A_{po}}{A_o}$$

$$R_o = \frac{1}{h_e}$$

$$R_{wo} = \frac{t_w}{12 k_w} \frac{A_o}{A_w}$$

$$R_{io} = \frac{1}{h_i} + R_{fi} \frac{A_o}{A_i}$$

$$R_{to} = R_o + R_{wo} + R_{io}$$

$$U_o = \frac{1}{R_{to}} \quad [\text{Btu/hr ft}^2 \text{ F}]$$

A.1.2 Pressure Drop Correlation

Staggered tube arrangement:

$$\begin{aligned}
 C_2 &= 0.075 + 1.85 \text{Re}^{-0.30} \\
 C_4 &= 0.11 \left(0.05 \frac{P_t}{d_o} \right)^{-0.7} \left(\frac{l_f}{s_f} \right)^{0.20} \\
 C_6 &= 1.1 + (1.8 - 2.1 \exp(-0.15 N_r^2)) \exp\left(\frac{-2 P_l}{P_t}\right) - \\
 &\quad (0.7 - 0.8 \exp(-0.15 N_r^2)) \exp\left(\frac{-0.6 P_l}{P_t}\right) \\
 f &= C_2 C_4 C_6 \left(\frac{d_f}{d_o} \right)^{0.5} \left(\frac{T_b + 460}{T_s + 460} \right)^{-0.25}
 \end{aligned}$$

Inline tube arrangement:

$$\begin{aligned}
 C_2 &= 0.11 + 1.4 \text{Re}^{-0.40} \\
 C_4 &= 0.08 \left(\frac{0.15 P_t}{d_o} \right)^{-1.1} \left(\frac{l_f}{s_f} \right)^{0.15} \\
 C_6 &= 1.6 - \left(0.75 - 1.5 \exp(-0.7 N_r) \exp\left(\frac{-0.2 P_l}{P_t}\right)^2 \right) \\
 f &= C_2 C_4 C_6 \left(\frac{d_f}{d_o} \right) \left(\frac{T_b + 460}{T_s + 460} \right)^{0.25}
 \end{aligned}$$

$$\begin{aligned}
 B &= \frac{A_n}{A_d} \\
 a &= \left(\frac{1 + B^2}{4 N_r} \right) \rho_b \left(\left(\frac{1}{\rho_2} \right) - \left(\frac{1}{\rho_1} \right) \right) \\
 P &= \frac{(f + a) G_n^2 N_r}{\rho_b 1.083 \times 10^9} \quad [\text{in H}_2\text{O}]
 \end{aligned}$$

Table A.4: Shah flow boiling correlation nomenclature

Notation	Description	Units
A	Area	m^2
Bo	Boiling number	
Co	Convection number	
d_h	Hydraulic diameter	m
Fr	Froude number	
g	Acceleration due to gravity (9.81)	m/s^2
G	Mass flux	$kg/m^2 \cdot s$
h	Heat transfer coefficient	$kW/m^2 \cdot K$
Δi_v	Enthalpy of vaporisation	kJ/kg
N	Intermediate dimensionless number	
Re_l	Reynolds Number for the liquid fraction of flow	
X	Vapour fraction	
μ	Dynamic viscosity	$Pa \cdot s$
ρ	Density	kg/m^3
Subscripts		
b	Bulk (Average) Property	
csa	Cross-sectional area	
i	Inner tube property	
l	Liquid property	
flux	Quantity per unit area	
nb	Nucleate boiling	
sat	Saturated fluid property	
v	Vapour property	

A.2 Shah Flow Boiling Correlation (1982)

$$\text{Re}_l = \frac{G(1-X)d_h}{\mu_{l,\text{sat}}}$$

$$G = \frac{\dot{m}}{A_{\text{csa}}}$$

$$\text{Bo} = \frac{\dot{Q}_{\text{flux}}}{G \Delta i_v}$$

$$\text{Fr} = \frac{G^2}{\rho_l^2 g d_h}$$

$$g = 9.81 \quad \text{Acceleration due to gravity [m/s}^2\text{]}$$

$$\text{Co} = \left(\left(\frac{1}{X} \right) - 1 \right)^{0.8} \left(\frac{\rho_{v,\text{sat}}}{\rho_{l,\text{sat}}} \right)^{0.5}$$

$$N = \begin{cases} \text{Co} & \text{for vertical tubes or horizontal tubes with Fr} > 0.04 \\ 0.38 \text{ Co Fr}^{-0.3} & \text{for horizontal tubes with Fr} \leq 0.04 \end{cases}$$

$$h_{\text{cb}} = 1.8 N^{-0.8}$$

$$h_{\text{nb}} = \begin{cases} 230\sqrt{\text{Bo}} & \text{if Bo} \geq 0.3 \times 10^{-4} \\ 1 + 46\sqrt{\text{Bo}} & \text{if Bo} < 0.3 \times 10^{-4} \end{cases}$$

$$h_{\text{bs},1} = \begin{cases} 14.7\sqrt{\text{Bo}} \exp(2.74(N^{-0.1})) & \text{if Bo} \geq 11 \times 10^{-4} \\ 15.43\sqrt{\text{Bo}} \exp(2.74(N^{-0.1})) & \text{if Bo} < 11 \times 10^{-4} \end{cases}$$

$$h_{\text{bs},2} = \begin{cases} 14.7\sqrt{\text{Bo}} \exp(2.74(N^{-0.15})) & \text{if Bo} \geq 11 \times 10^{-4} \\ 15.43\sqrt{\text{Bo}} \exp(2.74(N^{-0.15})) & \text{if Bo} < 11 \times 10^{-4} \end{cases}$$

$$h = \begin{cases} \max(h_{\text{cb}}, h_{\text{bs},2}) & \text{if } N \leq 0.1 \\ \max(h_{\text{cb}}, h_{\text{bs},1}) & \text{if } 0.1 < N \leq 1.0 \\ \max(h_{\text{cb}}, h_{\text{nb}}) & \text{if } N > 1.0 \end{cases}$$

$$h_i = h h_l$$

Appendix B

Simulation Results

This appendix chapter provides the full results of the heat recovery steam generator simulations.

Table B.1: HRSG simulation results at 382 MW, for the Basic heat exchanger model.

Heat Exchanger	Q	UA	$T_{\text{shell,inlet}}$	$T_{\text{shell,outlet}}$	$P_{\text{shell,inlet}}$	$P_{\text{shell,outlet}}$	\dot{m}_{shell}	$T_{\text{tube,inlet}}$	$T_{\text{tube,outlet}}$	$P_{\text{tube,inlet}}$	$P_{\text{tube,outlet}}$	\dot{m}_{tube}
	kW	kW/C	°C	°C	bar	bar	kg/s	°C	°C	bar	bar	kg/s
HP Superheater 2	10061.17	235.11	574.51	561.90	1.30	1.29	654.06	497.62	547.78	116.73	114.53	75.20
Reheater	37371.16	551.43	561.90	514.75	1.29	1.26	654.06	355.51	541.32	30.98	29.68	88.23
HP Superheater 1	49485.08	897.52	514.75	451.44	1.26	1.22	654.06	323.41	497.62	118.03	116.73	75.20
HP Evaporator	92318.22	1979.23	451.44	330.42	1.22	1.17	654.06	320.17	323.41	118.03	118.03	75.20
IP Superheater 2	1564.47	53.49	330.42	326.79	1.17	1.17	376.61	271.98	317.19	31.18	30.58	13.03
HP Economiser 2	33783.31	1639.08	326.79	281.46	1.17	1.13	654.06	234.45	320.17	119.73	118.03	75.20
IP Superheater 1	1465.80	68.33	281.46	277.13	1.13	1.12	298.97	236.36	271.98	31.38	31.18	13.03
IP Evaporator	21192.03	899.95	277.13	248.38	1.12	1.10	654.06	236.36	236.36	31.38	31.38	13.03
LP Superheater 2	1074.01	44.64	248.38	245.82	1.10	1.09	373.73	190.78	240.69	5.45	4.95	9.90
HP Economiser 1	25288.79	1051.61	245.82	202.47	1.09	1.07	522.60	158.66	234.45	120.53	119.73	75.20
IP Economiser	6679.49	300.63	245.82	200.29	1.09	1.07	131.47	157.10	236.36	32.78	31.38	13.03
LP Superheater 1	790.99	33.56	202.03	199.18	1.07	1.06	250.05	156.51	190.78	5.65	5.45	9.90
LP Evaporator	20715.94	805.06	199.18	170.53	1.06	1.05	654.06	156.51	156.51	5.65	5.65	9.90
Preheater	50996.58	2178.72	170.53	99.19	1.05	1.02	654.06	62.43	156.77	18.33	15.83	127.75

Table B.2: HRSG simulation results at 326 MW, for the Basic heat exchanger model.

Heat Exchanger	Q	UA	$T_{\text{shell,inlet}}$	$T_{\text{shell,outlet}}$	$P_{\text{shell,inlet}}$	$P_{\text{shell,outlet}}$	\dot{m}_{shell}	$T_{\text{tube,inlet}}$	$T_{\text{tube,outlet}}$	$P_{\text{tube,inlet}}$	$P_{\text{tube,outlet}}$	\dot{m}_{tube}
	kW	kW/C	°C	°C	bar	bar	kg/s	°C	°C	bar	bar	kg/s
HP Superheater 2	8655.08	235.11	574.47	562.12	1.30	1.29	573.71	503.35	553.32	102.61	100.41	66.96
Reheater	33304.06	551.43	562.12	514.21	1.29	1.26	573.71	357.80	547.05	26.98	25.68	78.11
HP Superheater 1	44354.15	897.52	514.21	449.49	1.26	1.22	573.71	313.83	503.35	103.91	102.61	66.96
HP Evaporator	88546.46	1979.23	449.49	316.88	1.22	1.17	573.71	309.10	313.83	103.91	103.91	66.96
IP Superheater 2	1270.71	53.49	316.88	313.51	1.17	1.17	330.34	263.92	307.91	26.87	26.27	11.14
HP Economiser 2	28184.94	1639.08	313.51	270.26	1.17	1.13	573.71	226.34	309.10	105.61	103.91	66.96
IP Superheater 1	1206.97	68.33	270.26	266.18	1.13	1.12	262.24	228.22	263.92	27.07	26.87	11.14
IP Evaporator	18414.68	899.95	266.18	237.62	1.12	1.10	573.71	228.22	228.22	27.07	27.07	11.14
LP Superheater 2	847.62	44.64	237.62	235.31	1.10	1.09	327.82	185.18	233.08	5.14	4.64	8.13
HP Economiser 1	21890.18	1051.61	235.31	192.42	1.09	1.07	458.40	152.24	226.34	106.41	105.61	66.96
IP Economiser	5711.17	300.63	235.31	190.82	1.09	1.07	115.32	150.90	228.22	28.47	27.07	11.14
LP Superheater 1	585.01	33.56	192.09	189.68	1.07	1.06	219.33	154.33	185.18	5.34	5.14	8.13
LP Evaporator	17205.61	805.06	189.68	162.50	1.06	1.04	573.71	150.82	154.33	5.34	5.34	8.13
Preheater	43448.96	2178.72	162.50	93.10	1.04	1.01	573.71	62.00	150.66	19.23	16.73	115.98

Table B.3: HRSG simulation results at 265 MW, for the Basic heat exchanger model.

Heat Exchanger	Q	UA	$T_{\text{shell,inlet}}$	$T_{\text{shell,outlet}}$	$P_{\text{shell,inlet}}$	$P_{\text{shell,outlet}}$	\dot{m}_{shell}	$T_{\text{tube,inlet}}$	$T_{\text{tube,outlet}}$	$P_{\text{tube,inlet}}$	$P_{\text{tube,outlet}}$	\dot{m}_{tube}
	kW	kW/C	°C	°C	bar	bar	kg/s	°C	°C	bar	bar	kg/s
HP Superheater 2	7721.37	235.11	577.22	564.22	1.30	1.29	486.45	507.77	560.25	92.07	89.87	58.19
Reheater	29598.97	551.43	564.22	514.01	1.29	1.25	486.45	356.32	554.14	24.29	22.99	66.88
HP Superheater 1	38829.91	897.52	514.01	447.17	1.25	1.22	486.45	306.00	507.77	93.37	92.07	58.19
HP Evaporator	82465.51	1979.23	447.17	301.17	1.22	1.17	486.45	295.74	306.00	93.37	93.37	58.19
IP Superheater 2	918.01	53.49	301.17	298.29	1.17	1.17	280.10	255.57	296.52	24.15	23.55	8.70
HP Economiser 2	21825.83	1639.08	298.29	258.64	1.17	1.13	486.45	219.84	295.74	95.07	93.37	58.19
IP Superheater 1	855.14	68.33	258.64	255.22	1.13	1.12	222.36	222.55	255.57	24.35	24.15	8.70
IP Evaporator	14395.33	899.95	255.22	228.83	1.12	1.10	486.45	222.55	222.55	24.35	24.35	8.70
LP Superheater 2	669.23	44.64	228.83	226.67	1.10	1.09	277.96	179.80	226.41	4.97	4.47	6.58
HP Economiser 1	18649.65	1051.61	226.67	183.47	1.09	1.07	388.67	146.86	219.84	95.87	95.07	58.19
IP Economiser	4619.66	300.63	226.67	184.14	1.09	1.07	97.78	145.69	222.55	25.75	24.35	8.70
LP Superheater 1	412.04	33.56	183.61	181.60	1.07	1.06	185.97	153.06	179.80	5.17	4.97	6.58
LP Evaporator	14046.58	805.06	181.60	155.38	1.06	1.04	486.45	145.69	153.06	5.17	5.17	6.58
Preheater	35845.59	2178.72	155.38	87.77	1.04	1.01	486.45	62.29	145.52	19.71	17.21	102.04

Table B.4: HRSG simulation results at 222 MW, for the Basic heat exchanger model.

Heat Exchanger	Q	UA	$T_{\text{shell,inlet}}$	$T_{\text{shell,outlet}}$	$P_{\text{shell,inlet}}$	$P_{\text{shell,outlet}}$	\dot{m}_{shell}	$T_{\text{tube,inlet}}$	$T_{\text{tube,outlet}}$	$P_{\text{tube,inlet}}$	$P_{\text{tube,outlet}}$	\dot{m}_{tube}
	kW	kW/C	°C	°C	bar	bar	kg/s	°C	°C	bar	bar	kg/s
HP Superheater 2	7111.28	235.11	581.23	567.38	1.29	1.28	420.01	511.88	567.09	84.35	82.15	51.78
Reheater	26359.73	551.43	567.38	515.63	1.28	1.25	420.01	358.12	560.66	22.12	20.82	58.51
HP Superheater 1	34891.73	897.52	515.63	446.06	1.25	1.22	420.01	299.81	511.88	85.65	84.35	51.78
HP Evaporator	77773.03	1979.23	446.06	286.25	1.22	1.17	420.01	282.34	299.81	85.65	85.65	51.78
IP Superheater 2	652.44	53.49	286.25	283.87	1.17	1.17	241.84	246.58	284.17	21.86	21.26	6.73
HP Economiser 2	17093.41	1639.08	283.87	247.79	1.17	1.13	420.01	213.95	282.34	87.35	85.65	51.78
IP Superheater 1	578.13	68.33	247.79	245.10	1.13	1.12	191.99	217.39	246.58	22.06	21.86	6.73
IP Evaporator	11103.50	899.95	245.10	221.47	1.12	1.10	420.01	217.39	217.39	22.06	22.06	6.73
LP Superheater 2	545.44	44.64	221.47	219.43	1.10	1.09	239.99	174.30	220.23	4.84	4.34	5.41
HP Economiser 1	16349.03	1051.61	219.43	175.50	1.09	1.07	335.59	141.76	213.95	88.15	87.35	51.78
IP Economiser	3747.15	300.63	219.43	179.42	1.09	1.07	84.42	140.71	217.39	23.46	22.06	6.73
LP Superheater 1	283.83	33.56	176.28	174.68	1.07	1.06	160.57	152.13	174.30	5.04	4.84	5.41
LP Evaporator	11672.98	805.06	174.68	149.40	1.06	1.04	420.01	140.77	152.13	5.04	5.04	5.41
Preheater	30110.49	2178.72	149.40	83.55	1.04	1.01	420.01	63.13	140.58	19.84	17.34	92.20

Table B.5: HRSG simulation results at 382 MW, for the Weighted heat exchanger model.

Heat Exchanger	Q	UA	$T_{\text{shell,inlet}}$	$T_{\text{shell,outlet}}$	$P_{\text{shell,inlet}}$	$P_{\text{shell,outlet}}$	\dot{m}_{shell}	$T_{\text{tube,inlet}}$	$T_{\text{tube,outlet}}$	$P_{\text{tube,inlet}}$	$P_{\text{tube,outlet}}$	\dot{m}_{tube}
	kW	kW/C	°C	°C	bar	bar	kg/s	°C	°C	bar	bar	kg/s
HP Superheater 2	10006.06	232.47	574.51	561.97	1.29	1.28	654.06	497.63	547.45	116.64	114.32	75.22
Reheater	37225.82	545.04	561.97	515.01	1.28	1.25	654.06	355.51	540.98	30.98	29.73	88.06
HP Superheater 1	49488.85	891.72	515.01	451.69	1.25	1.22	654.06	323.33	497.63	117.91	116.64	75.22
HP Evaporator	92221.96	1967.11	451.69	330.81	1.22	1.17	654.06	320.45	323.33	117.91	117.91	75.22
IP Superheater 2	1534.19	52.89	330.81	327.25	1.17	1.17	376.61	273.01	317.65	32.15	31.56	12.84
HP Economiser 2	33631.80	1620.68	327.25	282.13	1.17	1.13	654.06	235.31	320.45	119.71	117.91	75.22
IP Superheater 1	1431.62	68.55	282.13	277.90	1.13	1.12	298.97	237.92	273.01	32.26	32.15	12.84
IP Evaporator	20801.99	901.64	277.90	249.69	1.12	1.10	654.06	237.92	237.92	32.26	32.26	12.84
LP Superheater 2	1097.77	44.14	249.69	247.08	1.10	1.09	373.73	191.24	241.46	5.52	5.13	10.10
HP Economiser 1	25610.55	1039.77	247.08	203.18	1.09	1.07	522.60	158.61	235.31	120.53	119.71	75.22
IP Economiser	6659.11	297.29	247.08	201.70	1.09	1.07	131.47	157.05	237.92	32.78	32.26	12.84
LP Superheater 1	812.92	33.67	202.88	199.95	1.07	1.06	250.05	156.51	191.24	5.65	5.52	10.10
LP Evaporator	21119.90	806.97	199.95	170.74	1.06	1.05	654.06	156.51	156.51	5.65	5.65	10.10
Preheater	50999.77	2154.27	170.74	99.41	1.05	1.02	654.06	62.41	156.73	18.33	16.67	127.77

Table B.6: HRSG simulation results at 326 MW, for the Weighted heat exchanger model.

Heat Exchanger	Q	UA	$T_{\text{shell,inlet}}$	$T_{\text{shell,outlet}}$	$P_{\text{shell,inlet}}$	$P_{\text{shell,outlet}}$	\dot{m}_{shell}	$T_{\text{tube,inlet}}$	$T_{\text{tube,outlet}}$	$P_{\text{tube,inlet}}$	$P_{\text{tube,outlet}}$	\dot{m}_{tube}
	kW	kW/C	°C	°C	bar	bar	kg/s	°C	°C	bar	bar	kg/s
HP Superheater 2	8346.94	209.19	574.47	562.56	1.24	1.23	573.71	501.64	550.09	102.94	100.82	66.45
Reheater	32481.30	490.46	562.56	515.84	1.23	1.20	573.71	357.80	543.04	26.98	25.83	77.84
HP Superheater 1	43716.29	802.42	515.84	452.09	1.20	1.18	573.71	313.94	501.64	104.07	102.94	66.45
HP Evaporator	85820.25	1770.12	452.09	323.72	1.18	1.14	573.71	313.94	313.94	104.07	104.07	66.45
IP Superheater 2	1329.52	47.60	323.72	320.21	1.14	1.13	330.34	266.60	311.57	27.89	27.36	11.39
HP Economiser 2	29464.77	1458.38	320.21	275.06	1.13	1.10	573.71	228.11	313.94	105.67	104.07	66.45
IP Superheater 1	1266.22	61.68	275.06	270.78	1.10	1.10	262.24	230.06	266.60	28.00	27.89	11.39
IP Evaporator	18809.22	811.35	270.78	241.65	1.10	1.08	573.71	230.06	230.06	28.00	28.00	11.39
LP Superheater 2	876.05	39.72	241.65	239.26	1.08	1.07	327.82	186.42	235.20	5.24	4.96	8.32
HP Economiser 1	22177.32	935.64	239.26	195.84	1.07	1.05	458.40	152.54	228.11	106.41	105.67	66.45
IP Economiser	5834.53	267.52	239.26	193.84	1.07	1.05	115.32	151.20	230.06	28.47	28.00	11.39
LP Superheater 1	616.21	30.30	195.44	192.90	1.05	1.05	219.33	154.33	186.42	5.34	5.24	8.32
LP Evaporator	17590.06	726.16	192.90	165.13	1.05	1.04	573.71	151.16	154.33	5.34	5.34	8.32
Preheater	43540.99	1938.54	165.13	95.63	1.04	1.01	573.71	62.10	150.98	19.23	17.91	115.90

Table B.7: HRSG simulation results at 265 MW, for the Weighted heat exchanger model.

Heat Exchanger	Q	UA	$T_{\text{shell,inlet}}$	$T_{\text{shell,outlet}}$	$P_{\text{shell,inlet}}$	$P_{\text{shell,outlet}}$	\dot{m}_{shell}	$T_{\text{tube,inlet}}$	$T_{\text{tube,outlet}}$	$P_{\text{tube,inlet}}$	$P_{\text{tube,outlet}}$	\dot{m}_{tube}
	kW	kW/C	°C	°C	bar	bar	kg/s	°C	°C	bar	bar	kg/s
HP Superheater 2	7118.46	183.17	577.22	565.23	1.18	1.17	486.45	504.97	553.96	92.96	91.15	57.34
Reheater	28333.34	429.46	565.23	517.20	1.17	1.16	486.45	356.32	546.61	24.29	23.33	66.60
HP Superheater 1	37848.22	702.61	517.20	452.11	1.16	1.14	486.45	306.41	504.97	93.91	92.96	57.34
HP Evaporator	77166.38	1549.95	452.11	315.84	1.14	1.10	486.45	306.41	306.41	93.91	93.91	57.34
IP Superheater 2	1065.29	41.68	315.84	312.52	1.10	1.10	280.10	260.64	305.71	25.31	24.91	9.26
HP Economiser 2	24923.03	1276.99	312.52	267.38	1.10	1.08	486.45	222.23	306.41	95.26	93.91	57.34
IP Superheater 1	986.77	54.01	267.38	263.45	1.08	1.07	222.36	224.79	260.64	25.40	25.31	9.26
IP Evaporator	15367.16	710.43	263.45	235.32	1.07	1.06	486.45	224.79	224.79	25.40	25.40	9.26
LP Superheater 2	694.20	34.78	235.32	233.09	1.06	1.06	277.96	182.23	230.17	5.10	4.90	6.72
HP Economiser 1	18884.62	819.27	233.09	189.42	1.06	1.04	388.67	147.34	222.23	95.87	95.26	57.34
IP Economiser	4875.85	234.25	233.09	188.26	1.06	1.04	97.78	146.16	224.79	25.75	25.40	9.26
LP Superheater 1	451.42	26.53	189.18	186.99	1.04	1.04	185.97	153.06	182.23	5.17	5.10	6.72
LP Evaporator	14335.05	635.84	186.99	160.26	1.04	1.03	486.45	146.21	153.06	5.17	5.17	6.72
Preheater	35945.80	1697.42	160.26	92.53	1.03	1.01	486.45	62.47	146.01	19.71	18.68	101.90

Table B.8: HRSG simulation results at 222 MW, for the Weighted heat exchanger model.

Heat Exchanger	Q	UA	$T_{\text{shell,inlet}}$	$T_{\text{shell,outlet}}$	$P_{\text{shell,inlet}}$	$P_{\text{shell,outlet}}$	\dot{m}_{shell}	$T_{\text{tube,inlet}}$	$T_{\text{tube,outlet}}$	$P_{\text{tube,inlet}}$	$P_{\text{tube,outlet}}$	\dot{m}_{tube}
	kW	kW/C	°C	°C	bar	bar	kg/s	°C	°C	bar	bar	kg/s
HP Superheater 2	6232.94	162.75	581.23	569.09	1.14	1.14	420.01	509.07	558.65	85.66	84.10	50.45
Reheater	24980.30	381.57	569.09	520.08	1.14	1.12	420.01	358.12	551.14	22.12	21.28	58.25
HP Superheater 1	33632.29	624.28	520.08	453.13	1.12	1.11	420.01	300.49	509.07	86.47	85.66	50.45
HP Evaporator	70127.82	1377.14	453.13	309.60	1.11	1.08	420.01	300.49	300.49	86.47	86.47	50.45
IP Superheater 2	888.07	37.03	309.60	306.38	1.08	1.08	241.84	255.46	300.81	23.11	22.79	7.80
HP Economiser 2	21567.19	1134.61	306.38	261.07	1.08	1.06	420.01	216.88	300.49	87.63	86.47	50.45
IP Superheater 1	804.20	47.99	261.07	257.35	1.06	1.06	191.99	219.96	255.46	23.18	23.11	7.80
IP Evaporator	13001.19	631.23	257.35	229.75	1.06	1.05	420.01	219.96	219.96	23.18	23.18	7.80
LP Superheater 2	565.48	30.90	229.75	227.64	1.05	1.05	239.99	178.06	225.61	4.99	4.85	5.52
HP Economiser 1	16497.22	727.92	227.64	183.39	1.05	1.04	335.59	142.24	216.88	88.15	87.63	50.45
IP Economiser	4190.49	208.13	227.64	182.96	1.05	1.04	84.42	141.18	219.96	23.46	23.18	7.80
LP Superheater 1	329.68	23.57	183.31	181.45	1.04	1.03	160.57	152.13	178.06	5.04	4.99	5.52
LP Evaporator	11880.72	564.95	181.45	155.76	1.03	1.03	420.01	141.29	152.13	5.04	5.04	5.52
Preheater	30183.37	1508.17	155.76	89.84	1.03	1.01	420.01	63.34	141.08	19.84	18.98	92.03

Table B.9: HRSG simulation results at 382 MW, for the Correlation heat exchanger model.

Heat Exchanger	Q	UA	$T_{\text{shell,inlet}}$	$T_{\text{shell,outlet}}$	$P_{\text{shell,inlet}}$	$P_{\text{shell,outlet}}$	\dot{m}_{shell}	$T_{\text{tube,inlet}}$	$T_{\text{tube,outlet}}$	$P_{\text{tube,inlet}}$	$P_{\text{tube,outlet}}$	\dot{m}_{tube}
	kW	kW/C	°C	°C	bar	bar	kg/s	°C	°C	bar	bar	kg/s
HP Superheater 2	10173.32	244.86	574.51	561.76	1.05	1.05	654.06	499.22	548.63	119.16	118.72	77.97
Reheater	37092.26	532.61	561.76	514.96	1.05	1.05	654.06	355.51	539.54	30.98	30.56	88.59
HP Superheater 1	51697.85	984.31	514.96	448.79	1.05	1.04	654.06	324.54	499.22	119.79	119.16	77.97
HP Evaporator	100599.20	2453.58	448.79	316.62	1.04	1.03	654.06	309.48	324.54	119.79	119.79	77.97
IP Superheater 2	1247.90	58.40	316.62	313.72	1.03	1.03	376.61	266.22	309.41	32.59	32.53	10.62
HP Economiser 2	29701.44	1899.06	313.72	273.75	1.03	1.03	654.06	234.86	309.48	120.14	119.79	77.97
IP Superheater 1	956.74	56.23	273.75	270.92	1.03	1.03	298.97	238.62	266.22	32.66	32.59	10.62
IP Evaporator	16644.61	885.47	270.92	248.33	1.03	1.03	654.06	238.62	238.62	32.66	32.66	10.62
LP Superheater 2	1095.70	41.20	248.33	245.71	1.03	1.03	373.73	188.21	238.89	5.58	5.51	10.06
HP Economiser 1	26970.48	1161.82	245.71	199.46	1.03	1.02	522.60	156.86	234.86	120.53	120.14	77.97
IP Economiser	6154.90	285.86	245.71	203.77	1.03	1.02	131.47	155.32	238.62	32.78	32.66	10.62
LP Superheater 1	738.86	31.12	200.32	197.66	1.02	1.02	250.05	156.51	188.21	5.65	5.58	10.06
LP Evaporator	21105.85	856.47	197.66	168.46	1.02	1.02	654.06	155.18	156.51	5.65	5.65	10.06
Preheater	50531.61	2211.51	168.46	97.75	1.02	1.02	654.06	61.89	155.01	18.33	17.42	128.26

Table B.10: HRSG simulation results at 326 MW, for the Correlation heat exchanger model.

Heat Exchanger	Q	UA	$T_{\text{shell,inlet}}$	$T_{\text{shell,outlet}}$	$P_{\text{shell,inlet}}$	$P_{\text{shell,outlet}}$	\dot{m}_{shell}	$T_{\text{tube,inlet}}$	$T_{\text{tube,outlet}}$	$P_{\text{tube,inlet}}$	$P_{\text{tube,outlet}}$	\dot{m}_{tube}
	kW	kW/C	°C	°C	bar	bar	kg/s	°C	°C	bar	bar	kg/s
HP Superheater 2	8604.01	225.78	574.47	562.19	1.04	1.04	573.71	503.10	551.67	105.23	104.83	69.06
Reheater	32515.57	489.20	562.19	515.42	1.04	1.04	573.71	357.80	542.36	26.98	26.59	78.35
HP Superheater 1	45728.15	899.17	515.42	448.70	1.04	1.03	573.71	315.18	503.10	105.82	105.23	69.06
HP Evaporator	94430.88	2268.86	448.70	307.07	1.03	1.03	573.71	300.79	315.18	105.82	105.82	69.06
IP Superheater 2	1039.85	52.53	307.07	304.31	1.03	1.03	330.34	258.57	300.86	28.31	28.26	9.29
HP Economiser 2	25446.88	1755.01	304.31	265.18	1.03	1.03	573.71	227.14	300.79	106.10	105.82	69.06
IP Superheater 1	807.52	50.50	265.18	262.45	1.03	1.02	262.24	230.80	258.57	28.38	28.31	9.29
IP Evaporator	14906.94	845.39	262.45	239.32	1.02	1.02	573.71	230.80	230.80	28.38	28.38	9.29
LP Superheater 2	865.98	36.11	239.32	236.97	1.02	1.02	327.82	182.76	231.48	5.29	5.23	8.27
HP Economiser 1	23247.87	1071.94	236.97	191.41	1.02	1.02	458.40	150.82	227.14	106.41	106.10	69.06
IP Economiser	5263.14	263.58	236.97	195.99	1.02	1.02	115.32	149.49	230.80	28.47	28.38	9.29
LP Superheater 1	543.29	27.34	192.33	190.10	1.02	1.02	219.33	154.32	182.76	5.34	5.29	8.27
LP Evaporator	17535.96	781.68	190.10	162.39	1.02	1.02	573.71	149.48	154.32	5.34	5.34	8.27
Preheater	43143.71	2040.16	162.39	93.49	1.02	1.01	573.71	61.53	149.29	19.23	18.47	116.35

Table B.11: HRSG simulation results at 265 MW, for the Correlation heat exchanger model.

Heat Exchanger	Q	UA	$T_{\text{shell,inlet}}$	$T_{\text{shell,outlet}}$	$P_{\text{shell,inlet}}$	$P_{\text{shell,outlet}}$	\dot{m}_{shell}	$T_{\text{tube,inlet}}$	$T_{\text{tube,outlet}}$	$P_{\text{tube,inlet}}$	$P_{\text{tube,outlet}}$	\dot{m}_{tube}
	kW	kW/C	°C	°C	bar	bar	kg/s	°C	°C	bar	bar	kg/s
HP Superheater 2	7406.68	204.20	577.22	564.75	1.03	1.03	486.45	506.75	556.42	94.92	94.58	59.41
Reheater	28504.28	439.66	564.75	516.42	1.03	1.03	486.45	356.32	546.91	24.29	23.96	66.99
HP Superheater 1	39503.84	806.84	516.42	448.44	1.03	1.03	486.45	307.58	506.75	95.43	94.92	59.41
HP Evaporator	85106.67	2054.12	448.44	297.71	1.03	1.02	486.45	292.36	307.58	95.43	95.43	59.41
IP Superheater 2	802.76	45.69	297.71	295.19	1.02	1.02	280.10	252.24	292.77	25.64	25.60	7.58
HP Economiser 2	20717.04	1587.15	295.19	257.54	1.02	1.02	486.45	221.49	292.36	95.64	95.43	59.41
IP Superheater 1	621.45	43.94	257.54	255.05	1.02	1.02	222.36	225.40	252.24	25.69	25.64	7.58
IP Evaporator	12253.27	772.66	255.05	232.59	1.02	1.02	486.45	225.40	225.40	25.69	25.69	7.58
LP Superheater 2	679.65	31.04	232.59	230.41	1.02	1.02	277.96	178.52	226.05	5.13	5.09	6.64
HP Economiser 1	19648.19	968.43	230.41	184.93	1.02	1.02	388.67	146.23	221.49	95.87	95.64	59.41
IP Economiser	4351.74	237.75	230.41	190.39	1.02	1.02	97.78	145.07	225.40	25.75	25.69	7.58
LP Superheater 1	390.54	23.54	186.03	184.13	1.02	1.02	185.97	153.06	178.52	5.17	5.13	6.64
LP Evaporator	14205.18	696.65	184.13	157.63	1.02	1.02	486.45	145.13	153.06	5.17	5.17	6.64
Preheater	35761.04	1842.14	157.63	90.21	1.02	1.01	486.45	62.06	144.92	19.71	19.10	102.22

Table B.12: HRSG simulation results at 222 MW, for the Correlation heat exchanger model.

Heat Exchanger	Q	UA	$T_{\text{shell,inlet}}$	$T_{\text{shell,outlet}}$	$P_{\text{shell,inlet}}$	$P_{\text{shell,outlet}}$	\dot{m}_{shell}	$T_{\text{tube,inlet}}$	$T_{\text{tube,outlet}}$	$P_{\text{tube,inlet}}$	$P_{\text{tube,outlet}}$	\dot{m}_{tube}
	kW	kW/C	°C	°C	bar	bar	kg/s	°C	°C	bar	bar	kg/s
HP Superheater 2	6575.52	186.84	581.23	568.42	1.03	1.03	420.01	510.88	561.68	87.36	87.06	52.37
Reheater	25221.71	400.12	568.42	518.93	1.03	1.03	420.01	358.12	552.20	22.12	21.84	58.56
HP Superheater 1	35155.31	733.73	518.93	448.89	1.03	1.02	420.01	301.57	510.88	87.80	87.36	52.37
HP Evaporator	78000.46	1890.69	448.89	288.71	1.02	1.02	420.01	284.08	301.57	87.80	87.80	52.37
IP Superheater 2	618.58	39.93	288.71	286.46	1.02	1.02	241.84	246.19	284.88	23.38	23.35	6.19
HP Economiser 2	17126.91	1448.50	286.46	250.33	1.02	1.02	420.01	216.62	284.08	87.97	87.80	52.37
IP Superheater 1	475.59	38.43	250.33	248.13	1.02	1.02	191.99	220.50	246.19	23.42	23.38	6.19
IP Evaporator	9868.59	669.96	248.13	227.15	1.02	1.02	420.01	220.50	220.50	23.42	23.42	6.19
LP Superheater 2	549.93	26.92	227.15	225.09	1.02	1.02	239.99	174.38	221.59	5.01	4.99	5.40
HP Economiser 1	17166.37	883.45	225.09	179.01	1.02	1.02	335.59	141.78	216.62	88.15	87.97	52.37
IP Economiser	3793.03	217.68	225.09	184.65	1.02	1.02	84.42	140.72	220.50	23.46	23.42	6.19
LP Superheater 1	277.87	20.47	180.15	178.58	1.02	1.02	160.57	152.13	174.38	5.04	5.01	5.40
LP Evaporator	11645.23	624.73	178.58	153.39	1.02	1.01	420.01	140.84	152.13	5.04	5.04	5.40
Preheater	30155.27	1680.52	153.39	87.50	1.01	1.01	420.01	63.13	140.63	19.84	19.33	92.23

Appendix C

DVD Contents

This appendix chapter lists the software provided on the accompanying DVD.

Table C.1: DVD contents.

Folder	Description
Basic heat exchanger	Basic heat exchanger classes.
Weighted heat exchanger	Weighted heat exchanger classes.
Correlation heat exchanger	Correlation heat exchanger classes.
Gas Turbine	Gas turbine model functions.
HRSG simulation	Functions and scripts related to the heat recovery steam generator simulation model.
Simulation results	Excel files containing all HRSG simulation results.